Tapered gain guides in diode lasers and picosecond Q-switched bow tie laser arrays

Kitcher, Daniel John

Award date:
1998

Awarding institution:
University of Bath

Tapered Gain Guides in Diode Lasers and Picosecond Q-Switched Bow Tie Laser Arrays

submitted by Daniel John Kitcher

for the degree of Ph.D.

of the University of Bath

1998

ProQuest LLC
789 East Eisenhower Parkway
P.O. Box 1346
Ann Arbor, MI 48106-1346

Abstract

The use of the tapered waveguide to simultaneously expand and amplify the output of a diode laser has recently led to an order-of-magnitude increase in the continuous power and the picosecond pulsed output that can be obtained from a diode laser in a single spatial mode. The theoretical and experimental investigation of gain-guiding has been used as a basis for detailed investigation of gain guided single taper lasers. It was found that the narrow gain guide was prone to launch a spatial mode structure with highly undesirable asymmetry from a high quality beam waist which was located at the apex of the taper. Symmetry could be restored and stabilised by a ground connection to the narrow region of the taper. This avoided divergence that is normally induced by gain-guiding in the narrow region.

Building on the achievements of bow tie lasers, further increases to power were sought by combination of many parallel stripes to create a novel bow tie array. Novel diode laser array structures were fabricated and measurements of the spatial mode properties of these are presented. Multiple contact laser arrays were tested with the narrow stripe regions in the centre used as a saturable absorber for Q-switching. Nanosecond current pulses were used to generate single Q-switched pulses of up to 17*W* peak power and down to 11ps duration (fwhm) from a monolithic diode laser. The potentially chaotic spatial and temporal nonuniformity of broad area diode lasers was observed to influence the performance of arrays within the duration of picosecond-range pulses. A trade-off of nonuniformity against pulse duration could be optimised by an external control voltage to the absorber. Optimised pulses could be generated with a subpicosecond rise time and 1.6ps relative jitter between stripes of the diode laser array.

Acknowledgements

I would like to thank all of the following:

EPSRC for funding

Prof.I.H.White*, the principle investigator of the Bow Tie Laser project

Dr.K.Williams* for help and advice on Q-Switching

Dr.I.Khrushchev* for the training and use of the $50GHz$ scope and autocorrelator, and for jointly performing measurements on Q-Switched Bow Tie Array lasers.

J.S.Roberts** for making the double heterostructure wafers.

Mr.T.Ryan*** for patient fabrication of literally hundreds of devices

C.Blay for enduring my unless suggestions for obscure experiments, and for taking the colour photographs of laser chips.

Kamil Abd-Rahman for my first initiation to the optoelectronics laboratory and for a C program that has evolved into several automated experiments.

J.Müller for developing the overshoot compensated avalanche pulse generator.

M.Tatar, P.Ford, M.Harriman, W.Lambson and B.Draper for technical, logistical, electronic, chemical and indescribable help.

* C.C.R., Dept.of Electrical Engineering, University of Bristol
I would like to acknowledge the help of Dr.Kevin Williams, Dr.Igor Khrushchev and Prof. Ian White. The measurements of Chapters 7 and 8 were performed with Dr.Khrushchev in the University of Bristol.

** EPSRC III-V Materials Growth Facility, University of Sheffield

*** Fabrication of lasers was performed in the Dept.of Electrical Engineering, University of Bath

Thanks to all of my colleagues from the Optoelectronics Group, who have included: M.Asghari, T.Burks, R.Cregan, P.Dowd, Z.Jiang, Kamil, J.Knight M.Owen, B.Mangan, P.Mason, P.Phillips, L.Raddatz, P.St.J.Russel, E.Squire, P.Snow, M.Stephens, Y.Sumailia, H.Summers, A.Wonfor, B.Zhu,

And a special thanks to Dr.Frances Laughton, my supervisor, without whom none of this would have been possible.

1. The Importance of Arrays and Tapered Structures

1.1 INTRODUCTION TO DIODE LASERS AND THEIR USES

Since the first demonstrations of Light Amplification by Stimulated Emission of Radiation in p-n diode junctions by several research teams[1-4] in 1962, semiconductor lasers have evolved from fragile cryogenic curiosities to being the most compact and reliable light sources known to man. The natural size scale of microns or less and consequent timescale of nanoseconds down to picoseconds was at first a technological barrier to the production of laser diodes and observation of their output, but has eventually resulted in development of optical sources of unprecedented intensity and compactness, suitable for novel mass market products including laser printers, magneto-optic drives and CD players. Red laser diodes have found widespread use as alignment tools for manufacturing and construction, and in bar-code scanners. The increased brightness and reliability in comparison to other optical sources has led to the use of diode lasers to optically pump larger crystal lasers[5-11]. A selection of diode laser uses are indicated on Figure 1.1, illustrating the most technologically important emission wavelengths. Into the far infra-red region[12], diode lasers at the appropriate absorption bands are used to detect carbon dioxide, for example, water, or hydrocarbons[13]. Diode lasers are achieving the power and delivery requirements for new surgical tools, remote sensors and manufacturing processes[14,15].

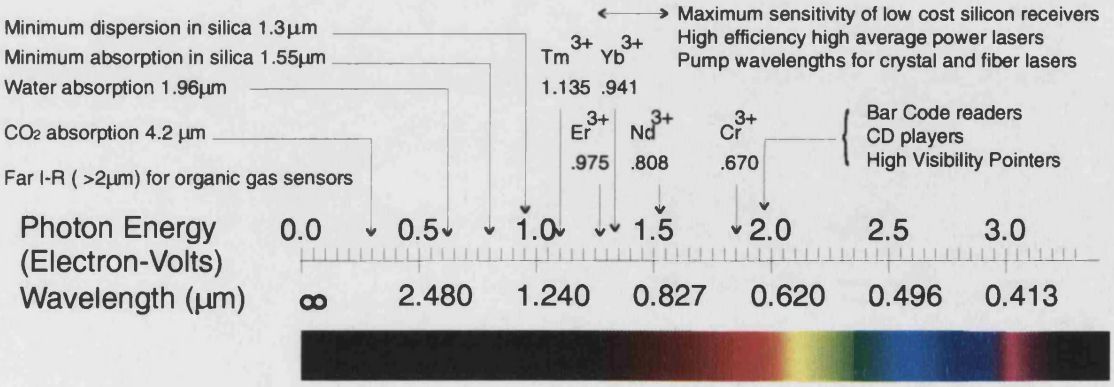

Figure 1.1 A selection of diode laser applications across the infra-red and red-visible spectrum. Important application wavelengths are labelled in micrometers. Energy (eV) and wavelength (μm) scales are plotted for comparison

The enormous potential for optical data transmission at high speed was soon recognised[16-18], and was a driving factor which demanded the investigation of optical fibers[19]. This in turn led to development of InGaAsP lasers[20,21] at 1.3 and 1.55μm, which are the most suitable wavelengths for long-haul transmission through silica fiber[22]. Feasible data rates which have been demonstrated[23-25] are above 100Gbit/s, which is well beyond the bandwidth limit of other communication channels, and could potentially be extended to approximately 50Tbit/s[22]. In the past decade, intercontinental optical fiber data links have aided the implementation of the global internet, providing a new opportunity for world wide co-operation and sharing of ideas.

1.2 HIGH-BRIGHTNESS CW SINGLE-MODE DIODE LASER STRUCTURES

1.2.1 Introduction

Kilowatt powers may be obtained from diode laser arrays combined as bars of arrays, and stacks of bars[26,27]. Incoherent and partially coherent groups of sources including these will be dealt with in chapter six. For comparison of the physical properties of lasers, the total optical power can be misleading, because for many systems it depends mainly on the number of duplicate lasers that have been installed, so the different material systems and types of laser structure are not comparable by raw power. Different regimes of pulsed operation further complicate a comparison.

1.2.2 Fair Comparison of Diffraction Limited Power

A convenient measure for comparison of the different laser structures is the sustainable continuous-wave (CW) power within the diffraction limit. The diffraction limit may be defined using the beam quality parameter M^2 of Equation 1.1 [27,28]. The near-field width w_0 of the laser spot and the far-field angular divergence θ_0 are conveniently represented by half-widths within which intensity falls to a factor of $1/e^2$ in comparison to the maximum.

Equation 1 $$\tan\theta_0 w_o = M^2 \frac{\lambda}{\pi}$$ *The diffraction limit*

The beam quality parameter M^2 is equal to 1.0 if the beam quality is optimum[27-28]. Otherwise, $M^2 > 1$. As a rule of thumb, the output from an imaging system is less intense at the best focus than the corresponding ideal Gaussian beam would be by a factor of approximately M^2. This becomes less accurate for peculiar shaped laser beams[166]. The maximum obtainable intensity is reduced by a further factor of typically 1.5 due to the non-Gaussian form of the fundamental mode of most wafer structures[166].

A selection of the most intense coherent laser diodes in the literature up to December 1997 are presented below, compiled from references[29-49]. Either the authors' quoted 'power within the diffraction limit' or the reported CW power, corrected by dividing by M^2 are compared.

Without exception, all of the optimised CW lasers used quantum well wafer structures. Conventional narrow stripe lasers were limited to approximately 0.1W within the diffraction limit. Lasers incorporating tapered gain sections within the laser resonator were able to deliver the best CW diffraction limited powers at long wavelengths, up to 1W[29-32]. In the 0.98μm and 0.85μm regions, even better performance, to 1.3W was obtained[36,37] by an Integrated Master Oscillator Power Amplifier (MOPA)[33], with a single pass tapered amplifier fed by an integrated Distributed Bragg Reflector (DBR) single mode narrow stripe laser. Other MOPA systems have achieved powers greater than 4W [34-38]. MOPA devices are now commercially available[26] at 0.5W for selected wavelengths from 1.6-0.63μm. Tapered diode amplifiers have been reported to deliver powers in excess of 4W using injection from a Ti:sapphire laser[34,35], and recently up to 5W using injection from an external diode laser[36]. A schematic plan of the major types of high power laser is show in Figure 1.2.

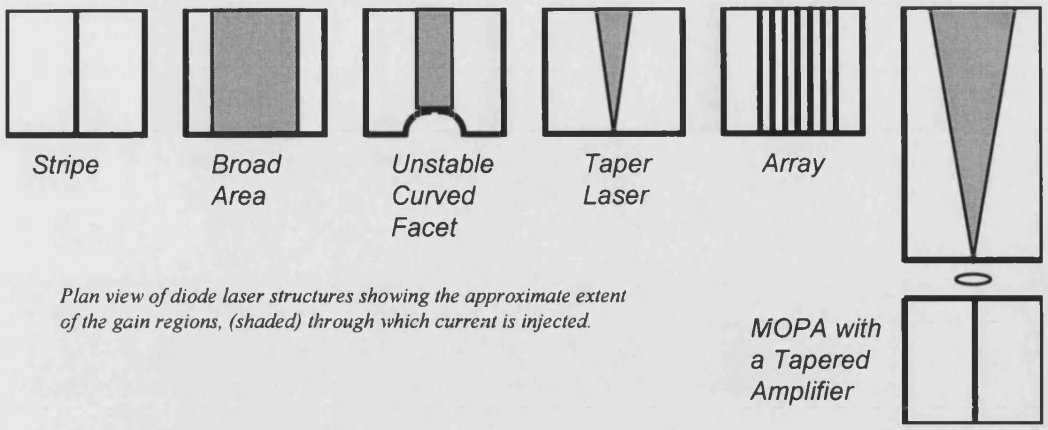

Plan view of diode laser structures showing the approximate extent of the gain regions, (shaded) through which current is injected.

Figure 1.2 Plan view of diode laser types. The threshold current, operating current and thermal power scale with the area of the current injection region (shaded). The optical output power scales with the width of the shaded regions.

A number of other novel structures have been demonstrated to produce high power (greater than 0.3W CW) within the diffraction limit. These include the MAG-MOPA, which used a narrow stripe DBR to feed a single longitudinal and spatial mode into a 5mm length 2nd order Bragg grating with gain and surface-emitting out-coupler regions[27]. The ARROW laser[39] emits a single transverse mode, selectively confined by a resonant effect at double-boundaries. The large refractive index step makes it insensitive to thermal and electronic refractive index changes which destabilise ordinary stripe lasers of the same width. Therefore an ARROW was able to emit a single mode over a very wide range of operating conditions at extremely high intensity. Several variants of unstable resonator lasers used a curved facet[41] or an integrated diverging lens train[42], which implemented similar benefits to a tapered laser, and achieved up to 0.5W within the diffraction limit. This review would not be complete without mention of the various phase controlled diode laser arrays which have been investigated, but only achieved moderate power (0.05-0.3W) within the diffraction limit. One special external cavity configuration[43-45] has achieved reasonable power (0.1W) and spatial mode selection. Phase conjugate feedback[46] attained 0.2W within the diffraction limit, while a Talbot Cavity[47] has achieved 0.5W. A unique approach to diode laser array construction is the Resonant Optical Waveguide (ROW) which places gain in low refractive index channels. By use of precise control of the refractive index step, stripe width, and emission wavelength, the ROW array strongly favours in-phase locking of all of the stripes of the array[27]. The CW diffraction limited power of typically 0.5W[48-49] is quite

high, and is obtained from a compact monolithic structure. The ROW array is suitable for duplication on large bars since it is reportedly less sensitive to defects and degradation than other high power laser designs[27].

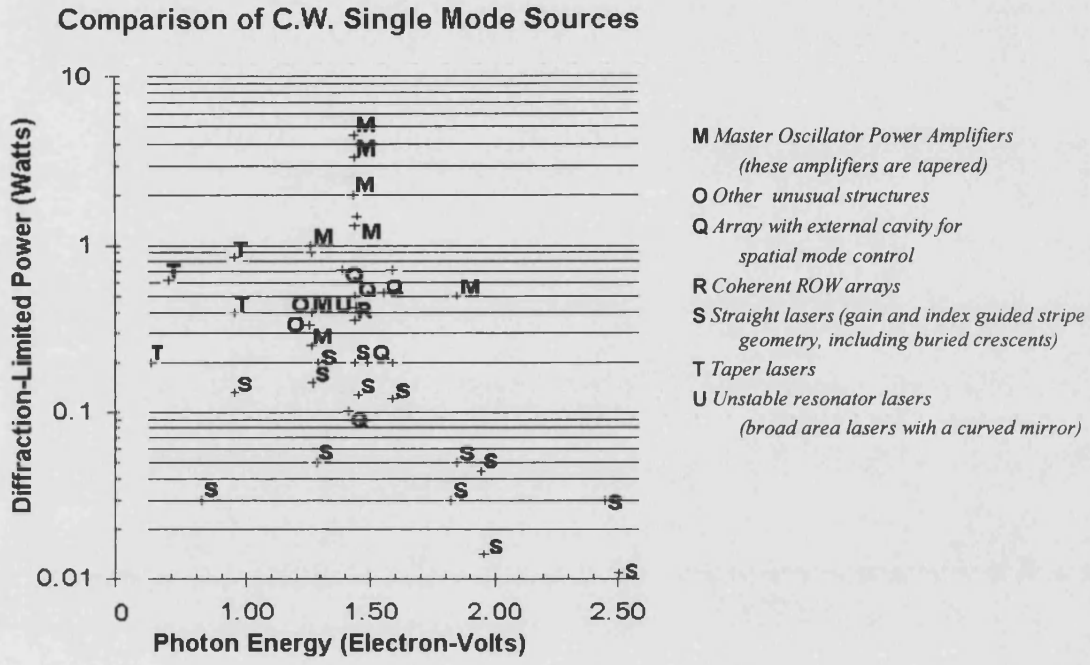

Figure 1.3 *Power within the diffraction limit for various laser structures. Isolated reports of higher power operation over very short lifetimes are not included since these cloud a comparison. Taper lasers marked 'T' deliver increased power at non-standard long wavelengths. ROW arrays and MOPA structures are available at restricted wavelengths, where they deliver the highest available intensity.*

1.2.3 Summary of Comparison

In summary, a number of laser structures have been reported which improve on the power performance of comparable narrow stripe lasers by an order of magnitude. These are coherent arrays (ROW, injection-locked, or external-cavity), unstable resonators (taper-lasers or curved-facet broad-area-lasers), integrated MOPAs (DBR-taper, DBR-grating emitter) and external amplifier MOPAs (broad area amplifier and tapered amplifier). Only the MOPA devices have exceeded One Watt diffraction-limited continuous-wave power.

1.3 OTHER DIODE LASER WAVELENGTH RANGES

At the time of writing, commercial diode laser materials are limited to emit at photon energies within the range of 0.40-2.0eV (2.0 to 0.62μm), with the highest efficiency and power in the middle of that range, (0.8-1.0μm). Some established wavelengths and uses were shown in Figure 1.1. Diode lasers which emit in the yellow[50] or yellow-green[51] have required cryogenic operation, and received little attention in recent years. Recent reports of blue-green, blue, indigo and violet diode lasers have been at lower power, with short lifetimes, and have lacked quantitative spatial mode data, but great improvements have been achieved[52-54]. Much progress is also being made in the mid infra-red[55-58]. Whenever fabrication uniformity is not a problem, the use of tapered gain sections to distribute current and optical output over an enlarged area whilst preserving a single spatial mode will be applicable at these new wavelengths also. The taper design can be implemented before accurate values of the material properties are known, in contrast to more complex architectures such as DFB-MOPA and ROW arrays which require detailed refractive index, bandgap and emission wavelength data, so tapered lasers are highly suitable for enhancement of brightness in new diode laser material systems.

1.4 LIMITS TO THE POWER AND RELIABILITY OF DIODE LASERS

1.4.1 Thermal Dependence of Threshold and Efficiency

With increasing temperature, threshold current increases, and the slope efficiency decreases[59], and at highly elevated temperatures, diode lasers are unable to operate. Common diode lasers with appropriate quantum wells can operate up to approximately 100^0C[59]. Internal heat generation is undesirable in all types of diode laser.

1.4.2 Electrical Contacts, Resistance and Cooling

The electrical power IV causes heating, especially in the vicinity of the heterojunction. In optimised lasers, the electrical to optical conversion (the 'wall-plug efficiency') may be as high as 66%,[61] but is usually lower. The rest of the power is dissipated as heat, and must be removed by conduction though the semiconductor[62]. Waste heat power

densities of the order of 100MW/cm^3 are released in conventional lasers. Therefore much effort has been devoted to improve the thermal packaging, ranging from ceramic or diamond plates to micro-groove water channel coolers[27], which become increasingly critical for larger high-current lasers. Common electronic component packages or copper heat spreader plates are sufficient for ordinary laser diodes.

1.4.3 Defects

A small number of defects are unavoidably frozen in during growth of laser structures. This led to extremely rapid degeneration of the early diode lasers. It is commonly observed that some defects proliferate, perhaps from excess optical absorption leading to further localised damage[59]. There are recognised mechanisms of growth of Dark Spot Defects (DSD) and Dark Line Defects (DLD)[63,64] which sometimes become evident within a few hours of device operation and eventually lead to failure of the whole laser. Observation of the power reduction during the first hundred hours of use allows selection of lasers which are free of serious defects of these kinds[59]. The initial defect density may be made low in lattice matched material systems such as (Al_xGa_{1-x})As/GaAs. Additional defects can be generated very easily, for instance during thermal expansion, optical damage, or nuclear radiation damage. Mechanical damage is avoided by careful handling of laser chips.

1.4.4 Catastrophic Optical Damage to Facets

The majority of high intensity diode lasers use cleaved semiconductor crystal facets to provide reflective surfaces which are highly uniform and absolutely parallel. The quality of these surfaces is critical to laser performance. Semiconductor materials undergo a modification to the density of states at the surface, and some materials, particularly AlGaAs are oxidised by contact with air[65]. Both the surface chemistry and surface states increase the optical absorption at the facet in comparison to the rest of the laser chip. This gives an excess temperature rise near to the facets[66-70], which further increases absorption. A destructive spiral of thermal runaway results in instantaneous permanent damage due to melting of the surface at positions of maximum optical intensity[69]. This is catastrophic optical damage (COD). A second destructive process is

the gradual degradation of facets during operation. Chemical reaction and defect creation cause a permanent reduction of laser efficiency, which becomes quite rapid at elevated temperature or at ultra-high intensity.

A number of processes have been evaluated which improve the stability of laser facets[71-82]. Contamination may be prevented by sealing lasers in vacuum or in a dry nitrogen atmosphere or by coating the facet with an inert solid before oxidation can occur. The use of $\lambda/4$ anti-reflection coating gives a further improvement in the COD intensity by a factor of three.[59,83]

1.4.5 Other Catastrophic Failures

COD is often the limiting factor for high power diode lasers containing AlGaAs. Other material systems, notably InGaAsP/InP have CW COD levels up to an order of magnitude higher than uncoated AlGaAs/GaAs[84]. Aluminium-free lasers can be manufactured with less strict anti-oxidation procedures, and much effort has been invested in developing InGaP/GaAs lasers at wavelengths which previously used AlGaAs[85-88]. One study of damaged pulsed InGaAsP lasers showed no evidence of optically induced failure, but traces of contact metals were found to have penetrated and destroyed the active region[89].

1.4.6 Intensity limit for operation of AlGaAs lasers

The accepted intensity limit[59] for COD of AlGaAs lasers is 6±2 MW/cm^2. This is derived from experimental data and suggests that the CW COD limit for the devices under test in this thesis should be equivalent to 0.9±0.3W per 100μm laser stripe width. The total power limit due to COD is proportional to the area of the facet region from which light emerges. It is assumed that the wafer structure supports a transverse mode of minimised width (necessary for low threshold), with an equivalent spot thickness d/Γ = 0.3μm. A 50% lateral fill factor is assumed, which is equivalent to replacing W by $\frac{1}{2}W$ to allow for lateral non-uniformity. The spatial modes are describe in more detail in Chapter 4. The COD level in GaAs is two orders of magnitude lower than the

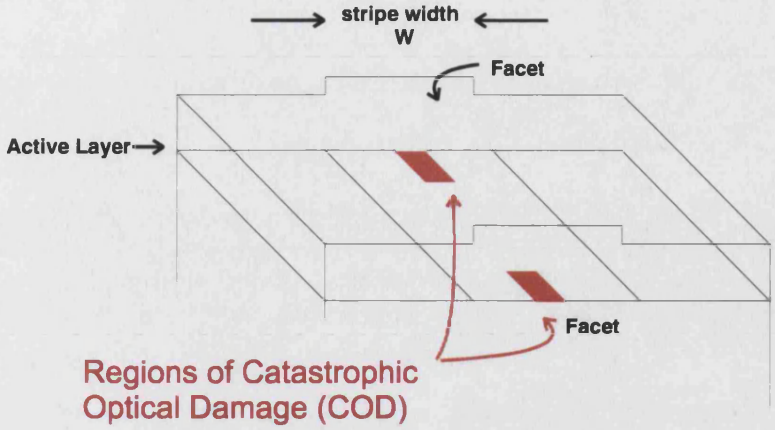

Figure 1.4 *The regions indicated receive the absorbed power during nonlinear self-focusing. The width of the vulnerable facet regions are 0.3-3μm, which can be much smaller than the typical width w of a stripe laser*

1.4.7 Intensity limit for Broad Area Lasers

Commercial broad area lasers[27] are usually operated at a conservative 0.25W per 100μm except in the well developed 0.8-1.0μm wavelength range, where 0.8-1.0W per 100μm (CW) is used reliably. Recent developments have raised the catastrophic failure limit during laboratory tests to as high as 4-11W (CW) per 100μm[90-92] but these use different wafer structures to the lasers under test in this thesis, and make use of protective facet coatings. Where improved materials prevent COD, the current density at the contact becomes the limiting factor. The use of a tapered contact which doubles the single-moded optical spot size also doubles the electrical contact area. Whether COD or electrical contact failure limits the lifetime, the taper structure permits a doubling of optical output power.

1.4.8 Catastrophic Failure Limit of Pulsed Lasers

The use of pulsed operation in any class of laser permits a further increase to the reliable output intensity. The localised heating which often determines the threshold of catastrophic failure may be separated into components of average heating (proportional to average power), and transient heating, which is a function of pulse energy and duration. By use of relatively short pulses (<0.01ms) and long intervals (low duty cycle)

duration. By use of relatively short pulses (<0.01ms) and long intervals (low duty cycle) less than typically 1%, the average heating can be decreased to less than 1^0C with simple external heat sink plates.

The maximum pulse energy then depends on the volume of the most loaded part of the laser system and the time available for heat to spread. In the case of uncoated AlGaAs, the depth of the absorbing region near to the facets (indicated in Figure 1.4) is of the order of 10μm, so the heated volume is of the order of 10×0.3×10μm in single-moded narrow stripe lasers. Thermal conduction is not significant on sub-nanosecond timescales. In other III-V optoelectronic materials, electrical contact nonuniformity on a similar size scale often leads to catastrophic failure. The heat capacity of GaAs is such that a 1K temperature rise should occur if 60pJ of energy is absorbed by the facet regions with a mass of 160pg in a typical stripe laser. In practice, the cladding AlGaAs has an intensity dependent nonlinearity which causes the optical distribution to self-focus into a narrow filament if Watt-level peak powers are approached. The self-focus facet heating volume could be destructively heated by up to 140K/nJ. Therefore picosecond pulses are limited to the picoJoule range when generated by single mode stripe geometry diode lasers.

1.5 PULSE GENERATION TECHNIQUES

The family of techniques for generating picosecond pulses from diode lasers has become almost as diverse as the laser structures themselves. The biggest distinction is between laser systems which have saturable absorbers of some kind, permitting Q-switching and in some cases mode-locking, against those which do not have saturable absorbers. Absorbers usually require an extra process in the manufacture of the laser chip but eliminate more sophisticated electronic drive or external optics which are otherwise needed to obtain the best output pulses.

Different techniques are marked on Figure 1.5 to indicate the typical behaviour under various schemes. Direct modulation of a laser diode optical output by application of current pulses is straightforward at rates of 100Mbit/s or less. At higher speeds, relaxation oscillations distort the output, so care is required in choosing the current

pulse shape and repetition rate. The oscillation features occur in timescales of 0.1 to 5ns, which is the timescale for carrier density fluctuations in the semiconductor, τ_s. Gain switching employs drive current pulses of short duration, ($<< \tau_s$) and substantially greater peak current than the threshold current I_{th}. The gain-switched pulses which are generated are an optimised relaxation oscillation. The short duration drive current rapidly increases the carrier population to raise gain well above the steady state threshold gain before the photon population has time to respond. Gain switching can be applied to large laser structures, leading to high peak power but with severe thermal limits to repetition, or can be optimised for short pulse generation by use of small single moded laser diodes. These are better suited for low current high speed current impulse generators such as a step recovery diode driven by an RF sinewave.

If a laser structure is modified to include a saturable absorber then Q-switching is possible. As discussed in Chapter 2, shorter pulse duration and greater power from a given laser structure is obtained by Q-switching in comparison to gain switching a structure with the same gain volume.

Mode-locking is used to obtain pulses in the picosecond and sub-picosecond regime. Pulses are of shorter duration and lower power than Q-switched and gain switched pulses, since only a fraction of the cavity length and carrier population overlaps with the pulse as it propagates up and down the cavity. Active mode-locking is the use of an external drive circuit to pump the laser gain section at the times to maximize the gain while the pulse passes through. This is generally limited by the speed and power of R.F. drive circuits. Passive mode-locking uses absorber self-saturation and recovery, and DC current to the gain sections. The limitation on pulse duration and repetition rate is then determined by gain and absorber recovery before and after the pulses. These in turn depend on carrier-carrier scattering rates, which can be in the sub-picosecond range. Colliding pulse mode-locking offers a further enhancement of speed at the expense of pulse energy, by coherently overlapping pulses in the absorber section, which effectively quadruples the intensity contributing to absorber saturation.

If a further decrease in pulse width is required, then complex systems using dispersion compensation elements to compress wide bandwidth pulses are used. For the maximum energy per pulse and increased power from semiconductor laser systems, an optical amplifier is required. The power in fibre coupled systems at the 1.55μm communication band can always be increased by passage through an Erbium doped fibre amplifier.

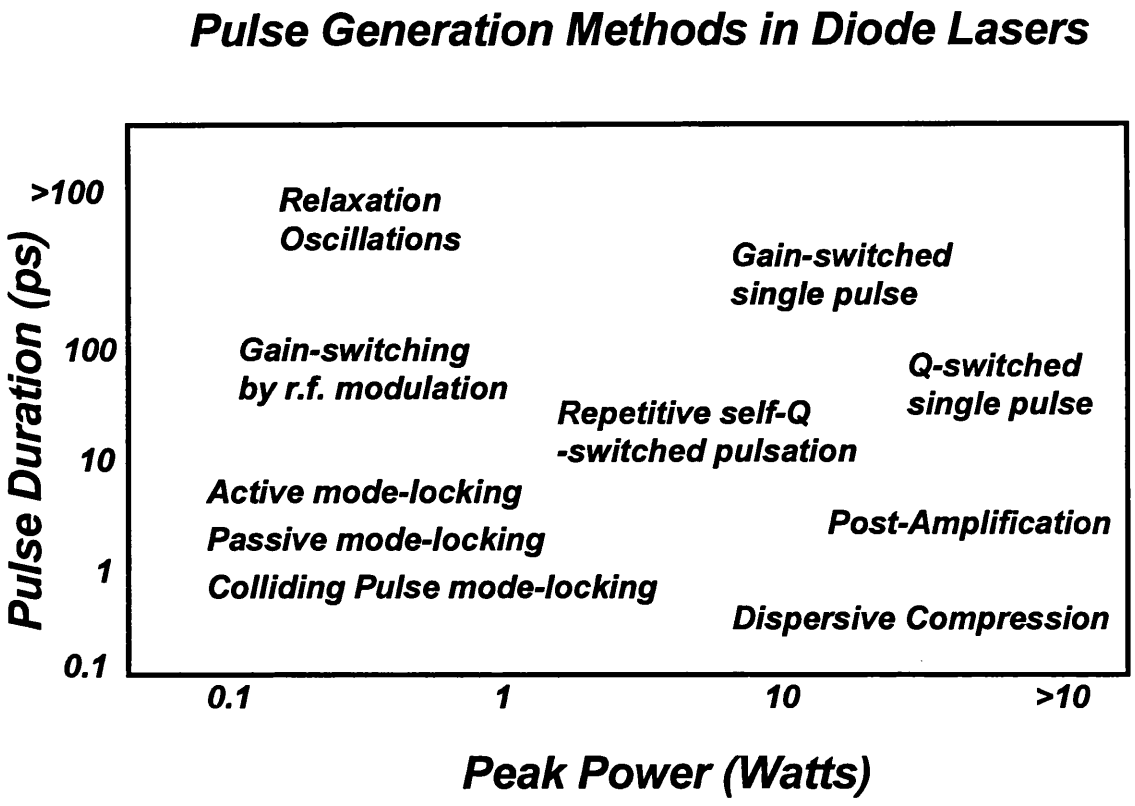

Figure 1.5 *The different regimes are labelled to indicate the approximate level of peak power and typical pulse duration. Q-Switched single pulses are of shorter duration and higher power than gain-switched pulses from the same laser. Gain switching can be applied to simpler laser structures. In comparison, mode-locking generates pulses of lower power, traded off for shorter duration and superior coherence.*

A review of pulse generation was written by Lau[93]. In the sections below, the power and pulse duration values are those stated in the references or inferred from pulse energy or average power. The same scaling of permitted peak power with laser size, structure, material and coating is found as for continuously operated lasers. Most of the pulsed

lasers are in quantum-well material at 1.3,1.55 or 0.85μm, except for the earliest reports which were for bulk GaAs/AlGaAs lasers.

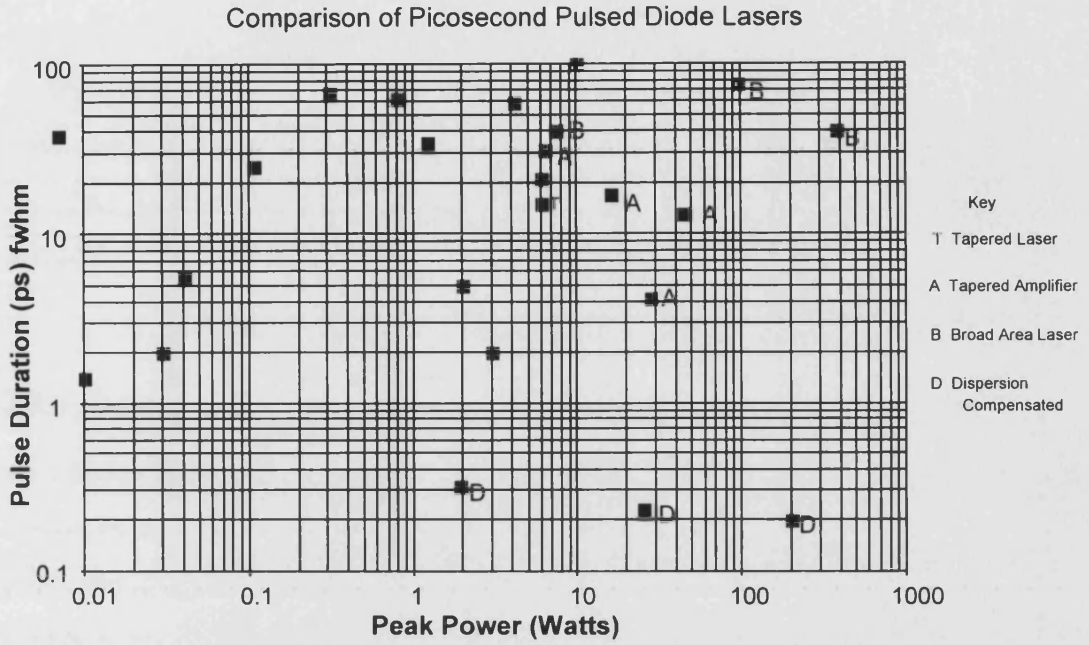

Figure 1.6 *A representative selection of pulse generation reports. Gain-switched and Q-switched broad area lasers 'B' appear in the top right of the figure, for maximum pulse energy and power up to hundreds of Watts according to the size of the lasers. Complex external optics were used to apply dispersion compensation 'D' and achieved high peak power. Tapered amplifiers 'A' and tapered lasers 'T' gave power in the 10W range with a single spatial mode. Ordinary straight laser structures (unlabelled) produce power which is one or two orders of magnitude lower.*

1.5.1 Direct Modulation

If the variation of current during one carrier lifetime (several nanoseconds) is small, or if a laser is DC biased above threshold, then the optical output follows the current above threshold according to the CW Light-Current (LI) characteristic[59]. It is simple to operate a laser in this way for 'slow' large-signal amplitude modulation or digital data transmission up to approximately 0.5GHz. Optical modulation of <600ps fwhm and <70ps rise time was obtained with electrical pulses of similar duration[94]. Applying modulation without significantly changing the gain has obtained small-signal modulation bandwidths beyond 40GHz.[101-102]

1.5.2 Gain Switching

If very rapid current variations significantly raise the gain in the laser cavity above its threshold value then relaxation oscillations may occur. If the excess gain is entirely depleted by the first oscillation then the optical pulse is described as gain-switched. A typical example of a gain-switched narrow stripe laser gave pulses of less than 100mW peak power and greater than 50ps duration[95]. Almost any laser structure may be gain-switched, from a single moded laser (4.1W, 14.5ps)[96] to a stack of bars of arrays (900W, 400ps)[97].

1.5.3 Q-Switching

As discussed in Chapter 2, the conversion efficiency of a short current pulse into a short optical pulse is improved if the Q of the laser cavity is switched to release a giant optical pulse and deplete the excess gain. This form of Q-switching has been used to generate pulses of up to 1.23W (34ps) from narrow stripe lasers[98] and 6W (15ps) from a single-moded double-taper laser[99], which is comparable to the pulses obtained from a multi-contact broad area laser using photoconductive switching to generate a near-instantaneous current pulse onto the absorber region.[100].

Use of an integrated modulator under external control to release optical pulses of small amplitude without significant depletion of the gain was also described as Q-switching[103]. Integrated modulators[104] have been used to generate pulse trains and bit sequences at ever faster data rates, usually at less than 50mW peak power.

1.5.4 Passive Q-Switching

It is useful to obtain stable pulse trains without the need for RF or impulse current supplies. Passive self-Q-switching is the repetitive process in which an absorber within a laser cavity becomes bleached by spontaneous emission, opening the Q-switch and emptying the gain region of most of the population inversion, then recovers absorption within the time required for the gain to rise back through threshold. Commercially available lasers[110] with ion implanted absorbers generated 0.5W 6-30ps pulses. Red single-mode narrow stripe lasers pulsated at a low power of 5mW (average), 25mW

(peak)[106,107]. Portnoi et al achieved an increase in laser volume to obtain 40ps 380W from giant broad area lasers with implanted absorbers[111]. A duration of 40ps and 7.5W peak power was obtained from a 100μm broad area laser with multiple contacts[108].

1.5.5 Passive Mode-Locking

If the pulsation frequency is near to the round-trip time of the laser chip (20-200GHz), or near to the round-trip time of an external cavity (0.1-20GHz) then the rapid amplitude modulation imposes side-bands on the optical spectrum, separated by the longitudinal mode spacing, the inverse of the round-trip time. This couples power between longitudinal modes, and can cause them to phase lock. This is a highly desirable condition, since successive pulses are coherent to one another, and as similar as possible. Pulsation at ultra-high frequency requires an ultra-fast saturable recoverable absorber. To date, suitable absorption states have had low saturation energy and relatively low unsaturated absorption coefficient, so mode-locking was limited to using a small fraction of the stored energy which is available to a Q-switched pulse from a particular laser structure. There is usually insufficient time between pulses for a high carrier inversion to accumulate.

Arahira reported mode-locked pulses at 1540GHz repetition rate[114], while Sanders[113] obtained 2ps 30mW pulses at 108GHz[113], and Zarrabi obtained 2W pulses at 40GHz from an array of thirteen ion implanted stripes under DC current[112].

1.5.6 Active Mode-Locking, Injection Locking

Deliberate injection of light or current at the cavity round-trip time has been shown to reduce the jitter and noise, and in some cases is necessary to initiate stable mode-locking. Transform limited 1.4ps pulses at low power (10mW) were produced in a multi-contact device with colliding pulses and RF modulation[115].

1.5.7 Travelling-Wave Pulse Amplification

Pulses which were generated by any of the techniques above may be injected into a diode laser amplifier with high gain. The amplifier must be AR coated to suppress internal lasing and pulse echoes. It also may require an optical isolator for more sensitive mode-locked schemes, so that residual reflections do not destabilise the pulse master oscillator. The final output is typically 20-30dB greater than can be obtained from a single mode laser, but pulse durations are lengthened by dispersion in the amplifier. Very high peak powers have been achieved from amplified gain-switched[115], mode-locked[116,117], and Q-switched[118] lasers. The highest powers were all achieved with AR coated tapered amplifiers.

1.5.8 Dispersion Compensation

Another approach is to take a pulse of moderate energy with large chirp, and to inject it into a passive dispersive element, such as a fiber grating or a prism-delay line. This can result in sub-picosecond output[120-125] if the dispersion is correctly matched to compress the input pulse towards its Fourier-transform limited duration. Up to 25W was achieved in this way from a single stripe laser diode[119]. More complex systems have been used to obtain up to 200W 0.2ps pulses from simple diode lasers[120-124]. The shortest pulses yet obtained from diode lasers were 0.065ps[123].

1.6 CONCLUSIONS

The multitude of available laser structures, materials and pulse generation schemes have been reviewed separately in sections 1.2, 1.3 and 1.5. There are several alternative structures which achieve a considerable improvement over conventional single-mode narrow stripe lasers. Of these, the tapered laser is most promising for ease of manufacture, and for exploiting new material systems. Tapered devices have dominated the field of high energy picosecond-range pulse generation from diode lasers.

2. Operating Principles of Diode Lasers

In this chapter, the basic operation of a diode laser will be reviewed, in order to state notation and approximations which are used elsewhere in the thesis. The principles and techniques are well documented in standard textbooks[125-129]. Pulse generation by gain switching and Q-switching is illustrated with the output of rate equation simulations.

2.1 DIODE JUNCTIONS, CARRIER DENSITY, RECOMBINATION

2.1.1 Cross-section and Band-Gap diagram of a typical Heterojunction

The heart of a laser diode is a p-n junction within materials such as Gallium Arsenide which have a direct band gap. Confinement of electrons and holes within the junction region is enhanced by the use of a double heterostructure, the central three regions of Figure 2.1.

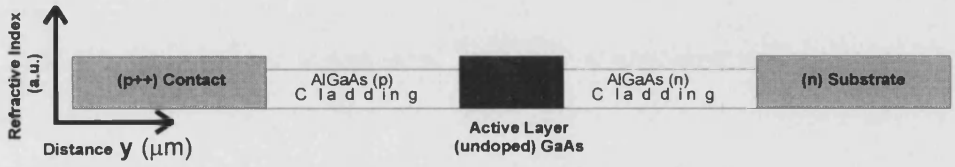

Figure 2.1 *Vertical (y) cross-section through a typical double heterostructure diode laser wafer. Cladding layers (for example, AlGaAs) surround a higher refractive index smaller band-gap core (for example GaAs). The cladding on one side of the active layer is p-doped and the other side is n-doped, which defines the diode junction. The active layer is usually undoped.*

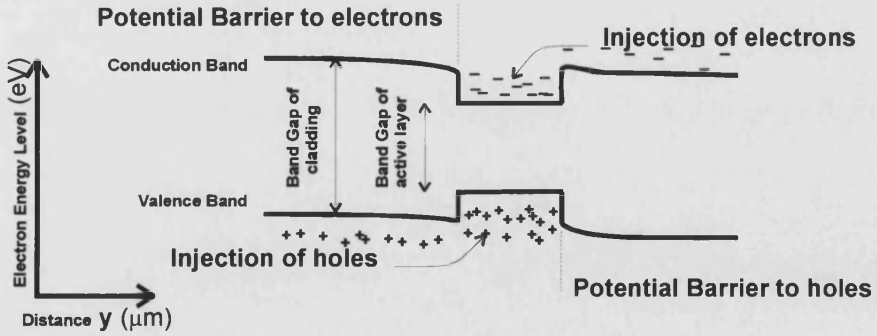

Figure 2.2 *Band edge diagram of a typical double heterostructure diode during high forward current flow. Current is carried through the p-doped layer by holes moving toward the diode junction. From the n-doped side, electrons are also moving toward the junction. The potential steps between the core and the wide bandgap cladding prevent injected electrons and holes from leaving the core layer.*

2.1.2 Stimulated Emission in Semiconductors

Energy E and momentum are both conserved by the interactions of electrons and holes with photons and phonons, (Equation 2.1). If a photon is liberated by an electron falling from an energy E_e in the conduction band into a hole energy level E_h in the valence band then its energy $\hbar\omega$ is given by Equation 2.1.

$$\hbar\omega_{photon} = E_e - E_h \qquad \textit{Equation 2.1}$$

Stimulated absorption can occur if a photon of resonant energy $\hbar\omega$ encounters an electron at a valence energy level, to generate an electron and hole pair at energy levels with a difference in energy of $\hbar\omega$. There should also be a negligible momentum difference ('k selection rule') for interactions in pure semiconductor. The k selection rule is relaxed in many-body interactions in which impurity atoms may carry momentum. This gives impurity states a relatively high importance in determining the gain function[125].

The interaction which promotes an electron from the valence band to the conduction band is stimulated absorption. The inverse process of stimulated emission can occur if a photon encounters an electron at the upper level and there is an unoccupied lower level available for it to fall to. This is represented as recombination of an electron with a hole.

The set of all available energy levels which differ by a particular energy $\hbar\omega$ rises steeply with increasing energy from near-zero for $\hbar\omega$ < the band-gap energy. This set, the joint density of states, is obtained by integrating the product of the density of electron states and hole states which differ by $\hbar\omega$. These states are capable of stimulated emission if occupied. If the number of occupied states exceeds the number of unoccupied ones then stimulated emission is more likely than stimulated absorption, equivalent to a population inversion[131]. Then photons experience gain on passing through the material. The photon density p grows exponentially with distance z at a rate g according to Equation 2.2.

$$\frac{dp}{dz} = p_{(0)} \exp(gz) \qquad \textit{Equation 2.2}$$

The gain coefficient g represents the average rate of amplification of photon density per unit distance through material in the z direction. If g is negative (loss) then the symbol α=-g is used in its place. Other losses (stated in section 2.1.3) require that g is substantially positive before the photon density p increases on passing through a semiconductor waveguide structure.

The simple two-level picture of gain is adequate for many purposes, but in semiconductors the situation is complicated by the quasi-continuous range of energy level transitions above the band-gap energy. The use of single numbers for carrier density n and photon density p is sufficient to describe processes in a single moded diode laser, in which the spatial average at the spectral peak is representative of the device. Validity of such approximations are discussed in the textbooks[125-129]. A thorough comparison of progressively more accurate but complex laser simulation models is presented by Hess and Kuhn[130].

There are large number of closely spaced excited electron states near to the bottom of the conduction band, which become filled sequentially, with the levels at lowest energies first. In the valence bands, the holes occupy the highest available states. In both bands, the density of states increases with distance from the band edge. The occupancy of these states decreases with energy above the band gap energy due to band filling. The joint density of states is a summation of all pairs of occupied electron and hole states which differ by a particular energy $\hbar\omega$. This function rises smoothly from near zero at the band edge. The density of occupied states goes through a maximum due to the increasing joint density of states, falling at still higher energies due to incomplete filling.

The semiconductor shows gain at high current, over a range of photon energies, determined by the energy levels of the crystal structure and doping sites[132]. This gives a gain spectrum which depends on temperature, strain, and especially on the carrier density n. A theoretical plot of the gain spectrum* of pure GaAs is shown in Figure 2.3.

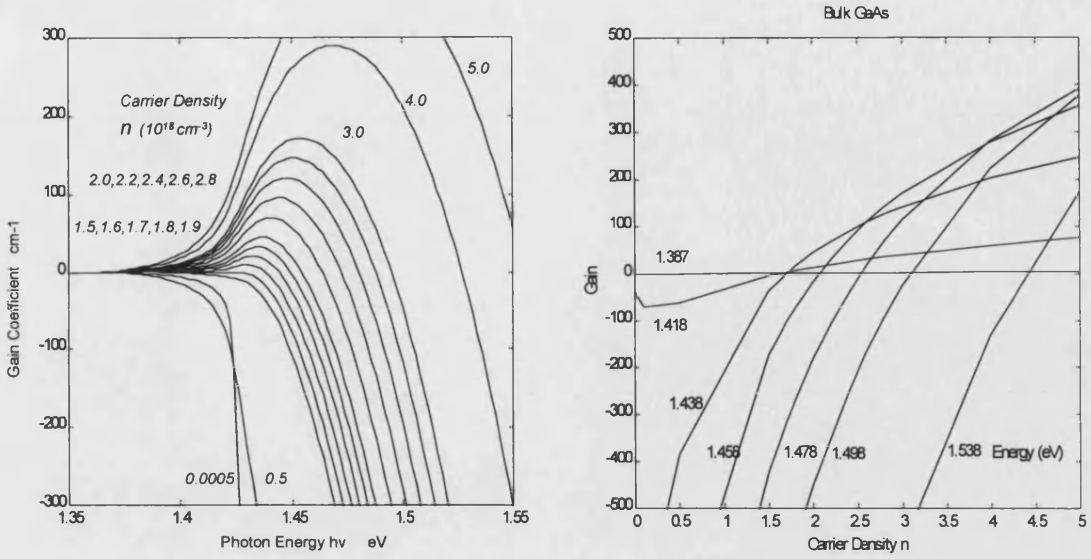

Figure 2.3 *A* *B*

A. Theoretical Gain Spectra g(ν) of bulk GaAs at room temperature. The gain is plotted for several carrier densities ranging from near zero to the values of the order of 10^{18} cm^{-3} which occur under high injection current. As current is increased, higher energy states become filled, giving gain further to the right of the gain spectra. The gain peak broadens and is blue-shifted (toward higher energy)

*B. Theoretical Gain Curves g(n) of bulk GaAs from the data of A along lines of constant frequency ν.[1] *1*

Below the band edge energy (nominal 1.387eV), GaAs is almost transparent. Well into the band (nominal 1.498eV), strong absorption or gain can occur due to the high density of available electron and hole states. As the photon energy increases, the gain slope *dg/dn* is enhanced, but to reach transparency requires a higher carrier density than at the band edge.

From the lasers tested in this thesis, the measured emission occurred at 885-888nm at 20°C, corresponding to 1.392-1.396eV. The gain spectrum of these lasers was offset from the simple theoretical results of Figure 2.3 by approximately 0.04± 0.01eV. This could be due to zinc diffusion from the *p* contact creating extra acceptor levels, 0.03eV inside the bandgap[125].

*[1] Data provided by Dr.H.Summers, Dept. of Physics, University of Wales, Cardiff [133]

2.1.3 Approximations to Gain Functions

Conventionally, a linear approximation to one of the gain curves is fitted to the region of interest,[125-129] and is a necessary simplification which allows many simple analytic conclusions to be derived for diode lasers. The differential gain a is measured from a tangent and inserted into Equation 2.3. For linear gain in a CW diode laser, the tangent at threshold carrier density is most suitable.

$$g = \frac{dg}{dn}\left(n - n_0\right) = a(n - n_0) \qquad \textit{Equation 2.3}$$

This linear function is valid for gain and loss, but is inaccurate away from threshold. To model an inhomogeneous laser, different values of a and n_0 are used for the various regions, which may be fitted from other tangents of the gain and loss curve near to the operating point of interest.

As can be seen from Figure 2.3B, the gain is a sublinear function of the carrier density n, passing through $g=0$ at a wavelength dependent transparency carrier density $n=n_0$. The carrier density in bulk GaAs heterostructures is a slightly sublinear function of the injection current density J (A cm^{-2}). An improved approximation is to use Equation 2.4, a logarithmic function for gain as a function of carrier density. The log function is not defined at $n=0$, so a better fit is required at very low carrier density. For the simulations used in this thesis, logarithmic gain has been used only above transparency. Using this form of gain function, the constant a defines $\frac{dg}{dn}$ at transparency, and an_0 equals the value of the gain at a convenient point $n = 2.719n_0$ which is fitted to the appropriate gain curve in Figure 2.3B. This is near to the operating point prior to giant pulse generation in semiconductor lasers.

$$g = an_0 \ln(n/n_0) \qquad \textit{Equation 2.4}$$

The rate of gain G per unit time is related to g by the speed of light within the laser material according to Equation 2.5.

$$G = \frac{c}{\mu} g \qquad \textit{Equation 2.5}$$

2.1.4 Effective Mirror Loss, Photon Lifetime

A laser cavity is formed by enclosing gain between reflective surfaces. If the optical power reflectivity of two mirrors a distance L apart is R_1 and R_2, then the loss per round trip at the mirrors can be expressed as an average mirror loss α_m defined by Equation 2.6. Other losses in the waveguide, including scattering loss α_S due to material inhomogeneity and surface roughness, and also free carrier absorption α_{fc}, contribute to the internal loss α_i. By convention[134], no confinement factor is used with α_i, which describes the mode-averaged loss constant.

$$\alpha_m = \ln\left(1/R_1 R_2\right)/2L$$
$$\alpha_i = \alpha_s + \alpha_{fc} \qquad \textit{Equation 2.6}$$

$$\frac{1}{\tau_p} = \frac{c}{\mu_z}\left(\alpha_i + \alpha_m\right) \qquad \textit{Equation 2.7}$$

The photon lifetime is typically of the order of 2.5ps. Comparison to the 12ps typical round trip time indicates large gain and loss, which are both characteristic of semiconductors. The Q-factor expresses the photon lifetime as the number of round-trips for the optical power to decay by a factor of *1/e*. In diode lasers, Q is typically 0.1 to 1, unlike gas laser cavities which have much lower gain available and have a Q factor much greater than 1.

2.1.5 Non-Radiative Recombination, Internal Efficiency, Carrier Lifetime

The average lifetime τ_s of an electron-hole pair in the active region is approximated by the following expression[129]:

$$\tau_s = 1/\left(A + Bn + Cn^2\right) \qquad \textit{Equation 2.8}$$

1/A is typically 6ns in Bulk GaAs.[125] At high carrier density, as found in amplifiers and lasers prior to gain-switching, the carrier lifetime decreases to typically 0.4ns.

2.1.6 Rate Equations

An ideal laser is defined in this thesis as one which obeys these rate equations:

$$\frac{dn}{dt} = \frac{I}{eV} - \frac{n}{\tau_s} - Gp \qquad \textit{Equation 2.9}$$

$$\frac{dp}{dt} = \frac{\beta n}{\tau_s} - \frac{p}{\tau_p} + \Gamma G p \qquad \textit{Equation 2.10}$$

The spatial distribution of optical power is constant with time, and is entirely represented by the confinement factor Γ, the fraction of optical power within the region of gain. For carrier density n which is less than the threshold value n_{th}, any photons are absorbed, creating excited carriers because the gain function G is negative. A spontaneous emission term $\frac{\beta n}{\tau_s}$ provides seed photons which are important prior to pulse generation and at low power. For currents greater or equal to the threshold current I_{th} required to reach $n=n_{th}$, the carrier density n settles to satisfy the threshold condition, Equation 2.11, for which the sum of gains and losses during a round trip, according to Equation 2.12 is zero.

$$\frac{I}{eV} - \frac{n_{th}}{\tau_s} = 0 \qquad \textit{Equation 2.11}$$

$$\Gamma g_{th} - \alpha_i - \frac{1}{2L}\ln\left(\frac{1}{R_1 R_2}\right) = 0 \qquad \textit{Equation 2.12}$$

For currents I greater than I_{th}, the output power L of an ideal laser is a linear function of excess current above threshold, which may be expressed in terms of the differential efficiency η.

$$\eta = \frac{1}{h\nu}\frac{dL}{dI} \qquad \textit{Equation 2.13}$$

The differential efficiency η_d depends on the internal efficiency η_i as well as the loss and output mirror reflectivity[135] according to Equation 2.14.

$$\eta_d = \eta_i \Big/ \left(1 + \alpha \frac{2L}{\ln(1/R_1 R_2)}\right) \qquad \textit{Equation 2.14}$$

2.2 DIODE LASER SIMULATION

The operation of an ideal diode laser may be simulated by numerically evaluating the right hand sides of the rate equations to calculate successive increments to n and p[136-137]. Effects of rapidly varying parameters and multiple-valued parameters to describe more realistic lasers are best investigated by simulation, as exact solutions of the rate equations only exist for special cases[130]. The simulation used in this thesis*[2] included a small number of spatially separate regions along the length of a monolithic laser cavity, and a discrete set of laser wavelengths, centred around the peak of a parabolic approximation to the gain spectrum of Figure 2.3A. The current, gain and carrier lifetime functions of the sections could be independently varied. Logarithmic gain was used, as described in Section 2.1.3.

2.2.1 Transient Response of Lasers and Steady State

The rate equations have a steady state solution given by Equation 2.12 if the current is above threshold. A numerical integration of the simple rate equations settles toward this steady state for all reasonable initial conditions, as does a common diode laser. Any change to conditions which is rapid in comparison to the rate of change of carrier density n can lead to a series of damped relaxation oscillations[125-129]. The photon population suffers a large oscillation when the carrier population overshoots the steady state.

2.2.2 Gain Switching

If a current change occurs at a rate that is much greater than I_{th}/τ_s then the overshoot is sufficiently great that p may return to near-zero after the first burst of light after the laser gain is switched well above threshold. This is illustrated in Figures 2.5 and 2.6. The energy contained in the pulse increases with the inversion ratio r, defined by Equation 2.15. The extraction efficiency η_e is defined as the fraction of carriers above transparency which are used in the first pulse. This is a simple function[93], if linear gain

*[2] Multi-moded multi-section Rate Equations Simulation written in C by members of the Optoelectronics Group, Dept. of Physics, University of Bath

is assumed, given by Equation 2.17 and shown in Figure 2.4. The pulse energy increases substantially with drive current amplitude and slew rate. The conversion factor to optical power depends on the internal efficiency at high carrier density, and is $h\nu\eta_i\eta_e(n_{max}-n_0)$ The duration of the optical pulse decreases steadily with r according to Equation 2.16 and also shown in Figure 2.4. However, it is not possible to achieve high r by gain-switching lasers without using current pulses of destructively high current density. The photon population rapidly builds up from the spontaneous emission after a brief turn-on delay time. Within typically 50ps of exceeding threshold, a pulse develops. The maximum r is typically 1.3, so only a fraction of the stored energy in the cavity is released as a gain-switched optical pulse.

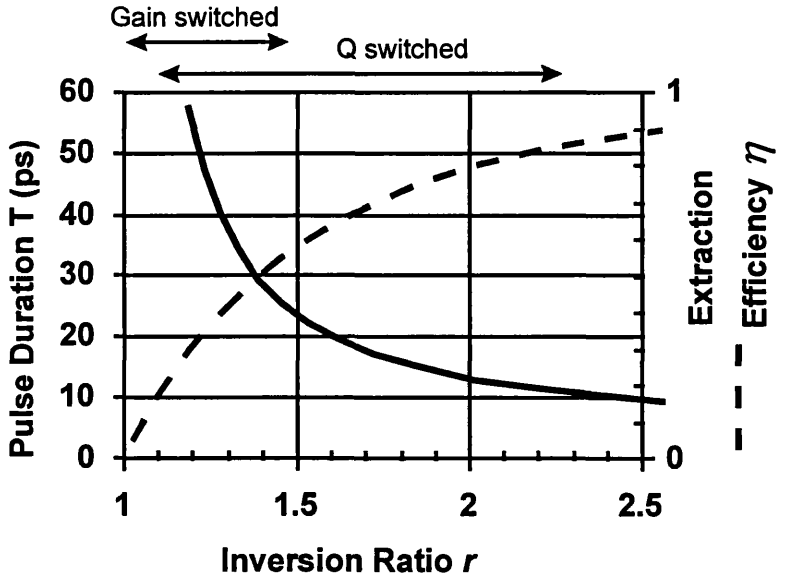

Figure 2.4 *Pulse duration $T_{1/e2}$ and extraction efficiency η_e as functions of the inversion ratio r, assuming linear gain. T was calculated assuming a photon lifetime τ_p of 2.55ps. Logarithmic gain would tend to stretch the r axis so that a higher initial inversion ratio is required to give a particular extraction efficiency.*

$$r \approx \frac{n_{max}}{n_0}$$ *Equation 2.15*

$$T_{1/e^2} = \frac{r\eta_e}{r-1-\ln r}\tau_p$$ *Equation 2.16*

$$\frac{1}{\eta_e}\ln\left(\frac{1}{1-\eta_e}\right) = r$$ *Equation 2.17*

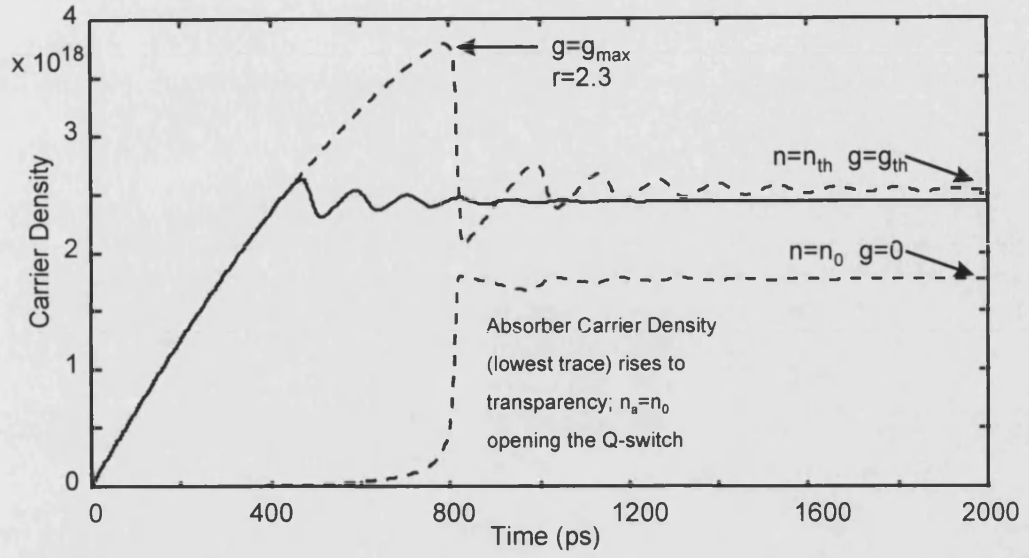

Figure 2.5 *Carrier dynamics for gain switching and Q-switching to generate a giant optical pulse. Parameters were chosen to model a bulk GaAs/AlGaAs laser with a total length of 500*μm. *The current was turned on abruptly from 0 to 4.0I_{th} at time t=0. Logarithmic gain was used above transparency. For the Q-Switched simulation (dashed) a 50*μm *absorber section was included, with an absorption constant greater than the gain constant by a factor of four. The same current density was used in both cases.*

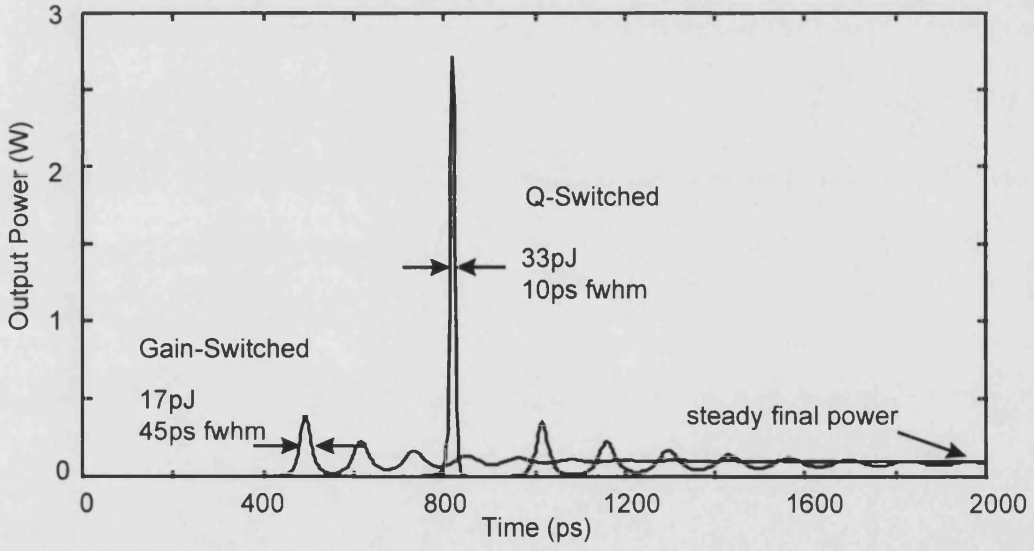

Figure 2.6 *Optical power output for gain switching and Q-switching, showing a giant optical pulse followed by relaxation oscillations. The pulse energy and powers were calculated for a stripe laser of width 5*μm. *From Figure 2.5, the saturable absorber permitted a very large population inversion to accumulate in the gain region. The energy released by the Q-switched pulse was doubled in comparison to gain switching a similar laser. The simulated peak power was increased by an order of magnitude, mainly due to a reduction in pulse duration.*

2.2.3 Q-Switching

In order to increase the inversion ratio r, and make full use of the energy storage of a laser cavity carrier population, a saturable absorber is used to spoil the cavity Q for as long a delay as possible after threshold is reached.[13-140] During the delay, the carrier population density continues to rise toward its limiting value of $I/(q_e V \tau_s)$ which can be of the order of twice the normal threshold before the non-radiative recombination rates have increased to excessive levels. At very high carrier density, the spontaneous emission bleaches through the absorber, abruptly switching the Q of the cavity to a higher value[139]. This is evident in Figure 2.5 as a rise in the absorber carrier density at time t=800ps. At this moment the absorber becomes almost transparent, and a giant optical pulse grows, following a similar history to a gain-switched pulse. As with gain switching, very high current and high initial gain are favourable. Figure 2.4 is still valid for linear gain. Figure 2.6 shows the evolution of a typical Q-switched pulse with high r due to high current density, with an absorber occupying 10% of the length of the laser cavity. The absorber carrier density in the latter half of the pulse is clamped at transparency, and its rate of absorption is governed by the absorbing volume and the non-radiative recombination rate. With very high current excitation, the pulse extraction parameter η_e can be as high as 0.8.

2.2.4 Latching of the Q-Switch

The absorber region modelled in section 2.2.3 has a carrier lifetime of approximately 2ns. Figure 2.5 shows that once the Q-switch has opened, it remains open for greater than the time for the gain to recover to the low-Q threshold. The relatively small rate of carrier recombination in the absorber is sustained by the relatively large optical power passing through it.

2.3 TYPES OF ABSORBER AND REPETITIVE PULSATION

An unpumped region or inhomogeneous current injection[17,93] offer a possible implementation of a semiconductor saturable absorber. The use of reverse bias voltage to sweep out carriers[108], the addition of high doping concentrations[103], or the use of damage sites generated by ion implantation[110,111] are three methods of increasing absorber recovery. If substantial absorption is restored before the gain section climbs back to the low-loss threshold (marked n_{th} on Figure 2.5) then quasi-CW operation does not occur after a giant pulse. Instead, the gain continues to rise until it reaches threshold above the recovered loss. Then another Q-switched pulse emerges, and the process repeats. If absorber recovery is complete, then the pulse repetition period T_R is given approximately by Equation 2.18. and the repetition rate $1/T_R$ increases linearly with current.

$$T_R = (n_{max} - n_{min}) / \frac{I}{Vq_e} \qquad \textit{Equation 2.18}$$

At high current, where the period is less than the absorber carrier lifetime multiplied by the ratio of differential gain/differential absorption, the absorber fails to recover. There is low amplitude ripple, and for higher currents, the absorber becomes permanently bleached. These cases are illustrated in Figure 2.7 for a laser with ordinary absorber carrier lifetime and an enhanced absorber differential gain constant.

In summary, the basic operation of diode lasers has been reviewed. The energy per pulse which can be obtained from a diode laser is maximised by use of Q-switching, which requires a saturable absorber. The process can be adequately described by a numerical simulation of rate equations.

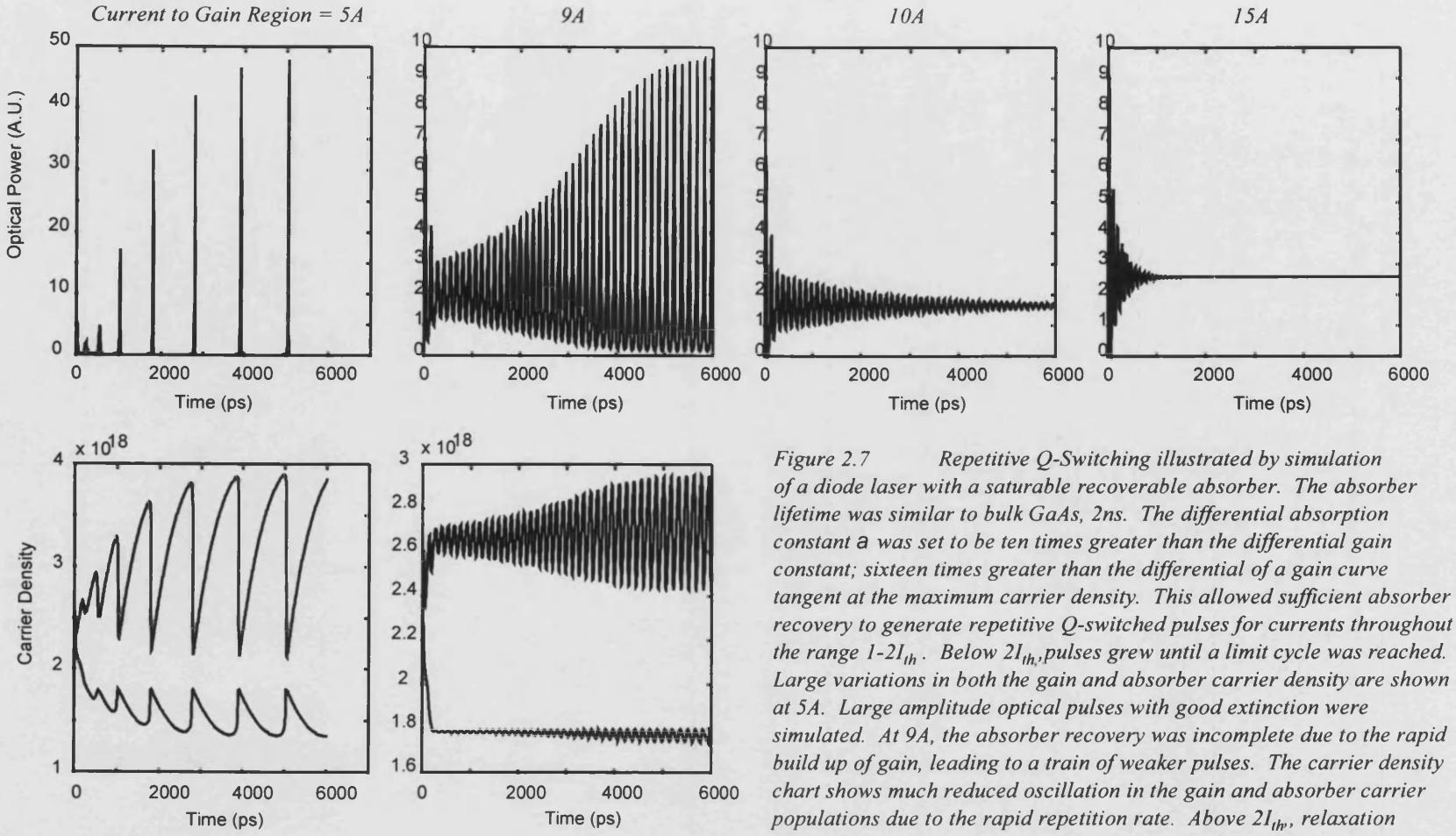

Figure 2.7 Repetitive Q-Switching illustrated by simulation of a diode laser with a saturable recoverable absorber. The absorber lifetime was similar to bulk GaAs, 2ns. The differential absorption constant a was set to be ten times greater than the differential gain constant; sixteen times greater than the differential of a gain curve tangent at the maximum carrier density. This allowed sufficient absorber recovery to generate repetitive Q-switched pulses for currents throughout the range 1-2I_{th}. Below 2I_{th},pulses grew until a limit cycle was reached. Large variations in both the gain and absorber carrier density are shown at 5A. Large amplitude optical pulses with good extinction were simulated. At 9A, the absorber recovery was incomplete due to the rapid build up of gain, leading to a train of weaker pulses. The carrier density chart shows much reduced oscillation in the gain and absorber carrier populations due to the rapid repetition rate. Above 2I_{th}, relaxation oscillations were damped, as is shown for currents of 10A and 15A.

2.4 SYMBOLS

Symbol	Description	Unit	Typical value
I	Current	A	1
J	current density	KA/cm^{-2}	2
g	gain constant	Cm^{-1}	200
a	Differential gain or absorption constant	cm^2	117×10^{18}
α	loss constant	Cm^{-1}	300
n	carrier density	Cm^{-3}	10^{18}
n	mode number	Integer	0
p	photon density	Cm^{-3}	10^{17}
R	mirror reflectivity	-	0.32
R	Resistance	Ω	0.6
Γ	overlap of optical and gain distributions	-	0.5
D	waveguide scale width	-	1.6
d	thickness of active layer	μm	0.17
L	length of laser cavity (or laser section)	cm	0.05
w	width of current injection stripe	μm	3
s	scale width of gain distribution	μm	4
S	scale width parameter	-	
u	complex near-field parameter	μm^{-1}	
β	spontaneous emission coupling factor	-	0.001
λ	laser emission wavelength = c/n, $=2\pi/\beta_0$	μm	0.885
ε	dielectric constant	ε_0	12.25
μ	refractive index		3.5
η	efficiency	-	-

2.4.1 Subscripts, which are applied to Symbols

th	value at threshold
0	value at transparency
e	Electron
h	Hole
p	Photon
eff	effective value; spatially and spectrally averaged
i	intrinsic or internal
x	*x* component of (lateral; in plane of junction)
y	*y* component of (transverse; perpendicular to junction plane)
z	z component of (longitudinal; along the principle optical axis)
$1/e^2$	full-width between points at $1/e^2$ of the maximum value
A	section *A* of inhomogeneous laser
B	section *B* of inhomogeneous laser
G	gain section of inhomogeneous laser
R	repetition; frequency or period

2.4.2 Exceptions: Symbols which do not fit the above rules

Symbol	Description	Unit	Typical value
θ_0	$1/e^2$ half-width of far-field intensity	Radian, deg	0.1745, 10°
W_0	$1/e^2$ half-width of near-field intensity	µm	
s_{eff}	$1/e^2$ full width of near-field = $2w_0$	µm	
α_H	line-width enhancement factor	-	5.5
b	see Chapter 5	-	3.5
η_D	slope efficiency dL/dI	-	0.33
η_i	internal efficiency	-	0.83
η_e	extraction efficiency of a pulse	-	0.5
β_0	propagation Constant $2\pi/\lambda$	cm^{-1}	70757

3. Measurement Techniques

An outline of techniques for characterisation of semiconductor lasers will be presented in this chapter. The implementation of these systems as used for experimental work in this thesis will be described. Estimates of the accuracy and limitations to the measurements will be presented wherever these affect further work.

3.1 PULSED POWER SUPPLY

3.1.1 The need for pulsed operation

Gain switching and Q-switching required the use of subnanosecond current impulses, for which special pulse generators were used. Even for basic characterisation, such as LI measurements, considerable power was dissipated. For example, a typical array laser was operated in the range 0.5-10A, which transiently dissipated 1-100W. This could only be sustained for a few microseconds before permanent thermal damage was expected. Therefore it was necessary to apply current pulses of less than a microsecond for a small fraction of the time, called the duty cycle. 2% duty was a safe limit for bulk GaAs/AlGaAs array lasers n-side down. <0.1% duty was preferred, so that the average temperature during measurements was almost independent of the current.

3.1.2 Impedance Matching

The lasers required current pulses of duration much less than a microsecond. The majority of high speed cables, pulse generators and accessories used 50Ω impedance. Figure 3.1 illustrates correct use of them. Resistors were added to construct a total load of 50Ω impedance. Similar rules apply for other impedance values; the source should match the load, and also the transmission lines and junctions in between. A miss-match could generate transient voltage spikes, which risked damage to the diode junctions of the lasers or power supply.

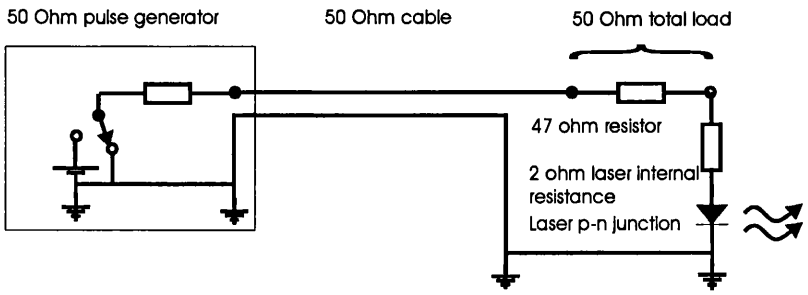

Figure 3.1 Equivalent circuit of 50 Ω pulse generator connected to a 50 Ω load

3.1.3 Pulse Generators

Systems which were used for the work in this thesis are tabulated below. For high current operation of arrays (1-10*A*) the 50Ω sources were not suitable, so the IRF and DLD were used. For short pulse high current work, the Avtech was required for adjustability and the Avalanche Pulse Generator (APG) provided the shortest possible pulse duration.

Pulse Power Device		Max. Current	Current Adjustment Range	Min. Pulse Duration, Containing 95% Power	Output Impedance Z
		(A)	*(%)*	*(ns)*	*(Ω)*
Lyons	a	0.2	99	15	50
HP214B	a	1.0 (2.0)	60	20	50
Blue Box	c	0.4	100	100	50
IRF511		4.0	95	40	10
IRF840		36	95	40	0.6
DLD-100	c	80	95	40	3
Avtech	a	10	95	4	5
Avalanche Pulse Generator (APG)	b	8 2	10 10	2 1.2	3 3

Table 1 Pulsed Current Supply Systems

a. Available commercially
b. Home built by J.Muller[140]
c. Computer control of pulse amplitude

A computer controlled LI measurement system was previously reported[141]. It made use of a pulse amplification unit under computer control, which was not intended to produce sufficient power to operate laser arrays. Based on components and software from this system, a modular approach was adopted, which permitted substitution of more powerful current pulse generators. The general system now in use is illustrated in Figure 3.2

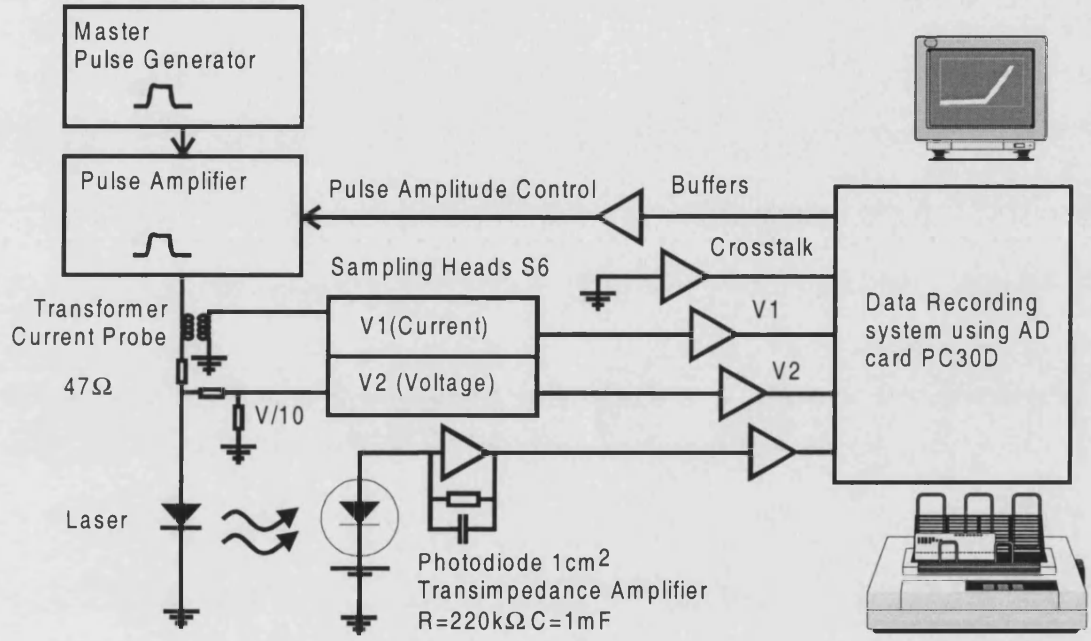

Figure 3.2 Block diagram of system for Light, Current and Diode Voltage Measurements

The voltage pulses (V1 and V2) were attenuated and examined on a Tektronics scope using S6 high speed sampling heads. A suitably short time interval was selected (the plateau of 250ns pulses or peak of 2ns pulses). The sampling heads produced output voltages which were fed via buffer amplifiers into Analogue-to-Digital Channels (ADC) of the PC30D card in a 286PC. A third ADC was used to record the average photocurrent from a $1cm^2$ silicon photodiode with reverse bias. Suitable optical attenuation was used if the peak light power exceeded 100mW, to avoid photodiode

saturation, as shown in Figure 3.3, or if the average power exceeded 100μW, to avoid amplifier saturation. The computer program[141] was adapted to subtract the 'zero offset' measured at the first point of a recording, and to subtract a crosstalk term from a grounded ADC. It was also restructured to average many ADC readings for each recorded point. As previously, the current, light and voltage were appropriately scaled, displayed on screen, and stored to the hard drive for future use. The current measurement with the IRF or DLD installed was performed by using software to take the differences of voltages across a small resistance in series with the laser.

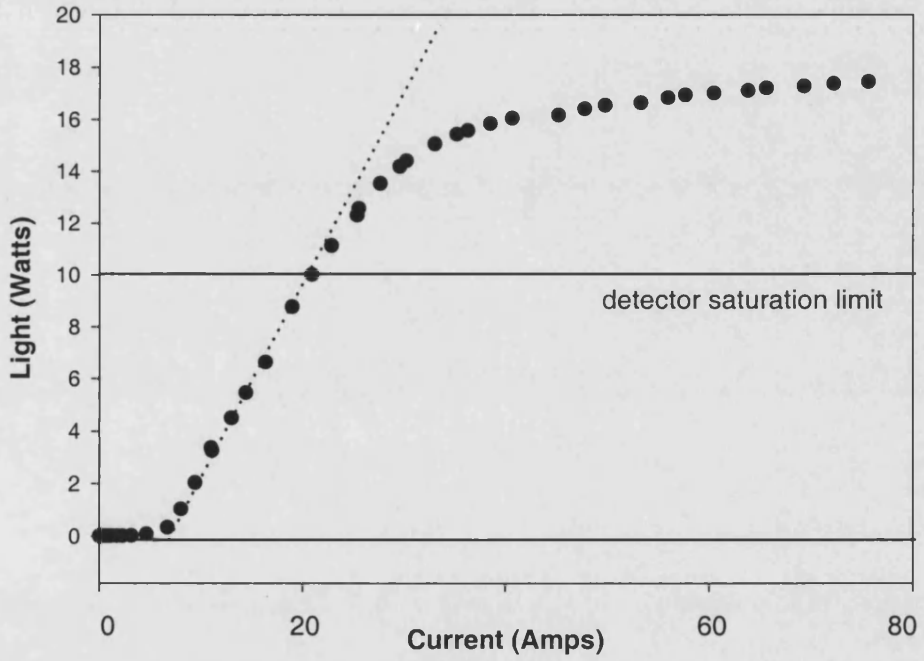

Figure 3.3 *L-I of a broad area laser showing photodiode saturation above approximately 10 Watts (100mW peak at the photodiode after filter attenuation to 1%) The LI characteristic of this laser diode (dotted) was known to be linear to at least 20W.*

Duty cycle = 200ns, 2000μs Filter=ND2, Pulse Generator=DLD100

3.2 NEAR- FIELD MEASUREMENTS

3.2.1 Definition

The near-field is defined as the optical field near to the laser facet[142]. For diode lasers, it is often not necessary to measure the additional non-radiating fields that are present in a true near-field[143-145]. The intensity distribution, proportional to the field amplitude squared ($I = c\varepsilon_o \varepsilon |E|^2/2$) of a magnified image at the output plane of the laser is conventionally presented as the 'near-field'. For edge emitting semiconductor lasers, as tested in this thesis, only the x dependence of intensity need be recorded, since the y dependence is constant and is determined by the wafer structure.

3.2.2 Magnification

A magnified image of the laser facet was viewed by a CCD camera and monitor. Where possible, a diode lens (L1 = Melles Griot, 14.5mm) was used, with a diffraction limit to resolution of 1.7μm. An ×16 microscope objective with poorer aberrations was required to observe an image of large (90-400μm) laser arrays without exceeding the CCD sensor size. The method is illustrated in Figure 3.4. The CCD width was known, and magnification was given by Equation 3.1:

$$magnification = \frac{s_2}{s_1} = \frac{s_2}{f\left(1 - \frac{f}{s_2}\right)} \approx \frac{s_2}{f} \qquad \textit{Equation 3-1}$$

The calculated scale factor was confirmed by lateral (x) movement of the lens so that the laser image crossed the scan range.

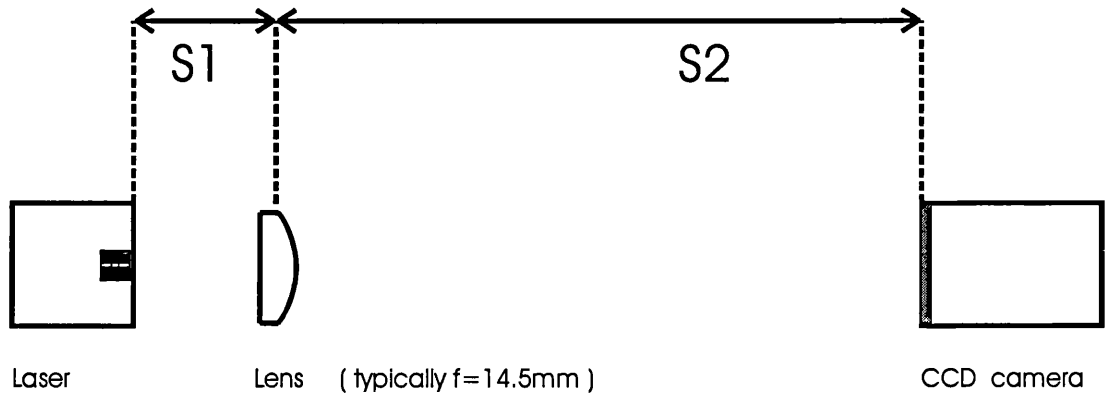

Figure 3.4 Geometry for Near-Field measurements. The ratio S1/S2 determines the magnification, which was approximately S2/f

3.2.3 Recording

The CCD image could be stored on a computer by a video analyser card. The apparatus is illustrated in Figure 3.5. An improved line scan could be obtained by storing a 2D image of the laser near fields, and summing several lines to reduce noise. The data processing steps are illustrated in Figure 3.7.

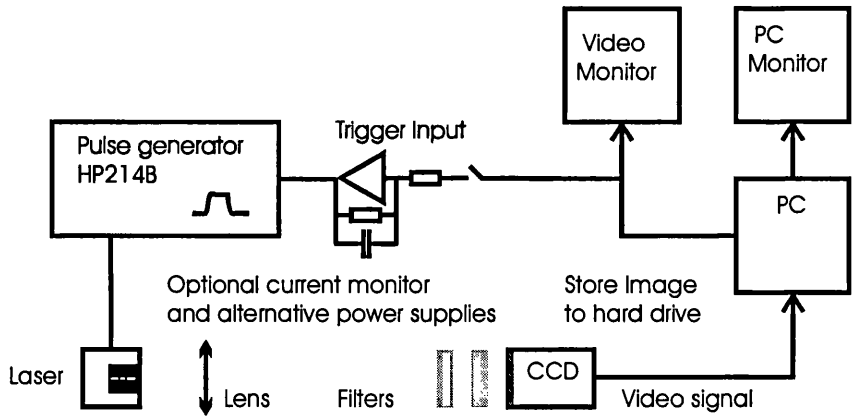

Figure 3.5 System for Near-Field observation and recording. The trigger input was used to synchronise the laser pulse to a period when the camera was most sensitive. This was useful to take near-field images of lasers at ultra-low duty cycle down to 1ns at 50Hz.

3.2.4 Sensitivity

It was found that a typical single pulse containing less than 8nJ optical energy saturated the whole video image. 1pJ onto 10×10 pixels gave a recordable spot on the camera. For standard near-field measurements, the camera was much too sensitive, so ultra low

duty cycle (1-1000ns at 50Hz) and neutral density (ND) filters were used to reduce the signal to a suitable range. The low duty helped to avoid laser degradation. An RG715 visible-blocking filter was permanently fitted so that the background level was less sensitive to ambient light, which was subdued but not blacked out. The camera sensitivity varied during its readout cycle, so the video new-frame signal was isolated using an active filter (RC = 30μs) and used to trigger a master pulse generator (HP214B) after a fixed delay of 3ms.

3.2.5 Post Processing

Stored images required processing before it represented the intensity profile. Firstly, the camera response was highly sub-linear. A fit to the camera response at 888nm is shown in Figure 3.6. The calibration measurements were observed in an image of spontaneous emission, as the duty cycle was increased from 0.00% to 0.1%. The response function was applied to each point of data to convert it to an intensity measurement and then plotted. This could be applied to line sections or to 2D images.

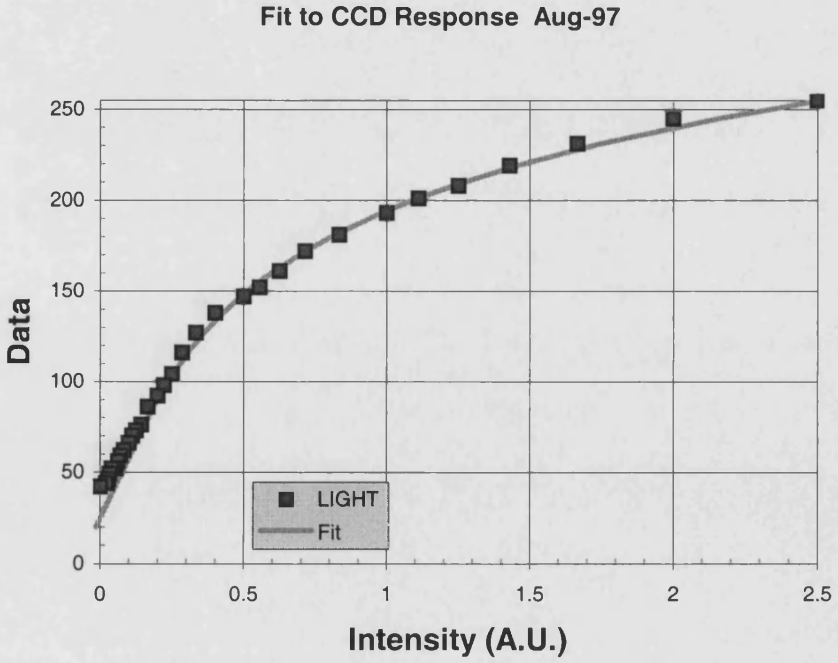

Figure 3.6 Silicon CCD camera response function at 888nm

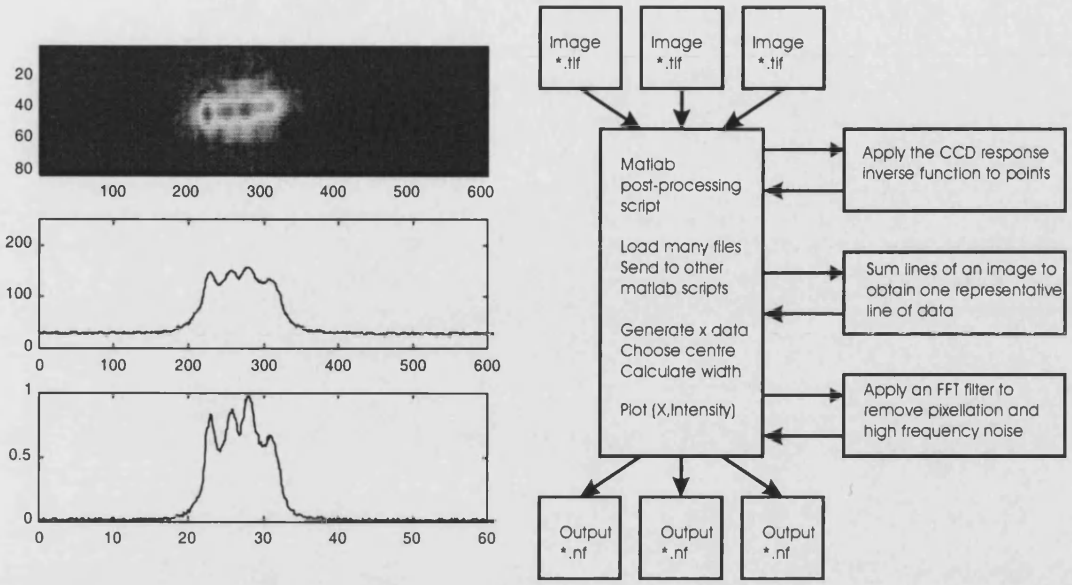

Figure 3.7 *Lines from a typical image (top) were summed (centre) and smoothed. Applying the camera response function influenced the width and severely influenced measurements of uniformity. The resulting near-field intensity line-scan of a multi-moded single taper laser is shown (bottom)*

3.2.6 Choice of Focal Plane, Beam Waists

The position z of the imaging lens required for a near field was selected as the position for minimum $1/e^2$ line width in the y direction. This is only the case if the transverse mode of the wafer structure is purely index guided. This lens position gave the sharpest silhouette of the front corners of several laser chips under back-lighting. The image broadened in y and contracted in x as the focal plane was moved inward through the laser, until a minimum $1/e^2$ width of x was reached. This was the beam waist from an astigmatic gain-guide[146]. The size of the beam waist indicates how closely the wave fronts matched a circular diverging pattern, and did not necessarily imply the existence of a real source of this size inside the laser.

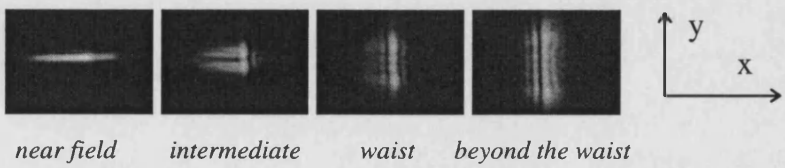

Figure 3.8 *Images taken as the distance from the laser the lens was decreased to move the imaged plane into the laser facet through the waist plane and beyond. The images are of a multimoded tapered laser number T51.*

The near-field was the most appropriate measurement to check for dark spot defects and symmetry, whilst the beam waist was most appropriate to measure the beam quality parameter M^2, in conjunction with measurements of the far-field[142].

3.3 FAR-FIELD MEASUREMENTS

3.3.1 Definition

The far-field is the optical field distribution far from a source or aperture[147]. It is conventional, in diode laser testing, to present a single line scan of the power incident on a detector as a function of angle θ. The geometry and measurement system are illustrated in Figures 3.9, and 3.10. As with the near-fields, the dependence of power in the y plane is a fixed property of the wafer, so only the dependence in the x plane was usually measured.

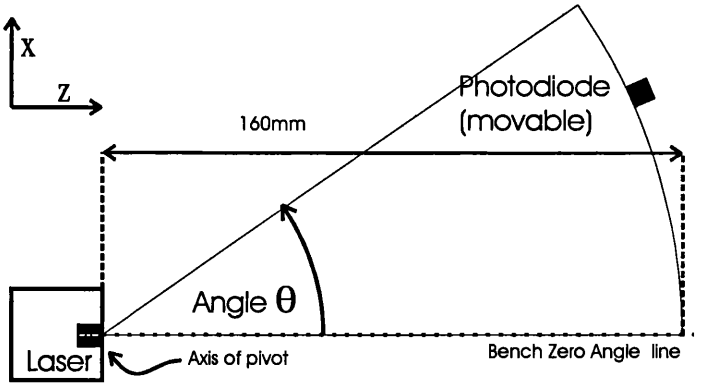

Figure 3.9 *Plan view of Far-Field measurement apparatus. The angle θ is defined from the normal to the laser facet, which was aligned using reflections from a HeNe laser. The photodiode was mobile along an arc within the plane of the page, which is the plane of the heterostructure layers..*

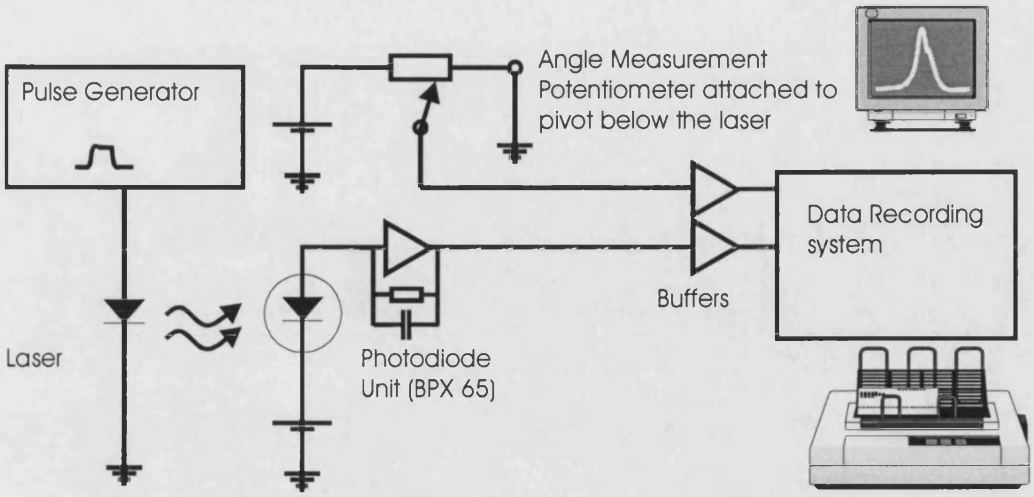

Figure 3.10 Far-Field measurement system. (electrical connections). The photodiode was suspended at the same height as the diode laser on a cantilever arm with a pivot about the y axis, below the laser diode facet. The plan view was shown in Figure 3.9. The angle was measured as a DC voltage on a potentiometer on the pivot axis. The signal from the photodiode gave a measurement of the intensity, which was recorded as a function of angle.

3.3.2 Angle measurement

A 20kΩ potentiometer was attached below the pivot of the detector arm. The output voltage depended linearly on angle, as confirmed by mechanical measurements presented in Figure 3.11. End stops were built so that -90°,+90° could be located repeatably to obtain the scale factors. The normal to the laser facet ($\theta_y = 0$) was not necessarily equal to the bench zero angle, because of movement of the silver epoxy when laser chips were mounted. A deviation angle ($2\delta\theta$) was measured by comparing the position of a HeNe reflection to a fixed marker. The correction $\delta\theta$ could be applied to sets of measurements when they were subsequently plotted. In a minority of chips, the waveguide axis was as much as half a degree off the crystal plane, so that the facet plane was not necessarily normal to the waveguide.

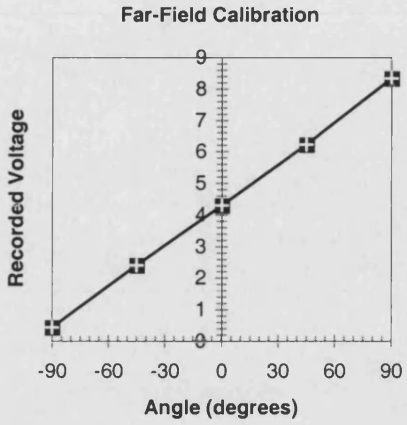

Figure 3.11 Calibration of Angle Measurement. The scale factor to convert voltage measurements to angle measurements was obtained from sets of ten measurements at several mechanically determined positions.

3.3.3 Resolution

The far-field may be expected to contain features whose angular extent is of the order of the diffraction limit θ_0 given by Equation 3.2 [28,143]. The limit is inversely proportional to the $1/e^2$ half-width w_0 of the laser output aperture. The slit size which subtends this angle at a distance of 160mm (the length of the measurement arm) is also listed. This shows that a 1mm detector approached the maximum permitted size for array experiments, so it degraded the results slightly. 1mm was quite acceptable for tapers and smaller lasers, as no features as small as the detector were expected. Where excess power was present from arrays well above threshold, a 0.1mm slit was inserted in front of the detector, for attenuation and resolution improvement.

$$\theta_0 = \frac{\lambda}{\pi w_0} \qquad \textit{Equation 3-2}$$

$$R_{\min} = {w_0}^2 / 2\lambda \qquad \textit{Equation 3-3}$$

The detector should lie outside the Rayleigh Distance R_{min} (Equation 3.3), in order that the Fraunhoffer far-field pattern is obtained. Inside of this distance, Fresnel diffraction patterns depend on the distance R to the laser. The value of R_{min} is tabulated below:

Laser Diode Configuration	Stripe Width $W \approx 2w_0$ (μm)	Diffraction Limit ($1/e^2$f.w.) *(radians)*	Rayleigh Distance R_{min} (mm)	Maximum Slit Width (mm)
Narrow Stripe	6	0.187	0.0051	30
Tapered Stripe	50	0.0225	1.41	3.6
Tapered Array	400	0.00281	90.4	0.451

Table 2 *Diffraction limited far-field angle $d\theta$ and minimum permitted distance to detector R_{min}. The width W is defined as the current injection ridge full-width at the output facet. For taper lasers and arrays, this is the width at the widest part of the device. The approximate width of diffraction limited far-fields on the 160mm arm of the apparatus is listed in the final column. The detector size or aperture slit should be an order of magnitude smaller.*

At least 99% of the vertical (θ_x) spread would usually be wasted if a point detector was used. Cylindrical optics were used to capture approximately 20% of a vertical slice of the far-field, and focus this onto the 1mm^2 silicon photodiode (BPX65) with an OP27 op-amp used as a 1MΩ transimpedance amplifier. This behaved as a tall thin slot detector since the lenses and laser were aligned in their vertical (y) axes.

3.3.4 Recording

Initially, an analogue chart recorder was used to make a paper copy of intensity signal vs. angle measurement voltage. Later measurements were recorded by digital storage adapter (DSA), or by the PC30D card and a new C program.

3.3.5 Sensitivity

Despite allowing digital recording, immediate printout, and improvement in the noise from older methods, care was required with mechanical stability. Good quality traces were obtained from 10μW average power. To study far-fields of smaller angular width, $< \pm 10^o$, from lasers of smaller facet size, <<50μm, best sensitivity was obtained from a CCD camera located directly in front of the laser.

3.4 CONCLUSIONS

The measurement systems for LI, VI, and spatial mode measurements which were used for work in this thesis have been described.

4. Gain Guided Lasers

In this chapter, optical waveguiding parameters will be found for the wafer structure and gain guides that were used for work in this thesis. Spatial mode data is used to determine gain, loss and the linewidth enhancement factor in 3μm stripe lasers.

4.1 SLAB WAVEGUIDE MODES

4.1.1 Wafer structures used for the lasers under test

The wafers QT476 and QT543R were used to fabricate all of the lasers which were tested for this thesis. The wafer composition and structure after processing are illustrated in Figure 4.1. The light was well confined to the GaAs core layer. A three layer symmetrical waveguide description gave accurate results. The three layer dielectric waveguide is dealt with by the standard textbooks.[125-129] The normalised width D defined in Equation 4.1 was less than π, therefore the slab waveguide was single moded.

$$D = d\beta_0\sqrt{\delta\varepsilon} \qquad \textit{Equation 4.1}$$

$$\beta_o = \frac{2\pi}{\lambda} \qquad \textit{Equation 4.2}$$

The dielectric constant step at the boundaries of the waveguide core layer was represented by Equation 4.3. Parameters of the lasers were $\delta\varepsilon=1.89$, $\lambda= 0.885\mu$m, $d = 0.17\mu$m, giving a value of $D = 1.66$.

$$\delta\varepsilon = \mu^2_{core} - \mu^2_{cladding} \qquad \textit{Equation 4.3}$$

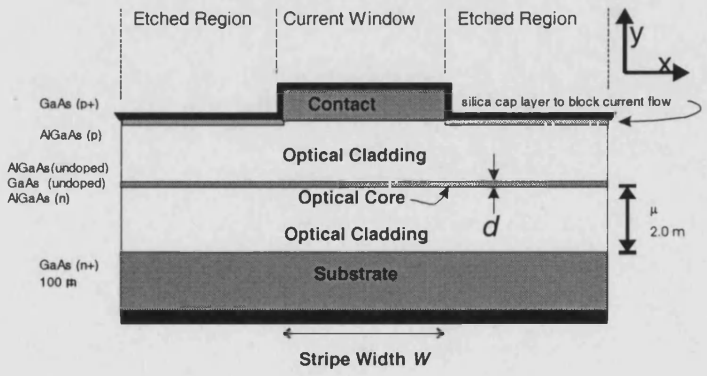

Figure 4.1 Cross section of the laser wafer structure under study

4.1.2 Slab Waveguide Modes of the wafer

Numerical solution of the one-dimensional time-independent wave equation was used to investigate the transverse (y) modes of the wafer multi-layer structure, which is illustrated in Figure 4.2. The wafer layers are listed in Table 4.1 and 4.2. It was found that the fundamental mode of the core layer was accurately approximated by the three layer analytical solution since the cladding layers of $(Al_{0.36}Ga_{0.64})As$ above and below were both much thicker than the penetration depth of the evanescent fields. The refractive index profile with depth, and the optical field amplitude, calculated at λ=0.885μm are displayed in Figure 4.2.

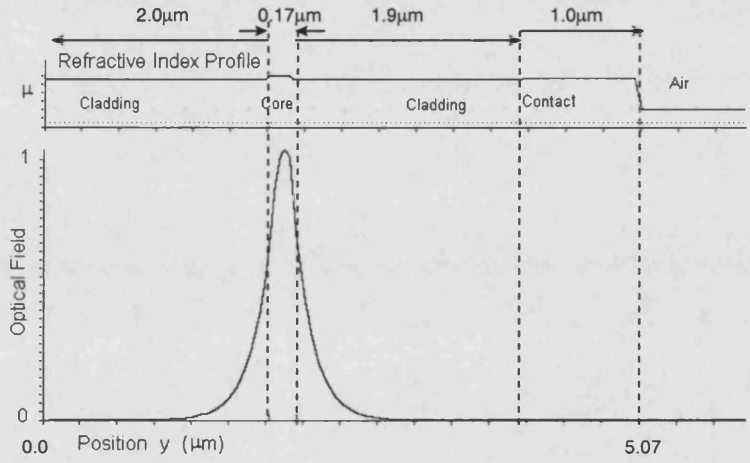

Figure 4.2 The Transverse Mode $H_y(y)$ of the bulk GaAs/AlGaAs wafers QT543R and QT476, which were used for all of the lasers which are reported in this thesis. The core and cladding refractive indices at the lasing wavelength were 3.64 and 3.37. The calculated effective index of the mode was 3.4732.

Layer	Composition	Ref. index, 885nm	Thickness μm	Dopant	Doping Density cm^{-3}
p Contact	GaAs	3.64	1.0	Zn	1.3 $H10^{20}$
p Cladding	$(Al_{0.358}Ga_{0.642})As$	3.37	1.6	C	2.9 $H10^{17}$
p	$(Al_{0.358}Ga_{0.642})As$	3.37	0.3	None	diffused Zn,C
Active core	GaAs	3.64	0.17	None	zero
n-cladding	$(Al_{0.358}Ga_{0.642})As$	3.37	2.0	Si	4.7 $H10^{17}$
n-buffer	GaAs	3.64	0.5	Si	2.0$H10^{18}$
n-substrate	GaAs 3^o	3.64	150	n	high

Table 4.1 Composition of bulk GaAs wafer QT476

Layer	Composition	Ref. index, 885nm	Thickness μm	Dopant	Doping Density cm^{-3}
p Contact	GaAs	3.64	0.3	Zn	1.3 $H10^{20}$
p Cladding	$(Al_{0.36}Ga_{0.64})As$	3.37	1.6	C	2.9 $H10^{17}$
p	$(Al_{0.36}Ga_{0.64})As$	3.37	0.4	None	diffused Zn,C
Active core	GaAs	3.64	0.17	None	zero
n-cladding	$(Al_{0.36}Ga_{0.64})As$	3.37	2.0	Si	4.7 $H10^{17}$
n-buffer	GaAs	3.64	1.0	Si	2.0 $H10^{18}$
n-buffer	GaAs 3°	3.64	150	n	high

Table 4.2 Composition of second bulk GaAs wafer QT543
Wafers and data were supplied by J.S.Roberts, EPSRC growth facility, Sheffield

The effective index μ_{eff} of a transverse mode is defined[125] as the ratio of the component of propagation constant β_z along the waveguide to the free space propagation constant β_o. Note that μ_{eff} lies between the refractive indices of the core and cladding materials. The value of the effective index for the TE mode of the waveguide was independent of the composition of the other layers outside of the AlGaAs cladding to at least eight decimal places, since there was negligible penetration of the cladding.

Using formulae and charts of Thompson[128], some further wafer parameters have been estimated. The effective $1/e^2$ width of the transverse mode was near to the minimum possible for the AlGaAs material system, approximately 0.25μm. The narrow mode width required a wide vertical far-field divergence. After allowance for obliquity factors, the full width half maximum was 63±6°, and less than 68% of the power lay within this range. The vertical confinement factor Γ_y describes the fraction of the optical power which is within the GaAs active layer. Its value was 0.58±0.05.

4.1.3 Effective Index Perturbation due to Etched Ridge Contact

If the contact layer was removed and the AlGaAs cladding thickness was reduced, corresponding to etching of the wafer, the effective index was not changed until the AlGaAs thickness was less than 1.2μm. A cladding thickness etched down to between

1.2 and 0.3μm gave a step in ε_{eff} which exponentially increased, approximately in proportion to the overlap between the material etched away and the evanescent field in the waveguide cladding. If the etch reached to within 0.3μm of the active layer, then the TE mode was no longer guided due to asymmetry. The effective index of the mode was calculated, and compared to the effective index of the unperturbed waveguide. This was squared to give the dielectric constant step which is plotted in Figure 4.3. The step was significant in compared to other effects in diode lasers if the cladding was thinned to 0.8μm or less.

Although small, this effective index step supports higher order lateral (x) modes[124,125] under a very wide ridge contact. Calculating the stripe width W for which the normalised width $D(W)$ exceeded π, the maximum single moded ridge width was calculated and plotted as Figure.4.4. A stripe laser that is wider than this limit always supports higher order lateral modes confined by the weak effective index perturbation at the edges of the ridge.

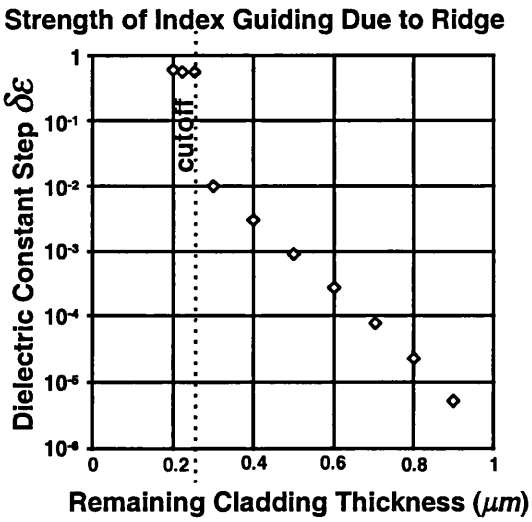

Figure 4.3
Dielectric Constant Step Δε after etching. The ridge was defined by etching to leave a reduced cladding depth on the top side. If greater than 0.3μm cladding was left after etching, then the layer structure supported a guided transverse mode. The effective dielectric constant of this mode differed by a small amount δε fromthe effective dielectric constant of the mode under the ridge center.

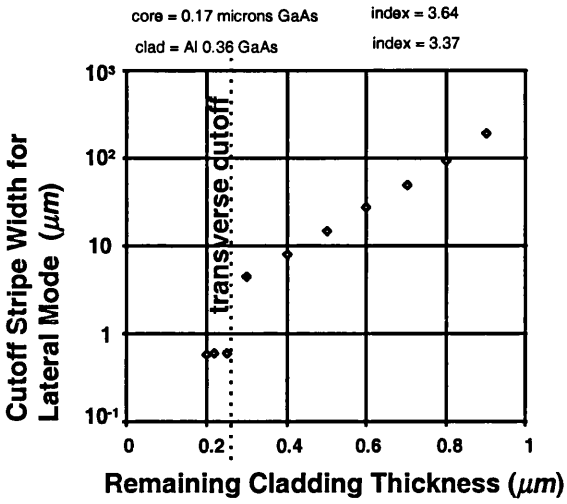

Figure 4.4
Cut-off width for higher order lateral modes due to the effective index step at the boundary of an etched ridge. The step in dielectric constant at the ridge boundaries supported higher lateral modes if a maximum ridge width was exceeded. This width is valid for materials which are uniform except at the step.

According to measurements with a Talystep mechanical surface profiler, the etch applied to lasers in this thesis left more than 1.1μm of cladding over the waveguide layers, even under the inter-contact isolation trenches of Chapter 7, and greater than 1.3μm cladding after the etch which defined the contact and ridge. Consequently, the effective dielectric constant step was less than 10^{-6}, which is unable to support higher lateral modes under a stripe of less than 1000μm width. This effective index step was insignificant in comparison to thermal guiding, non-uniformity and gain guiding.

4.2 INTRODUCTION TO GAIN-GUIDING

4.2.1 Description of modes of the Parabolic Gain-Guide

Electromagnetic waves can be guided by a region of high refractive index, such as the core of an optical fibre or the core layer in the slab waveguide example above.[125-129, 148-152] The process of gain-guiding is quite different to this, but can still support transverse modes, which may be defined as the time-independent bounded solutions of the wave equation in the structure under consideration. Time-independence requires that the device is monochromatic and in a steady state. The lateral modes are often an accurate fit to the observed lateral fields in real devices. A detailed treatment of gain-guiding in semiconductor lasers is presented by Thompson[128], and early experimental results are illustrated by several authors.[125-127,1467]

Material absorption or gain may be represented by an imaginary component $\mathrm{Im}(\beta_z) = g/2$ of the complex propagation constant β_z so that equation 4.4 describes damped travelling waves.

$$E_{(Z)} = E_{(Z=0)} \exp[jwt - j\beta_z z] = E_{(Z=0)} \exp[jwt - j\,\mathrm{Re}(\beta_z)z]\exp[gz/2] \qquad \textit{Equation 4.4}$$

Complex β_z is the propagation constant of photons in material of mode-averaged refractive index $\mathrm{Re}\sqrt{\varepsilon_z}$ and with an intensity gain coefficient of g. The complex (relative) dielectric constant ε_z is defined from Equations 4.5 and 4.6.

$$\beta_0^{\,2}\varepsilon_z = \beta_z^{\,2} \qquad \textit{Equation 4.5}$$

$$g = 2\,\mathrm{Im}\left(\beta_0\sqrt{\varepsilon_z}\right) \approx \beta_0\,\mathrm{Im}(\varepsilon_z)\Big/\left|\sqrt{\varepsilon_z}\right| \qquad \textit{Equation 4.6}$$

At the same location as an increase to gain in a semiconductor with increasing carrier density, there is a decrease to the real refractive index due mainly to other effects of the change to the carrier density δn. These are free carrier (plasma) interactions and Kramers-Kronig[153] effects, which contribute approximately $-1.23\times10^{-20}(\mathrm{cm}^3)\times\delta n$ and $-3\times10^{-20}(\mathrm{cm}^3)\times\delta n$ respectively for GaAs/AlGaAs lasers.[146,154,155] For small changes about the threshold carrier density $n \sim n_{th}$, as found in lasers, the gain function $g(n)$ is approximately linear, and the real and imaginary components of refractive index are proportional by Equation 4.7. This defines b, which is approximately equivalent to the linewidth enhancement factor[156-159], more usually called α_H after Henry[160].

$$b = -\alpha_H = 4\frac{\pi}{\lambda}\left(\frac{d\mu_{eff}}{dn}\right)\left(\frac{dn}{dg}\right) \qquad \textit{Equation 4.7}$$

On its own, the negative real refractive index change due to current injection would anti-guide light to the lossy material at the sides. However, these edge losses are exactly compensated by gain in the stripe centre. The modes of such a structure are necessarily diverging waves, which transport optical power from the excess gain at the stripe centre to the regions of absorption at the edges, in addition to transporting power along the structure. Averaged over a cross section, the modal gain g_z is just sufficient to

compensate for mirror losses and scattering losses to satisfy the round trip condition for threshold, Equation 2.12. The value of g_z is equivalent to the threshold gain of a broad area laser of the same length. At the stripe centre, the maximum gain, g_m, is somewhat greater.

The most important features of any structure with a smoothly varying distribution of charge carrier density are illustrated in the exact solution of a parabolic gain-index distribution, which are given by Thompson[128] and investigated experimentally in gain guided lasers by Cook and Nash[146]. In this model, the transverse dependence of the gain (and loss) is given by the parabola of Equation 4.9, which determines that the complex dielectric constant also follows a parabola, according to Equation 4.10.

$$g(x) = g_m\left[1-\left(\frac{2x}{s}\right)^2\right] \qquad \textit{Equation 4.8}$$

$$\varepsilon_{eff(x)} = \varepsilon_m - \Delta\varepsilon\cdot(b+j)\left(\frac{2x}{s}\right)^2 \qquad \textit{Equation 4.9}$$

The parabolic gain profile is consistent with the transverse component of the time-independent wave-equation if the field is a Hermite-Gaussian solution[161-165]. The first member of the solution set, the zero-order lateral mode is given by Equation 4.10. This optical field satisfies the standard Gaussian beam propagation properties in one dimension[166,152], but is astigmatic. Higher order complex Hermite-Gaussian functions are also solutions of the parabolic gain-guide.

$$H_y(x) = H_0\exp\left(\frac{-ax^2}{2}\right) \qquad \textit{Equation 4.10}$$

The complex constant a is separable into real and imaginary parts:

$$a = a_1 + ja_2 \qquad \textit{Equation 4.11}$$

Due to antiguiding, a is complex and wavefronts are curved. The location of the waist is several μm inside the cleaved output facet[146]. The corresponding solution to a parabolic real dielectric waveguide (for instance a graded index fiber) is a similar Gaussian function, except that a_2 is zero, locating the waist in the facet plane.

4.3 NARROW STRIPE LASERS

4.3.1 Device Description

The stripe lasers were fabricated from GaAs-AlGaAs double heterostructure wafer QT543R which is described in section 4.1. The 3μm stripe width W was defined by removing highly doped contact layers and adding a 0.2μm silica insulating layer to block current except for a current window through the ridge contact. Due to current spreading and diffusion, the gain guide was expected to be somewhat wider than the stripe.

4.3.2 Fitting to measurements of Threshold Current

The threshold gain Γg_z for lasers of 500μm length was estimated from Equation 2.12 to be 55±5cm^{-1}. The measured threshold currents in the range 140-180mA indicated that the current density into the contact stripe was 15-20kA/cm^2. From the gain curves of Figure 2.3 and the carrier lifetime $\tau_s(n)$=1.5ns, the broad area threshold carrier density n_{th}=2.45×10^{18}cm^{-3} required a threshold current density of only 4.4±0.2kA/cm^2. The ratio between the observed and broad area current densities gave an indication that substantial current spreading and diffusion over an area up to two times wider than the injection stripe were present in these lasers.

4.3.3 Near-Fields of 3μm Stripe Lasers

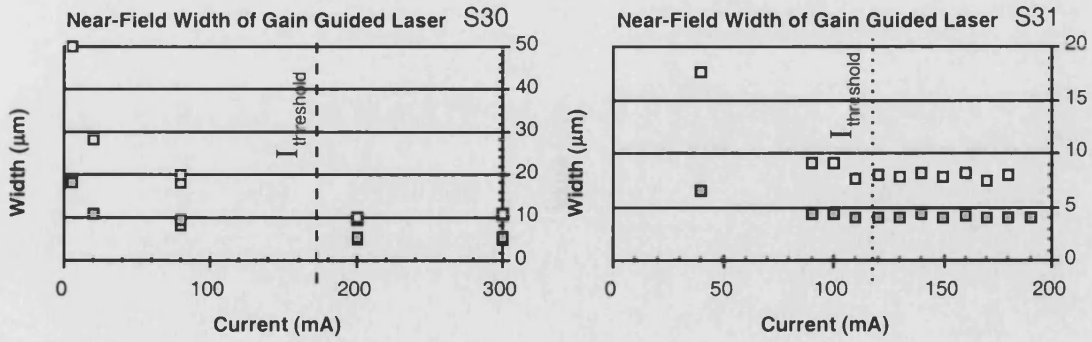

Figure 4.5 *Widths of near-field optical intensity profiles in two nominally identical 3μm stripe lasers S30 and S31 under various current injection levels. Lower (grey) f.w.h.m., upper (white) full 1/e^2 intensity widths. Above threshold, the near-fields were approximately constant.*

As illustrated in Figure 4.5, the width of the optical mode in the narrow stripe lasers was approximately constant for currents above $1.1I_{th}$. The fwhm of laser S31 above threshold was 4.0±0.2μm, and the $1/e^2$ full width was 8.0±0.5μm. The exact values were stable but varied substantially between similar laser chips. The measurements on S31 were repeated for current pulses of 12ns and 250ns duration. Above threshold, there was no significant difference due to pulse duration, indicating that thermal and other 'slow' processes did not influence these near-fields. Similar measurements on S30 found a fwhm of 5.2±0.2μm and $1/e^2$ full width of 10.5±0.5μm, also independent of pulse duration.

4.3.4 Far-Field and Beam Waist of 3μm Stripe Laser

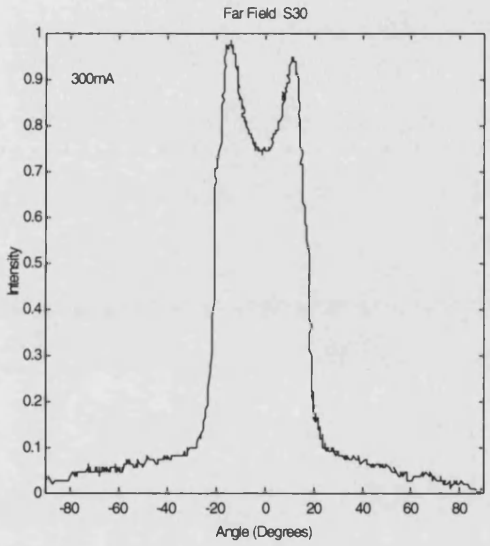

Figure 4.6 Intensity distribution in the far-field I=300 mA, $1.7I_{th}$, P=16mW

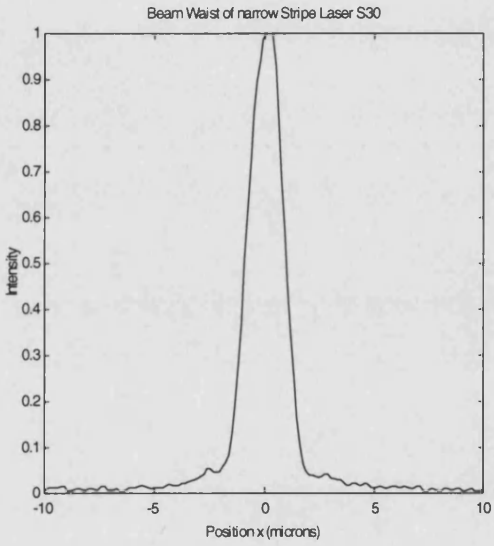

Figure 4.7 Lateral beam-waist intensity

The width of the far-field, shown in Figure 4.6, was almost constant with current, and independent of pulse duration in the range of 10-1000ns. The $1/e^2$ full-width was 40 ± 1^{o}. The two peaks were separated by 24 ± 1^{o} . The ratio of the central minimum/peak was 0.75±0.05 at 300mA. The two peaks became gradually better resolved as the current was increased. The single beam waist, shown in Figure 4.7, confirmed that the double peaked far-field was not due to higher order lateral modes, since one well-defined waist was observed. The width of the waist was 2.0±0.2μm.

4.4 MODES OF THE COSH^{-2} GAIN GUIDE

The measurements presented above are not consistent with modes of a parabolic gain guide, and are better described by the fundamental mode of the cosh^{-2} gain distribution. The properties of cosh^{-2} waveguides are explained in detail in the literature.[128,165]

4.4.1 Description of Cosh^{-2} Gain Guide

Let H_y be the optical magnetic field strength. The modes satisfy the time-independent wave-equation.[150]

$$\nabla^2 \underline{H}_y + \frac{(\nabla\varepsilon)}{\varepsilon}\nabla \times \underline{H}_y + \varepsilon \beta_o{}^2 \underline{H}_y = 0 \qquad \textit{Equation 4.12}$$

$$-\frac{\partial^2 H_y}{\partial^2 x^2} = \left\{\varepsilon_{eff}(x)\beta_0{}^2 - \beta_z{}^2\right\}H_y \qquad \textit{Equation 4.13}$$

Let the dielectric constant ε vary slowly with x and z, so that the separable solutions of the wave equation are accurate. Then the x-dependence of the field H satisfies Equation 4.14 for a discrete set of propagation constants β_z.

$$-\frac{\partial^2 H_y}{\partial^2 x^2} = \left\{q^2\right\}H_y \qquad \textit{Equation 4.14}$$

$$\varepsilon_{eff}(x) = \varepsilon_{fringe} + \frac{(\Delta\varepsilon)(b+j)}{\cosh^2(2x/s)} \qquad \textit{Equation 4.15}$$

The cosh^{-2} gain guide is described by Equation 4.16, with terms defined in Figure 4.8. The modes of this guide have a set of complex constants u for integer mode numbers n which simultaneously satisfy 4.14 and 4.17, giving the solution $H_y(x)$ which is stated in Equation 4.18. If the guiding is too strong, then higher order transverse mode(s) similar to Equation 4.19 are also supported.

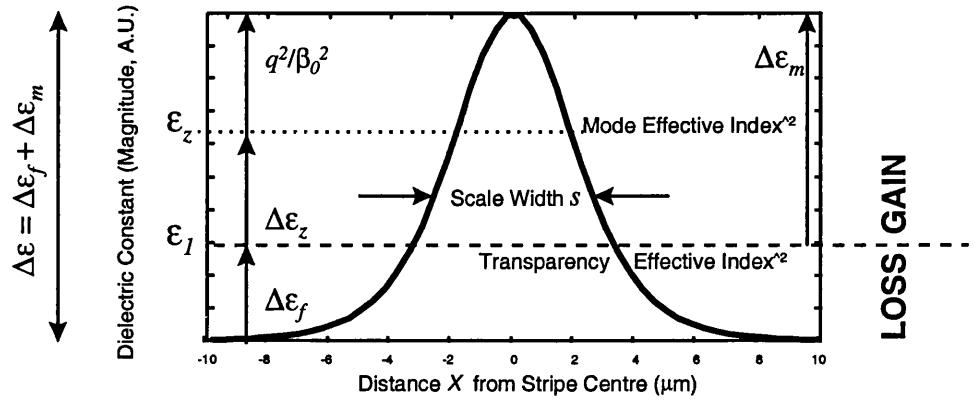

Figure.4.8 *Parameters to describe a cosh² gain distribution using a cosh² complex dielectric constant variation across the waveguide.*

$$q^2 = \left(\frac{2}{s}\right)^2\left(\frac{(u+n)(u+n+1)}{\cosh^2(2x/s)} - u^2\right) \qquad \textit{Equation 4.16}$$

The fundamental mode is Equation 4.17 with a value of u which satisfies 4.16 for $n=0$.

$$H_y = H_0 \cosh^{-u}(2x/s) \qquad \textit{Equation 4.17}$$

If the first higher order solution is guided then an n=1 solution exists to Equation 4.16 and the field is given by Equation 4.18. However, the higher order modes spread further into the region outside of the stripe than the fundamental mode, so is even more prone to distortion by defects and deviations from the $\cosh^{-1}$ profile that occur outside the stripe.

$$H_y = H_0 \cosh^{-u}(2x/s)\tanh(2x/s) \qquad \textit{Equation 4.18}$$

The complex constant u may be written as its real and imaginary part:

$$u = u_1 + ju_2 \qquad \textit{Equation 4.19}$$

The far-field $I(\theta)$ is most easily described if a scale width θ_0 is introduced:

$$\sin\theta_0 = \frac{2}{\beta_0}\frac{u_2}{s} \qquad \textit{Equation 4.20}$$

$$I(\theta) = \left[\left\{\frac{u_1}{u_2} + \frac{u_2}{u_1}\left(\left(\frac{\sin\theta}{\sin\theta_0}\right)^2 - 1\right)\right\}^2 + 1\right]^{-1} \qquad \textit{Equation 4.21}$$

This expression is not accurate for fitting to the form of the measurements in this thesis, but the measured width θ_0 in may be used to fit to u_2/s. In the limit of exponential near-field, the far-field is split a function with two Lorentzian-like peaks at angles $\pm\theta_0$ given by Equation 4.21 and plotted in Figure 4.9

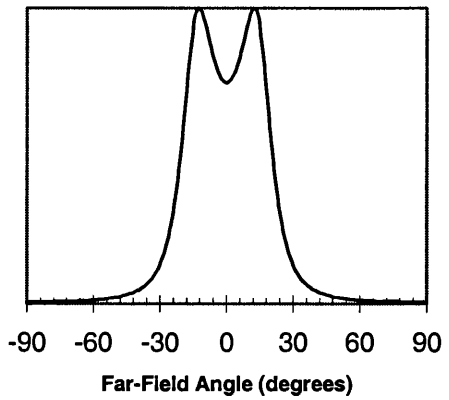

Figure 4.9 Approximate far-field intensity profile; limit U_1<<1,

4.4.2 Fitting of parameters

The $1/e^2$ full width of the far-field was fitted by a width parameter θ_0 of 20±1°. The good quality of the beam waist justified the assumption that a single mode was dominant. Then Equation 4.17 could be compared to the measured near-field widths, to add a second constraint to values of the three parameters s, u_1 u_2. A third constraint was obtained from matching to the depth of the on-axis minimum of the far-field, giving the parameters for theoretical near and far fields which were a reasonable approximation to the measurements.

The near-field of laser S30 was widened in comparison to the other narrow stripe lasers which were tested. There was some variation in the near-field widths around 10.5μm $1/e^2$ intensity full width. This was equivalent to the $1/e$ width of the amplitude function of Equation 4.17. The set of s and u_1 which matched the observed width satisfy Equation 4.22, gave the lower line of Figure 4.10

$$s\cosh^{-1}\left(\exp^{1/U_1}\right) = 10.5\,\mu\text{m} \qquad \textit{Equation 4.22}$$

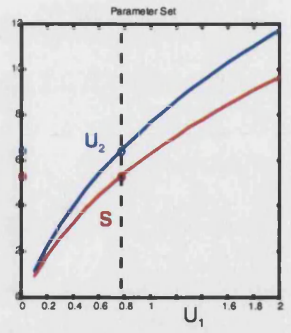

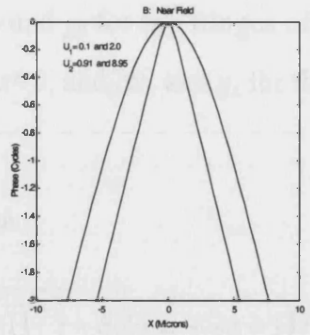

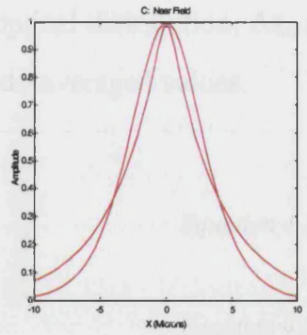

4.10 *4.11* *4.12*

Fig.4.10 *Parameter sets which matched the observed near-field and far-field $1/e^2$ widths according to Equations 4.21 and 4.23*

Fig.4.11 *For $U_1 >> 1$ the phase fronts in the near-field tend toward a parabolic form*
For $U_1 << 1$ the phase fronts tend toward a 'V' shape causing the far-field to split

Fig.4.12 *For $U_1 >> 1$ the near-field tends toward Gaussian form*
For $U_1 << 1$ the near-field approaches a two sided exponential.

The set of near-field intensity profiles for the parameter set u_1=0.1 0.2 0.3 … 1.9 2.0 are plotted in Figure 4.13 below. The corresponding far-fields are shown in Figure 4.14

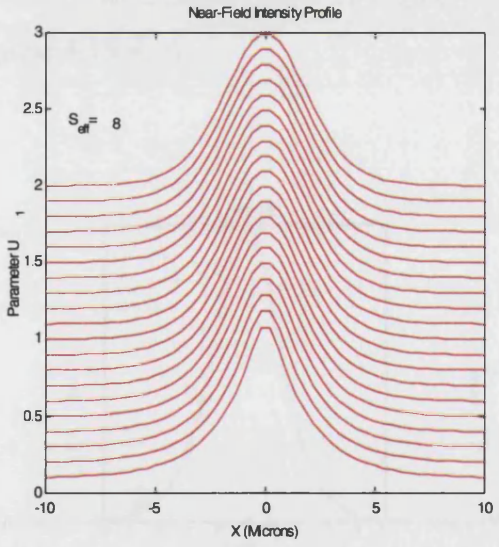

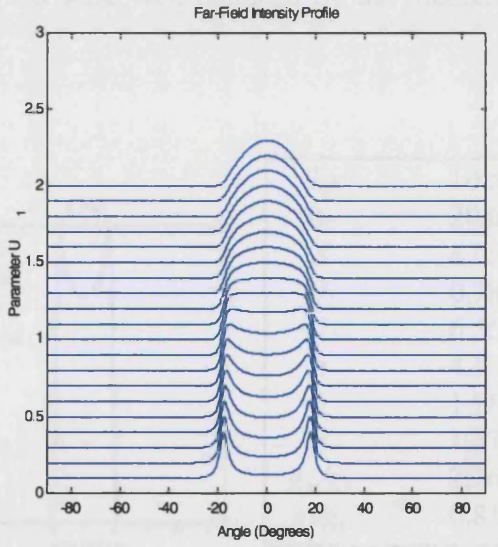

Figure 4.13 *Figure.4.14*

The set of theoretical near-field and far-field intensity profiles which match the measured $1/e^2$ widths of laser S30. The Y axis shows normalised intensity (A.U.) offset by the value of parameter u_1. For u_1>2, Gaussian optics gives a reasonable approximation to the modes.. For u_1=1, the far-field has a plateau which is flat over most of the range $\pm\theta_0$.

The measured values of u_1 and u_2 were used to estimate parameters F,h and b in Equations 4.23 and 4.24, which define the gain and loss of the gain-guide according to 4.25 and 4.26. Following the notation of Thompson[128], the dielectric constant

perturbations and gain are $\Delta\varepsilon_f$ and g_f for the fringes of the optical distribution, $\Delta\varepsilon_m$ and g_m for the maximum value, at $x=0$, and $\Delta\varepsilon_z$ and g_z for the mode-averaged values.

$$u_1 = \left[(2n+1)\{F(h+1)-h\}\right]/2h \qquad \textit{Equation 4.23}$$

$$u_2 = \left[\pm\sqrt{\left\{b^2+1-(2u_1+2n+1)^{-2}\right\}}-b\right](2u_1+2n+1)/2 \qquad \textit{Equation 4.24}$$

$$F = \frac{\Delta\varepsilon_f}{\Delta\varepsilon_m}+1 = \left|\frac{g_f}{g_m}\right|+1 \qquad \textit{Equation 4.25}$$

$$h = \frac{\Delta\varepsilon_m}{\Delta\varepsilon_z}-1 = \left|\frac{g_m}{g_z}\right|-1 \qquad \textit{Equation 4.26}$$

In all of the stripe lasers which were tested, the mode number n was zero, as a narrow single beam-waist implied fundamental mode operation. The beam-waist size approached the diffraction limit of 1.6μm, with a beam quality parameter M^2 as low as 1.12. The measurements of Figure 4.5 and 4.6 were well-matched by the theoretical plots 4.15,4.16

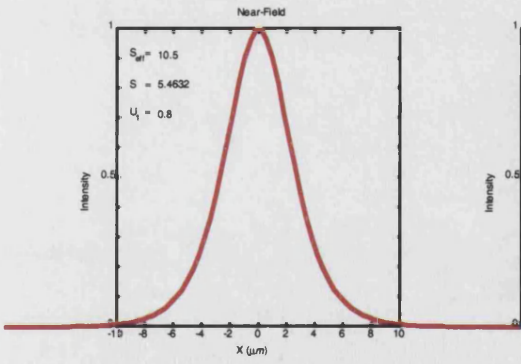

Figure 4.15 Near-Field

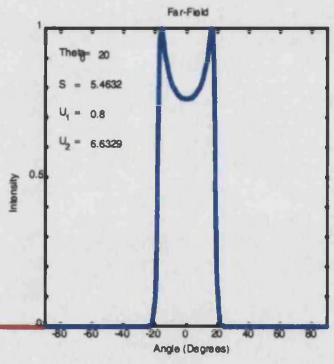

Figure 4.16 Far-Field

S_{eff}	10.5
θ_0	20.0
S	4.08
U_1	0.78
U_2	6.50
b	-4.52
h	1.16
F	1.37
g_m/g_z	2.16
g_f/g_z	0.81

Table 4.3 Parameters

Typical parameter values for laser S30 are listed in Table 4.3. F and h relate g_m and g_f, and scale to actual gain and loss values if the mode gain g_z is known. The ratios g_m/g_z and g_f/g_z were extremely sensitive to the value of observed near-field width, varying by a factor of two within the 20% variation of observed s_{eff}.

Two conclusions came from these measurements: Firstly, the linewidth enhancement factor b was approximately 4.5, which is an acceptable value for GaAs. Secondly, the fringe loss g_f to either side of the stripe was rather low. Estimates of the fringe loss with s_{eff}=10.5μm are g_f=82cm^{-1} and a peak gain of g_m=220cm^{-1}, assuming a mode gain of $\Gamma_y g_z$=59cm^{-1}.

4.4.3 Lateral Carrier Diffusion

Once injected into the active layer, the approximate carrier density function with distance x from a contact edge may be described by a diffusion length l_D, so that n falls according to Equation 4.27 [125].

$$n_{(x)} = n_{(0)} \exp^{-\frac{|x|}{l_D}} \qquad \textit{Equation 4.27}$$

The near-field spontaneous emission intensity distribution at half-threshold was observed to follow a bi-exponential form with a *1/e* decay distance of 4±1μm in laser S30 at $I=0.5I_{th}$. (Its value was 7±2μm in two nominally identical stripe lasers, all operating at half threshold, assumed to be near to transparency). The carrier diffusion length is double this, assuming a spontaneous recombination rate proportional to the square of the carrier density. The diffusion length at threshold is reduced by a factor of 1.6 due to the carrier lifetime decreasing. The reduction is from 2.0ns at $0.5I_{th}$ to 0.8ns at the high carrier density at the stripe centre during normal operation. From the estimated diffusion length of 5μm around a 3μm stripe, a current spreading factor of 3/13 was applied to the contact threshold current density J_{th} to give an estimated current density of 2.7kA/cm^2. The maximum carrier density which can be supported by this current density is 4×10^{18}cm^{-3}.

Consulting the gain curves g(n) of Figure 2.3B (or also Casey and Panish[125]), a reasonable fit to the gain g_m was obtained for 58meV offset from the bandgap. The appropriate gain curve $g(E)$ is plotted in Figure 4.17

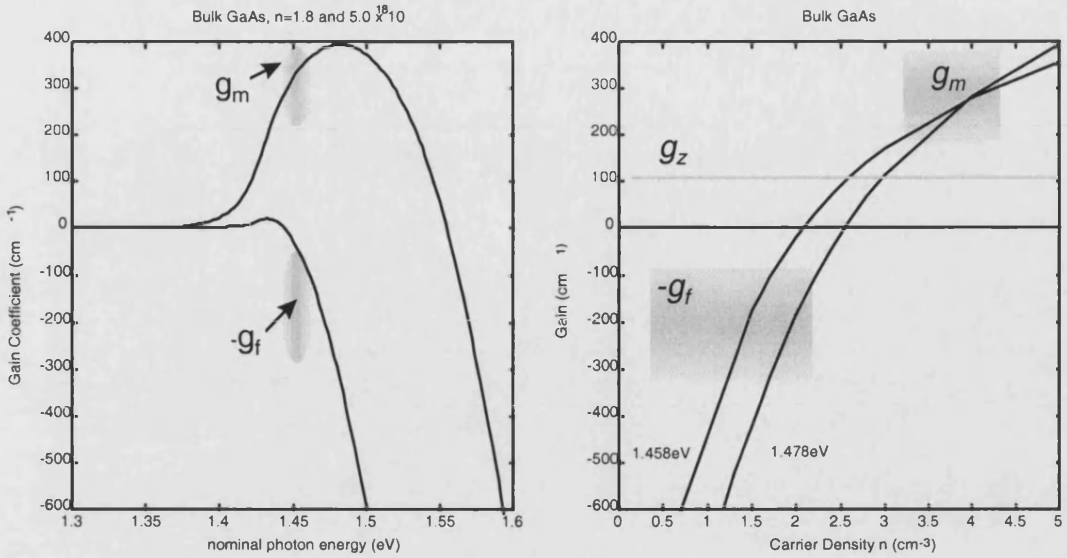

Figure 4.17 Gain spectra and probable operating points for the maximum (stripe centre) and fringe regions (both shaded). The spatial mode measurements determined the minimum possible value of the stripe-centre gain. It was assumed that the emission wavelength was close to the gain peak at high carrier density, 1.48eV on the spectrum above. Two g(n) curves are plotted for probable emission wavelength values. $n>4.5\text{-}5\times10^{18}cm^{-3}$ was required to reach g_m. The fringe carrier density was not determined, and is assumed to be near to transparency..

Finding a gain curve to fit to the fringe loss $-g_f$, required an arbitrary estimate of the fringe carrier density. The figure indicates the region of operation near to the gain peak, and shows probable gain spectra at the centre and fringes of the laser.

4.5 MATCHING TO TAPERED AMPLIFIERS

The beam divergence is inversely proportional to the scale width s of the gain distribution through Equation 4.21. The divergence also depends on u_2, which increases proportionally with the linewidth enhancement factor. Divergence gives astigmatism, which can be corrected with cylindrical lenses, and near-diffraction limited beams were observed after correction. A wide divergence is desirable for the purpose of launching into tapered gain regions of maximum volume in minimum length. The observed 20° $1/e^2$ half-angle in air corresponds to 5.7° within the laser. Therefore 5.7° is the maximum recommended taper half-angle for abrupt coupling to GaAs tapered gain regions. The optimum distribution for injection into tapered regions of uniform gain has $0.9>u_1>1.2$ The plateau in the far-field indicates that the taper could be injected with a

uniform fan of light. In order to compensate for spatial hole burning depleting the on-axis gain in the taper, a distribution with a more of a centred peak may give a more uniform final output of the taper.

With the current window geometry, there is little potential for further reduction of the gain-guide width to increase the taper angle, because the stripe is already much narrower than current spreading or diffusion lengths. Lateral p-n junctions or proton implanted stripe boundaries are suitable methods to reduce the width of the stripe laser. Changing from gain guided to strongly index guided confinement would give wide divergence determined by design, and would be less sensitive to random material variations and degradation than gain-guides. However, the maximum near-field width for a single mode decreases from approximately ten microns for gain guides to approximately three microns for sufficiently strong index guiding to achieve the desired wide far-field. This lowers the maximum power throughput of the stripe that satisfies COD limitations within the laser chip by a factor of three.

4.5.1 Suggestion for further study

A full numerical beam-propagation investigation is required to model the operation of a gain guided stripe integrated with a gain guided taper. A straight gain-guided stripe is adequately described by the $\cosh^{-2}$ gain distribution model.

4.6 BROAD AREA LASERS

4.6.1 Historical Development of Broad Area Lasers

Edge emitting diode lasers with an active stripe width W greater than 20λ are described as 'broad area'. The early diode lasers[1-3] employed uniform current injection through an active region of typically 400×200μm. Improved reliability was obtained by keeping the current away from the defect ridden side walls, using loss on either side of a contact stripe. An example structure is illustrated in Figure 4.18. Substantial advances have been made in the power and lifetime capability, mainly through improved quantum well materials and facet coatings[85-92]. The broad stripe laser is many times too wide to produce a spatially coherent output[167].

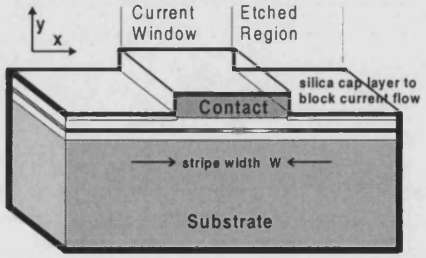

Fig.4.18 Typical Broad Area Laser structure, which emits in ± z directions

4.6.2 Example of Far-Field

The far-field of a laser with a stripe width W of 50μm, of the same length and composition (0.5mm, bulk AlGaAs/GaAs wafer QT476) as the arrays is shown below. The far-field well above threshold filled a wide range of angles. Fresnel's law dictates that the facet transmission decreases with angle, and Snell's law transforms the internal angular distribution to a more peaked external angular distribution. The far-fields demonstrated an uncontrolled optical distribution which was severely non-uniform and almost as wide as the spontaneous emission.

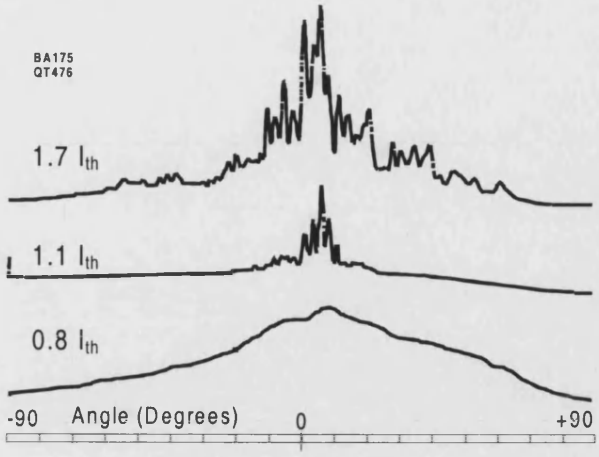

Figure 4.19
Far-Field from a 50μm broad area laser comparable to other lasers in this thesis. Even near to threshold, the output was highly multi-moded,and degenerated with increasing current as even more spatial modes were excited

This laser was expected to have 8 filaments with a beam quality parameter of $M^2 \approx 69$. The observed far-field widened with current from 5 to 30 times the diffraction limit.

4.6.3 Lateral Modes

The confinement of light within the active layer was illustrated in Section 4.1.2. From Figure 4.3 and 4.4, a dielectric constant step as small as 2×10^{-5} due to perturbation of the transverse mode will permit the $n=1$ lateral mode in a typical broad area laser of width $W=100\mu m$. The approximate number of lateral modes which are guided is proportional to the D parameter, calculated with from Equation 4.1, for a width $\delta\varepsilon$ due to the perturbation and $d=W$. The unavoidable variations in gain and temperature which are found in lasers lead to complex dielectric constant changes which are considerably greater than 10^{-5}. These support higher modes[167]. Single moded operation is not obtained in broad area lasers. The devices studied in this thesis had negligible confinement due to the ridge, so there were no well defined edge points to dictate symmetry and mode number. Therefore the term 'lateral mode' has to be used rather loosely in order to define a set of spatial field structures in these gain guided lasers. The 'modes' are a complete set of bounded solutions to the wave equation which propagate unchanged through a particular dielectric and gain distribution, which may vary with drive current, temperature, and defect distributions, which vary from device to device. The optical distributions do not form an orthonormal set, and are not precisely odd or even[168]. In contrast, modes of strongly index guided broad area lasers are nearly periodic within the ridge waveguide, with odd or even symmetry. Index guided lateral modes have been investigated in detail.[169]

4.6.4 Filamentation

Even in an infinite slab of uniform laser material, nonuniform lateral modes can develop from noise in the initial conditions, due to the interaction between the photon density and carrier density.[130,170-172] Suppose that an initially uniform gain slab contains an initially uniform plane wave mode, which circulates between cleaved facets. An excess photon generated by spontaneous emission makes the field at x_0 fractionally greater than at neighbouring regions. Excess photons deplete excess carriers at x_0 in comparison to the average rate of stimulated emission. The round trip time of most laser cavities is of the order of picoseconds, which is negligible in comparison to carrier diffusion and injection. The carrier density at x_0 is still depressed when photon returns one round trip later. The depleted carrier density (and depleted gain) leads to a local increase in the refractive index given by the linewidth enhancement factor. Therefore the region around x_0 acts as a very weak converging lens. After further round trips, x_0 attracts more photon density by its raised refractive index, giving further depletion of the carriers. The process can continue to deepen the gain depletion until a concentration gradient drives substantial diffusion of carriers from neighbouring regions into x_0, giving a self-focused spot.

4.6.5 Factors Influencing Filamentation

The proportionality between gain depletion and refractive index increase is usually expressed by the linewidth enhancement factor[158-160] α_H, and increasing it increases the tendency for self focusing[171]. Non-uniformity in the gain and carrier profile is damped out by carrier diffusion and by changes to the resistive current spreading outside of the active region. A short diffusion length (due to a short carrier lifetime) permits large non-uniformity to develop. Both of these effects increase if the average carrier density is high, therefore broad area lasers with a high threshold gain and current are most susceptible to self induced non-uniformity. It has been noted that if α_H is reduced from 5, typical for AlGaAs-GaAs lasers to less than 0.4, the self-spatial modulation instability of the laser near-field tends to become more damped by diffusion[172]. If a Kerr nonlinearity intensity-squared self-defocus is present[171] (perhaps in the AlGaAs cladding layers) then this partly offsets the self-focus effect, and the limit on α_H is relaxed to approximately 2. This value is approached, but not quite reached[158] by

quantum well lasers. These show greatly reduced spatial modulation and a narrowed lateral far-field in comparison to bulk active region lasers.

4.6.6 Temporal Instability

Even if the current is constant and the material is uniform, a Broad Area Laser may show microwave fluctuations in its output power. Take an example of a spectrum containing only two components, which differ by 0.02nm around 885nm, typical for a diode laser which supports two lateral modes. The temporal output from a point on the output facet is then modulated by mode beating at 7.6GHz. This is acceptable in some applications, such as thermal power delivery[172] and optical pumping of solid state laser rods. The spectra of broad area lasers contain several spatial mode components for each longitudinal mode. These are not necessarily phase locked, and can lead to mode beating noise across the full spectral bandwidth of 2nm, from DC to at least 0.5THz.

4.6.7 Coupled Spatio-Temporal Instability in Broad Area Lasers

For the example of two lateral modes in a broad area laser, the near-field oscillates from side to side at the beat frequency[130]. With an increased number of lateral modes, more complex structures develop.[173-176] The local regions which experience the largest peaks of oscillations can deplete the carriers, leading to the same self-focus effects as discussed in section 4.6.5. The rapidly shifting spatial modes observed by streak camera[173] preferred to linger and intensify around filament centres, where the observable DC near-field image showed enhanced brightness. These centres could form around any defect or weakly gain-guiding feature in the laser.

4.6.8 Preferred Filament Width

Mehuys[171] quoted a simple formula for the distance f between maxima of the near field of a broad area laser. Using the notation common to this thesis, and substituting the mode gain at threshold Γg_{th} for Equation 2.12, the following form is obtained. It is clear that low α_H and low mode-averaged gain Γg_{th} both increase f, i.e. improve the beam quality.

$$f = \sqrt{\frac{\lambda\pi}{\mu\alpha_H \Gamma g_{th}}} \qquad \textit{Equation 4.28}$$

Inserting the parameters of stripe laser S30 into Equation 4.29, the filament spacing expected for broad area lasers is 6±0.6μm. Comparison to the laser stripe width gives an order-of-magnitude estimate of the number of modes M and the beam quality M^2 to be expected.

4.6.9 Conclusions

From one dimensional numerical solution of the wave equation in the real refractive index structure of the AlGaAs/GaAs laser diodes, the effective index under the ridge and etched regions was calculated for the devices under study. It was shown that the ridge had negligible effect on the optical distribution. The dominant process of gain guiding was illustrated for the exact solutions of parabolic and $\cosh^{-2}$ distributions of gain vs. distance from the stripe centre. A good qualitative match to the measured near-field, far-field and beam waists of narrow stripe gain guided AlGaAs/GaAs lasers was observed. This was used to estimate the gain at the stripe centre and the loss at the stripe edges. These parameters govern the performance of novel laser designs in the same material which will be investigated in later chapters. It was also noted that the observed distributions varied substantially among nominally identical devices. This is to be expected, since the distribution was at a critical point where the spatial mode was extremely sensitive to small variations in the gain and loss of the laser material. This made the gain-guided lasers susceptible to imperfections in inhomogenous material.

The temporal and spatial instability of broad area lasers was reviewed. Broad area bulk AlGaAs/GaAs heterostructure lasers are expected to show filamentation with spatial structures of the order of 6μm.

5. Gain-Guided Tapers

5.1 INTRODUCTION

Following the successful demonstrations of bow tie lasers,[176-181] it was necessary to investigate the guiding parameters and optical spatial distribution. The single taper, sketched in Figure 5.1a loses the main advantage of the bow tie symmetrically double tapered design of Figure 5.1b. This was to increase the output power level within the catastrophic optical damage limit on low-cost uncoated chips by use of widened output waveguides at both ends. The purpose of the study of the single tapers described in this chapter was to obtain access to an optical distribution similar to that found in the straight sections in the middle of bow ties. Practical single taper lasers would require low reflectivity coatings at the output facet, in order to prevent excessive optical power from returning to the narrow end, which easily reaches the intensity threshold of damage.

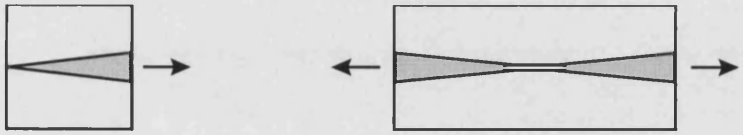

a. Taper Laser b. Bow Tie Laser

Figure 5.1 The single taper laser (a) is useful to produce high output power with high efficiency from the wider output facet region, marked ″. The design directs much of the output power in one direction. The symmetrical 'bow tie' design (b) has a higher facet COD limit, since both facets are wide.

5.2 DEVICE DESCRIPTION

The lasers which are described in this chapter were fabricated in the University of Bath from the same wafer, QT543R, and by the same batch processes as the narrow stripe gain guided lasers of Chapter 4,*[1]. The current windows and ridge (shaded in Figure 5.1) were defined on the p-side of the wafer according to a bow tie mask pattern with a taper half-angle of three degrees. Laser chips were cleaved to obtain single taper lasers, which included approximately 50×3μm of straight gain guide feeding into a gain guided

*[1] The tapered lasers were fabricated by Mr.T.Ryan, Dept.of Electrical Engineering, University of Bath.

linear taper. A sketch of the structure is shown in Figure 5.2. The lasers were further etched using a second mask to define gaps through the gold and highly doped p-contact to separate multiple electrical contacts along the length of the device.

Figure 5.2
Twin-contact taper lasers. Shading indicates current injection regions, which are labelled A and B. The etched trench which separated A from B had a resistance of the order of 1kΩ and negligible optical reflectivity, since it did not penetrate far into the optical cladding layer. Notation for dimensions of tapers is indicated on the figure.

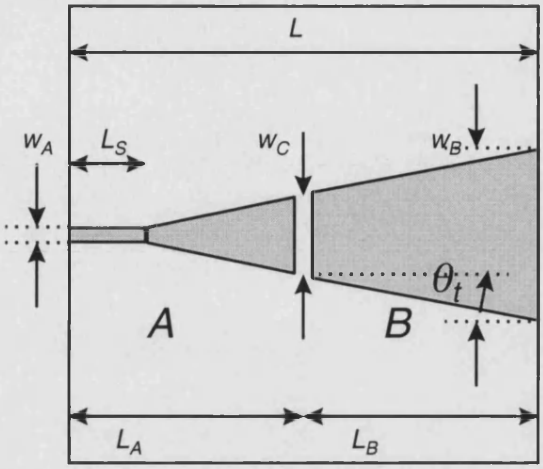

Figure 5.2

Throughout this thesis, particular laser chips are identified by a device number with letters to describe the structure; 'S' for straight, 'T' for tapered, or 'A' for array. Several variants of the 3° twin contact taper were tested, which are illustrated below in Figure 5.3.

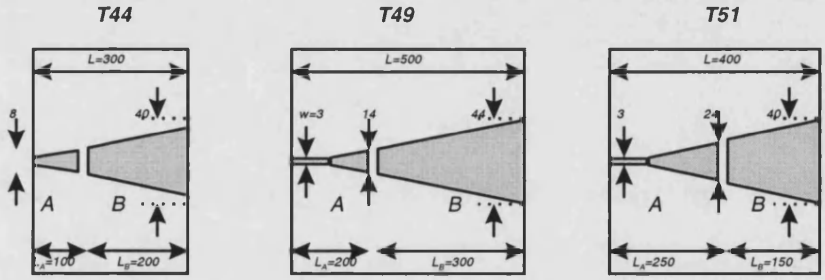

Figure 5.3 *Dimensions of twin-contact taper lasers (μm). A variety of structures were tested. All had an output facet width W_B in excess of 40μm, which is multi-moded in a conventional broad area gain guided laser. The current injection stripe width tapered down to 3μm at W_A*

5.3 SPATIAL MODES OF TAPERS WITH UNIFORM VOLTAGE

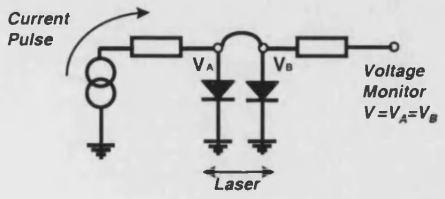

Figure 5.4

Contacts A and B were joined so that the external voltages V_A and V_B were equal, as in Figure 5.4. This was equivalent to a single contact over a whole taper. The gain at the

centre of A was less than at B, because roughly constant current density at the gold contact supplied lateral spreading and diffusion, as well as gain at the stripe centre. The centre gain g_m increased gradually with local taper width. Saturable absorption due to this longitudinal variation was not significant, since no step in the Light Current (LI) curve due to absorber saturation was observed. Therefore A was in a state between transparency and threshold gain during normal operation of the lasers.

5.3.1 Far-Fields

The far-fields of taper T44 with contacts A and B joined are shown in Figure 5.5. Measurements were observed from the front of the wide output facet. As is typical for gain-guided lasers of greater width than the natural filament size, the far-field optical distribution could show multiple emission lobes, and the content of those modes was sensitive to conditions[182-183]. Each lobe had a width greater than the plane-wave diffraction limit for the output aperture width W_B. The number of lobes and their angular separation increased with current above threshold. The minimum width observed was 4.5°(fwhm). The far-fields from the front of T49 were qualitatively similar. At higher currents, above $1.5I_{th}$, more spikes were clearly evident in the far-field, shown in Figure 5.6. At currents below or near to threshold, a wide continuous distribution of spontaneous emission was present.

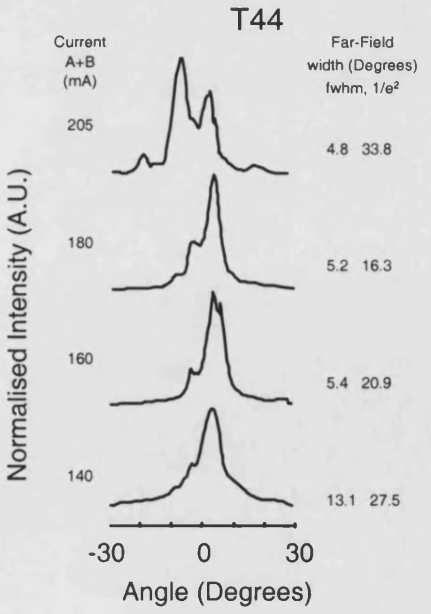

Figure 5.5

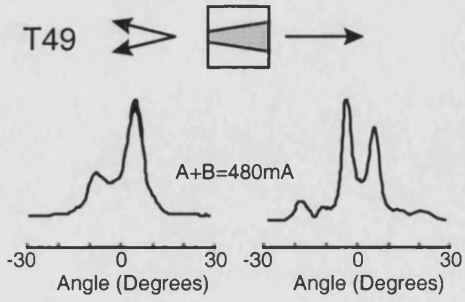

Figure 5.6

The far-fields observed from the narrow end of tapers consisted of two broad lobes, which were usually asymmetric and of unequal intensity. An example far-field from the narrow end of T49 is included in Figure 5.6. The measurement pair was taken under identical conditions. The angular separation of far-field maxima from the narrow end was persistently greater than for the wide end.

5.3.2 Near-Fields

Spontaneous emission near-fields were recorded at low currents of 15mA which was less than $0.1I_{th}$, and also 80mA, approximately transparency. The distribution of spontaneous emission showed no dark spots, and had a width (fwhm) similar to W_B, the contact width at the output of the taper. The near-fields at threshold were narrowed by typically 30%, but still single-lobed. At higher currents, above $1.5I_{th}$, the near-field could develop asymmetry, as in T49 (Fig.5.7) or a minimum at the centre of the stripe, as in T51 (Fig.5.8)

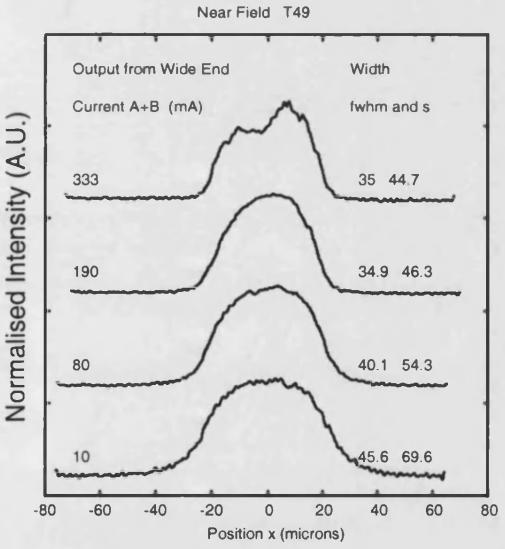

Figure 5.7

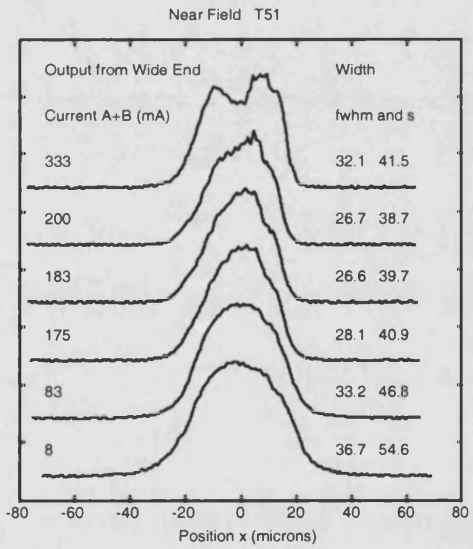

Figure 5.8

The near-fields widths from the rear facet A were, as expected, much wider than W_A which was 3-8μm. The spontaneous emission showed a width (fwhm) of 18μm at $0.1I_{th}$. The laser mode width above threshold was not less than 8.6μm, rising steadily and eventually splitting at very high current.

5.3.3 Beam Waists

By moving the imaging lens toward the laser facet by 50-110μm, a single virtual source within the laser could be imaged onto the CCD detector, as with the gain-guided modes of Chapter 4. Examples are shown for lasers T49 and T51 in Figures 5.9 and 5.10. The extremely small size of these beam waists, down to 2μm, showed that the outputs of the wide end of the taper were almost perfectly circular wavefronts in the lateral plane. The astigmatism distance multiplied by the waveguide effective index of 3.5 was generally very close to the length of the taper section, if viewed from the wide end, and negligible if viewed from the narrow end. Therefore the output can be approximated by assuming a point source which generates circular wavefronts from the apex of the taper.

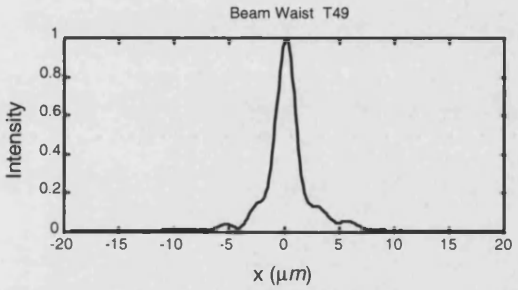

Figure 5.9 Beam Waist of T49

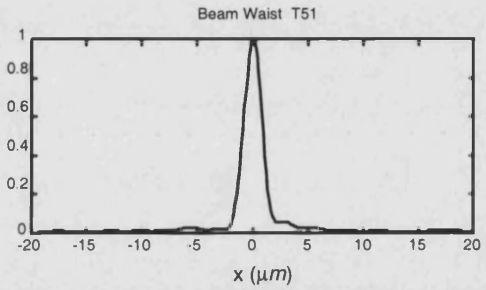

Figure 5.10 Beam Waist of T51

Intensity profiles through the beam waist at $1.5I_{th}$ with contacts A and B joined. The waist widths and positions were constant, showing no change under conditions which produced a multi- peaked near-field and far-field.

5.3.4 Beam Quality Parameter

The value of the beam quality parameter M^2,calculated from the measured far-field and beam waist size was greater than 1.3 close to threshold, and considerably greater at higher currents, in proportion to the increasing far-field width. This showed that the fundamental mode of the gain-guide close to threshold was not exactly Gaussian. The M^2 value was never quite as low as 1.2, which was observed for single moded stripe lasers in Chapter 4. As power was increased above $1.1I_{th}$, the M^2 value increased as the far-field broadened and developed additional peaks. However, a single beam waist of high quality remained stable and was present for all currents above threshold.

5.4 SPATIAL MODES OF TAPERS WITH GROUNDED NARROW SECTION

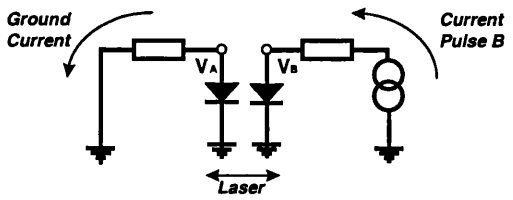

Figure 5.11

Lasers were connected according to Figure 5.11, with the narrow end contact A shorted to ground through a path of 100Ω. Currents of typically -10mA maintained the voltage on grounded contact A at +1V or greater. Above threshold, the shorted contact became clamped at the bandgap voltage of +1.4 indicating that absorber saturation occurred. Due to the intrinsic absorption α_i of 30cm^{-1}, the region under contact A was slightly absorbing, and approaching transparency for operation above $1.05I_{th}$.

5.4.1 Far-Fields

The far-fields emitted from the wide ends of tapers were consistently improved in symmetry and in width if A was grounded while current was applied to B. The improvement was most pronounced near to threshold. At high current, the symmetry of the far-field was much improved with A grounded, as can be seen by comparing Figure 5.4 to Figure 5.11 and by comparing 5.5 to 5.12. Similar far-field narrowing was previously observed in bow-ties[141].

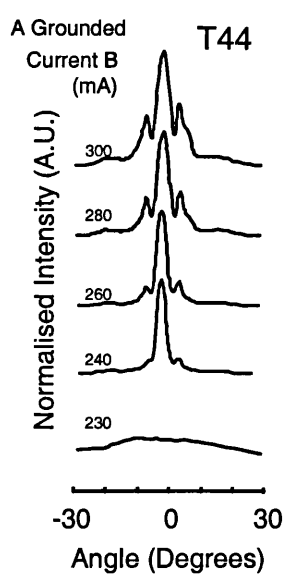

Figure 5.12

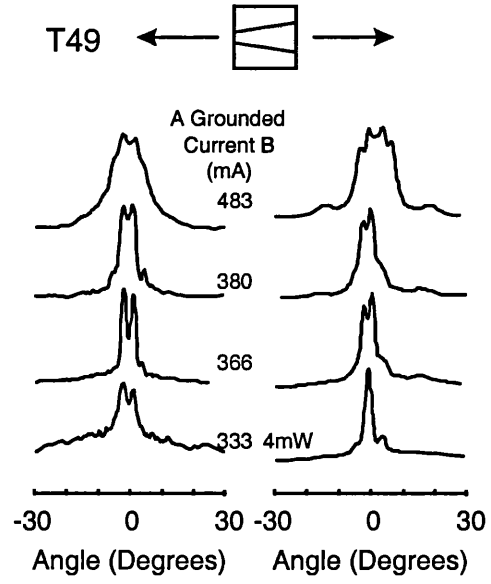

Figure 5.13

Even so, the output was not precisely perpendicular to the laser facet, and showed some minor asymmetry. Observation under a microscope showed that the waveguide ridge was 0.5° off axis, and this may have led to the observed offset. As the current to B was increased above threshold, multiple peaks developed, but symmetry was much improved from the uniform current case. The same observation has been made in bow tie lasers[176], where grounding or DC reverse voltage to the narrow stripe region was found to significantly improve the spatial mode uniformity and to reduce the far-field width.

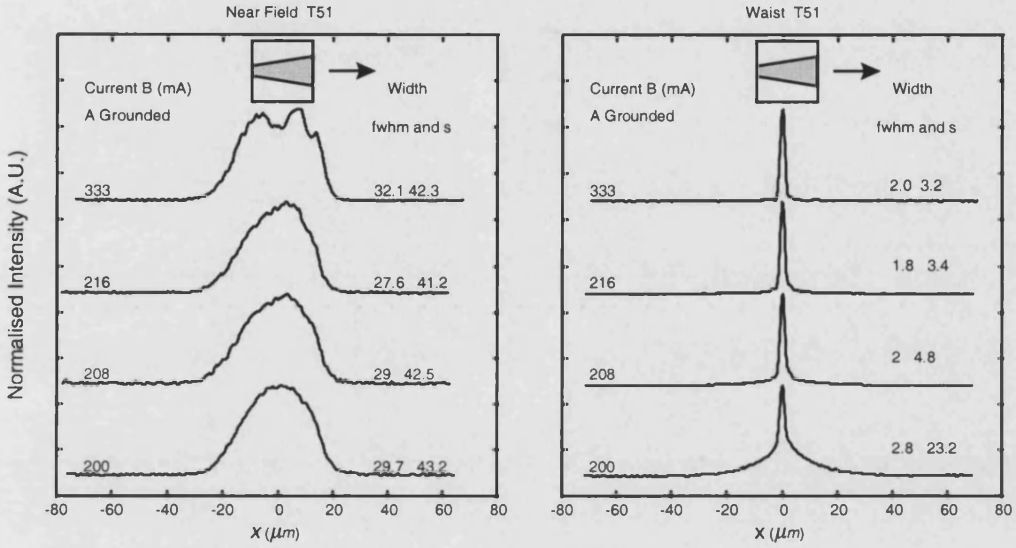

Figure 5.14 Near-field intensity profiles and beam waists of T51 from threshold (200mA) to 1.66I_{th}. At high currents, the near-field begins to split into multiple peaks, but a single beam waist remains.

5.4.2 Near-Fields, Beam Waists and M^2

The near-fields of T49 and T51 with the narrow section grounded were similar to the output with the whole devices driven. The output of T51 is shown in Figure 5.14, along with the beam waists after astigmatism correction. Multiple peaks suggesting higher order modes were significant at similar optical power levels as with uniform current, approximately 1.6I_{th}, for which the power was approximately 40mW and the peak intensity of the order of 0.4MW/cm^2 at the wide facet. The optical output from the wide end of the taper had a width of typically 35μm (fwhm) and 45μm (1/e^2) from a device width of 40μm, showing optimal filling of the available gain region, and maximum spreading of the optical output. Compared to a narrow stripe laser, the near-field width from T49 B was increased by a factor of four, so the power limit for catastrophic optical

damage corresponding 6MW/cm^2 should be raised in proportion, to approximately 0.7W. However, this level was still too high for single tapers, as the narrow end had a smaller near-field mode, and tended to suffer COD at lower power. The beam waist width remained less than 2-3μm, as with uniform pumping. The value of M^2, taken from the measured far-field and beam-waist size was as low as 1.05 close to threshold, and greater at higher currents, in proportion to the increasing far-field width. This shows that the output of tapers under non-uniform current injection could approach the diffraction limit, but only close to threshold.

5.4.3 Comparison of emission from front and rear facets

The near and far-fields of T49 and T51 were observed from both the +z and -z direction. The rear far-field of T49 was never single peaked, especially with contacts A and B joined together (top traces of Figure 5.15). This was observed even for conditions for which the wide (front) end emitted a single lobed far-field. At high currents, the rear far-fields were even broader, but retained some symmetry.

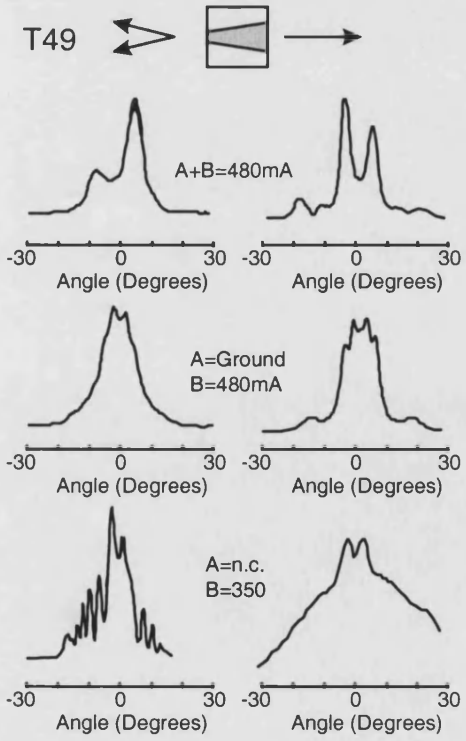

Figure 5.15

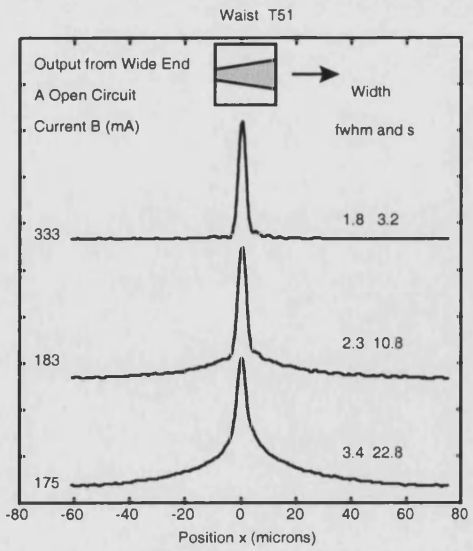

Figure 5.16

In the case of contact A grounded, the front and back far-fields were more similar and more symmetrical, but contained spike features with unequal angular separations comparing front to rear. The example in Figure 5.15 is at high current. When A was not connected (n.c.), the symmetry remained almost intact, but the width increased, both front and back. The rear far-field developed many sub-peaks. It is noteworthy that in another laser, T51, under similar conditions, with a multi-spiked far-field out of A (according to observations on IR card), there was still a single well-resolved beam waist observable from B, pictured in Figure 5.16.

5.5 SPATIAL MODES WITH NON-UNIFORM CURRENT INJECTION

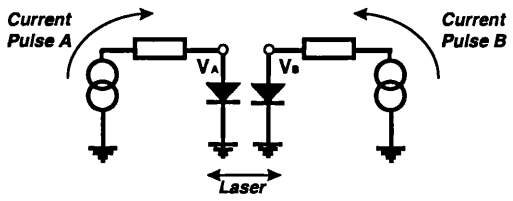

Figure 5.17

The currents into sections A and B were independently variable, using twin current pulse generators (Lyons Instruments) as in Figure 5.17. The aim of these measurements was to see whether the spatial mode, symmetry, and efficiency could be optimised at higher power, and to seek guidelines to avoid spatial mode hops. From exhaustive measurements with one current as a parameter and the other varied continuously, it was observed that kinks in the LI were repeatable but followed no obvious pattern, and varied among similar devices. The kinks did not occur at any fixed optical power level or current density. The representative LI of Figure 5.18 give almost as much information as the full set of measurements. The total threshold current was 12% higher and the average slope efficiency was lowered if the current was directed through A in comparison to the same current flowing into B.

Figure 5.18

Tapers were tested with unequal current density injected into sections A and B. One current was set as a parameter and the other was ramped steadily. Typical behaviour is illustrated by the selection of L-I curves plotted for laser T44.

The operating point for a narrow far-field from the front side is marked 'x'

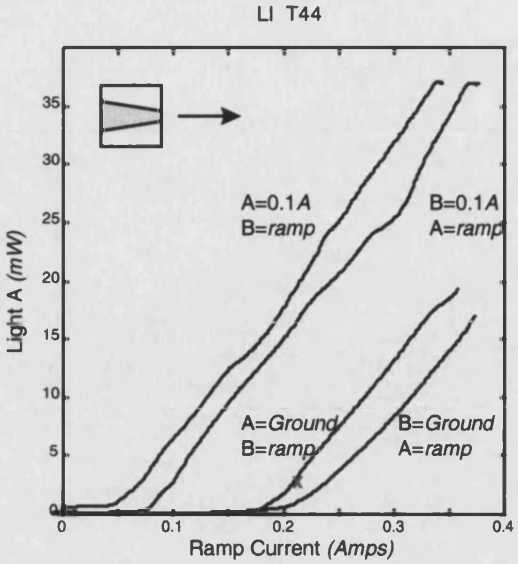

5.5.1 Far-Fields

The far-field from the front of T44 at constant total current was asymmetric until a mode hop at B=100mA, A=100mA. There was an abrupt mode hop leading to good symmetry if contact A was grounded to draw a small negative current. Good symmetry was only obtained while current A was negative. Figure 5.19 shows a set of traces at constant total current A+B. Figure 5.20 shows a similar mode collapse in switching from A grounded (-10mA) to a small injection current (+10mA) into A.

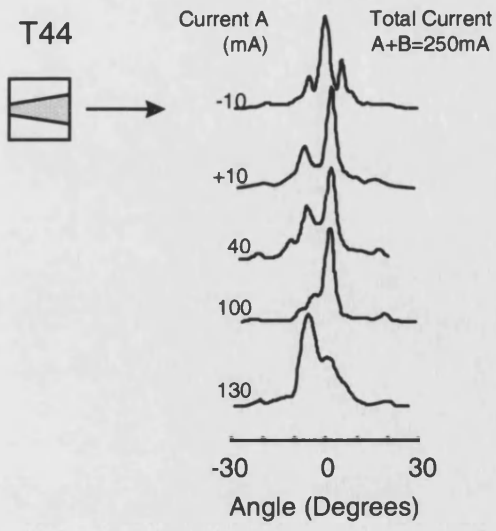

Figure 5.19

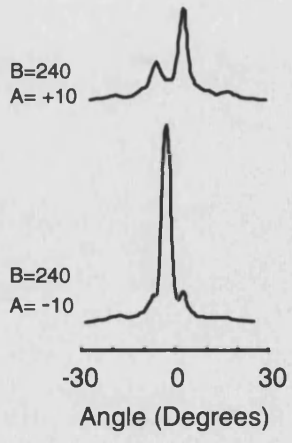

Figure 5.20

5.5.2 Comparison to theoretical modes of cosh-2 guides

In the limiting case of exponentially decaying carrier distribution to either side of the guide; $u_1 << 1$ the far-field develops two sharp spikes corresponding to linear phase lag with distance from the optical axis. The form of the observed far-field at the narrow end was indeed two peaked, and was also three to four times narrower than the far-field when current was applied to the narrow stripe sections, which would have allowed true gain guiding to occur. The difference in far-field widths was accounted for as follows: In the current pumped case, the carrier density at the waveguide centre was as high as the threshold gain value, estimated at $350cm^{-1}$, whilst in the grounded case, the centre carrier density was approximately three times lower, transparency. Therefore the carrier concentration gradient was reduced by a factor of three by grounding A, and the far-field width decreased by a similar factor.

The propagation of light under the grounded contact cannot be formally described by 'modes', and the structure cannot accurately be described as a 'waveguide' as it is lossy, so it does not support guided time-independent modes. However, the non-uniform loss was observed to influence the spatial distribution of light passing through it in a similar manner to a gain guide. Section A was bleached to near-transparency, and was bleached to a greater degree at the stripe centre than at the stripe edges. The propagation in this region was expected to have the same form as that of a gain guide; antiguiding due to the carrier induced refractive index profile with a real minimum and imaginary maximum in the centre. The decaying optical field remained narrow despite the antiguiding because there was strong loss to either side. This imposed a phase distribution which lagged at the guide edges, generating a far-field with two peaks in exactly the same manner as the gain guide.

5.6 CONCLUSIONS

The output from the wide end of a gain-guided tapered laser can be approximated, to first order, by an astigmatic Gaussian beam, with the transverse waist in the near-field plane and the lateral waist located at the apex of the taper. A beam waist of this type was observable under all operating conditions above threshold. The diffraction limited far-field was only observed at powers below 4mW and was only observable if contact A was grounded through a resistor and sinking a small absorbed photocurrent. The absorber current was typically $-0.06I_{th}$. The LI became nonlinear if any significant current $>0.05I_{th}$ was injected into section A. If A and B were joined, equivalent to use of a single electrical contact, the spatial mode became asymmetric and subject to mode shifts at all useful power levels. The taper lasers under test had a maximum width W_B of 40μm and an average width of typically 24μm. The average width was greater by a factor of three than the maximum recommended for single mode operation of straight lasers[184]. The spatial mode behaviour was intermediate between that which is typical for a broad area laser or a narrow gain-guide.[186-188]

6. Bow Tie Arrays: Device Structure and Spatial Modes

6.1 INTRODUCTION

In this chapter, a novel design of laser array will be described and characterised.

6.1.1 Tapered and Bow-Tie lasers

Bow tie arrays are a development of the bow-tie laser, which integrates a single moded stripe waveguide with tapered amplifiers within the laser cavity[176-181]. The gradual broadening of the optical mode as it gains energy allows an increase in power with reduced carrier depletion near to the facets and a higher COD limit compared to a straight narrow-stripe laser. The bow-tie design reduces gain saturation, and reduces the effective line width enhancement factor, to improve the average power, peak power, efficiency, and picosecond pulsed performance in most operating conditions.

6.1.2 Increasing the power and output aperture of Bow Tie Lasers

In order to raise the output power, the light must be distributed over a widened output aperture to avoid COD. To maximise the Q-switched pulse energy, the volume of gain material within a single spatial mode should be maximised[111].

Possible modifications to further increase the volume of a laser structure are to use a custom wafer with a thick active layer, to widen the taper angle[141], or to lengthen the amplifier sections. Some further improvement should be possible by optimising the width function of a non-linear taper[191-195]. It has been found experimentally in Bath that if the linear taper angle exceeded 6° in a GaAs bow tie laser of length 400μm, then the spatial output was multimoded[141]. The length was chosen by considering the trade-off of maximum gain volume for high energy against short cavity length for minimum photon lifetime and minimum pulse duration. Excessive length also degraded the spectral performance by increasing chirp[196]. The pulse energy could be increased by widening the taper further, but stable single pulse generation required the single lateral mode.[190] A short cavity, hence a short photon lifetime, was required to minimise the pulse fall-time.[129]

The investigation reported in this thesis was primarily into the laser contact shape, therefore several other parameters were deliberately not varied, so that a comparison against the literature would not be confused by the many possible improvements which can be made. The use of a wafer with a thick active layer or the use of low-loss multi-quantum well gain material were avoided, as were coatings. HR/AR coatings can immediately double the power by directing most of the output to one facet. Coatings destroy the inherent symmetry of the bow tie structure, preventing the possibility of high energy colliding-pulse mode locking.

For CW and quasi-CW operation, a different trade-off exists than for short pulse generation. The current density should be low so that resistive heating is reduced[184]. The threshold gain decreases with length until the outputs from the mirrors become less significant in comparison to intrinsic losses[197,198]. Low threshold current density allows operation in a regime where the gain is not saturated. As well as maximising the internal efficiency, the linewidth enhancement factor α_H is not increased unnecessarily, which would degrade device performance, whether pulsed or CW. The length of the laser chips was chosen so that the equivalent mirror loss α_m was lower than the waveguide intrinsic loss α_i For the wafers considered in this study, the intrinsic loss was estimated to be $36cm^{-1}$, which exceeded the distributed equivalent mirror loss for devices longer than 320μm. The actual length of 500μm slightly larger than the CW optimum, aiming to include as much gain volume as possible for high energy picosecond pulse generation. So nominally identical devices were tested both q-CW and also for short pulse performance.

6.1.3 Bow Tie Arrays

An additional way of creating an enlarged device without lengthening is by lateral replication. Several bow ties were combined in an array pattern, parallel to one another with some overlap of gain regions. The designs are illustrated by Figures 6.1-6.3.
An array is pictured in Figure 6.2, and the four major variations are shown in Figure 6.3. Arrays with further variations were made and tested[199]. The measurements presented in this chapter were all performed on five-stripe arrays with a central stripe width of W_A=5μm.

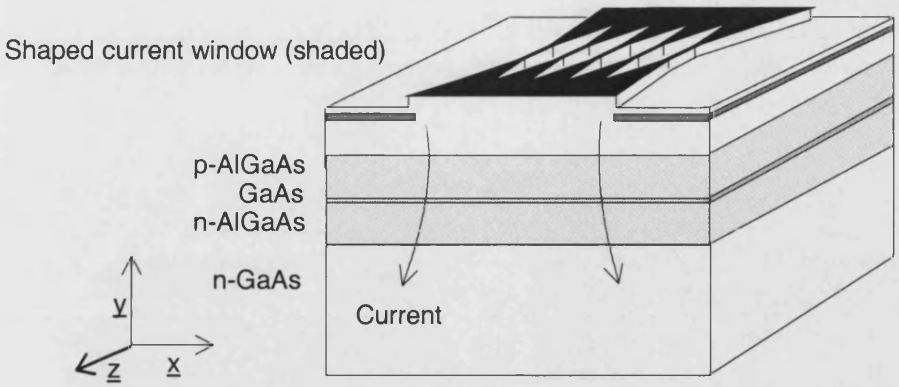

Figure 6.1 *The bow tie array. The composition and dimensions of the wafer structure were stated in Figure 4.1, which is essentially 0.17μm bulk GaAs clad by AlGaAs. The transverse mode H(y) was plotted in Figure 4.2. The current window structure influences the lateral modes H(x) by gain-guiding. A silica current blocking layer and shaped contact ridge define the current window.*

It was suggested that the neighbouring laser stripes might couple, giving a coherent bow tie array. A set of arrays were fabricated. Photolithographic processing was used to define current windows, of the multiple bow-tie shapes, which are shown in more detail in Figures 6.1-6.4. The shaded shaped area on the top surface of Figure 6.1 marks a current window, of identical composition and ridge step to the contacts of the stripe lasers of Chapter 4. The unshaded regions were insulated by a 0.2μm cap layer of silica, also identical to the non-current regions of stripe lasers. The carrier distribution under the current window formed a gain guide as in the stripe and taper lasers.

6.1.4 Estimate of the COD power limit of a Bow Tie Array

The arrays under test had output apertures ranging from 91-402μm. Therefore the catastrophic optical damage limit for reliable quasi-CW operation of uncoated devices of 6MW/cm^2 corresponded to the range 1.6-7.1W, depending on array type. Scaling up the Q-Switched performance of a single bow tie laser[176], a picosecond pulsed output power in excess of 50W was the ultimate theoretical limit for the largest output aperture design of bow tie array.

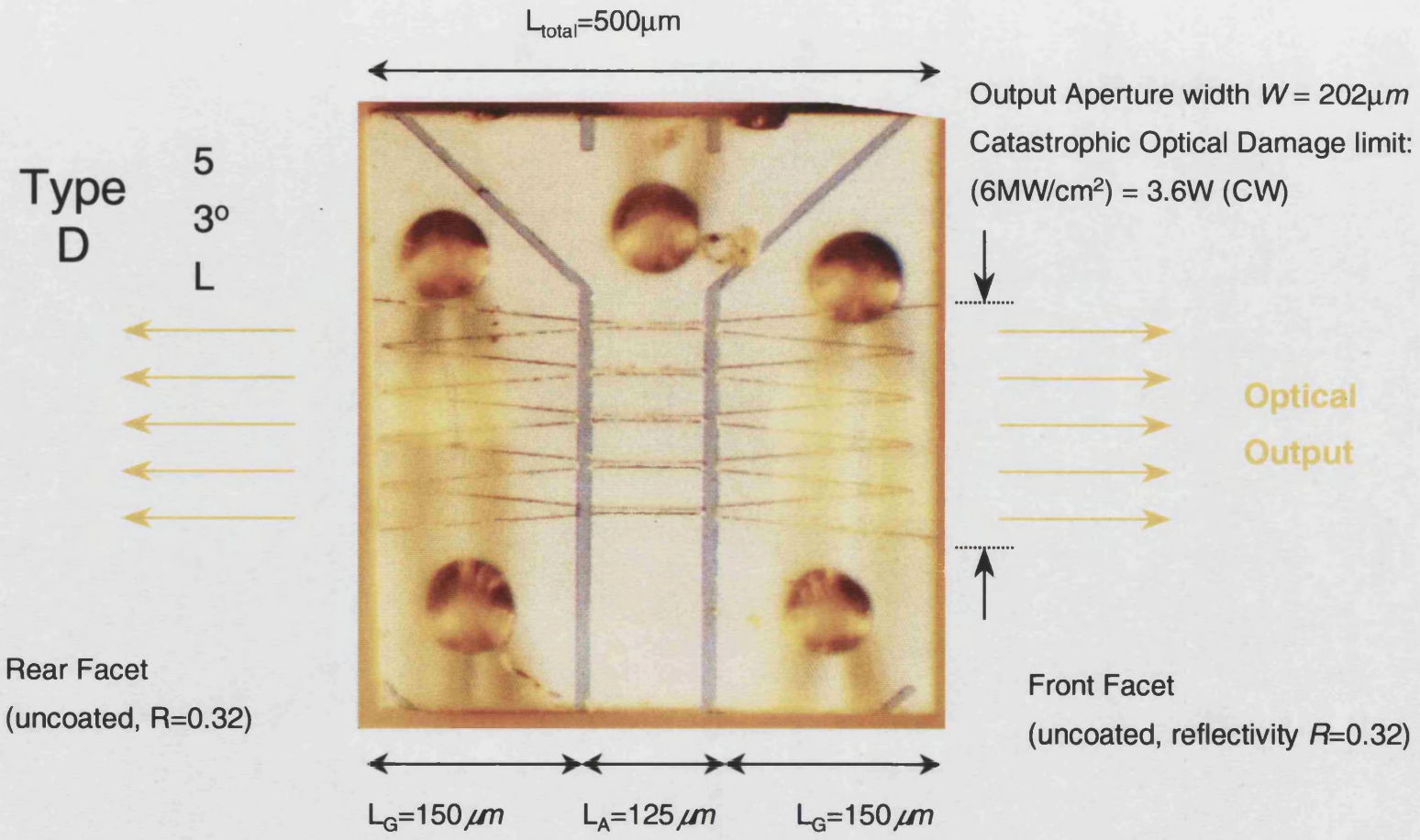

Figure 6.2 *Photograph and dimensions of Bow Tie Array type D. Fine brown lines are the etched edges of the patterned current window ridge. Vertical bands are etched trenches which electrically isolated the array into three longitudinal sections. The bond-wire to the central section was connected to a pad above the picture. The four bond-wires connected to the two end-sections were joined at a pad below the picture. The geometrical parameters were: 5 stripes, 5° taper half-angle, with a short region near to the facets where the tapers merged into a broad area section.*

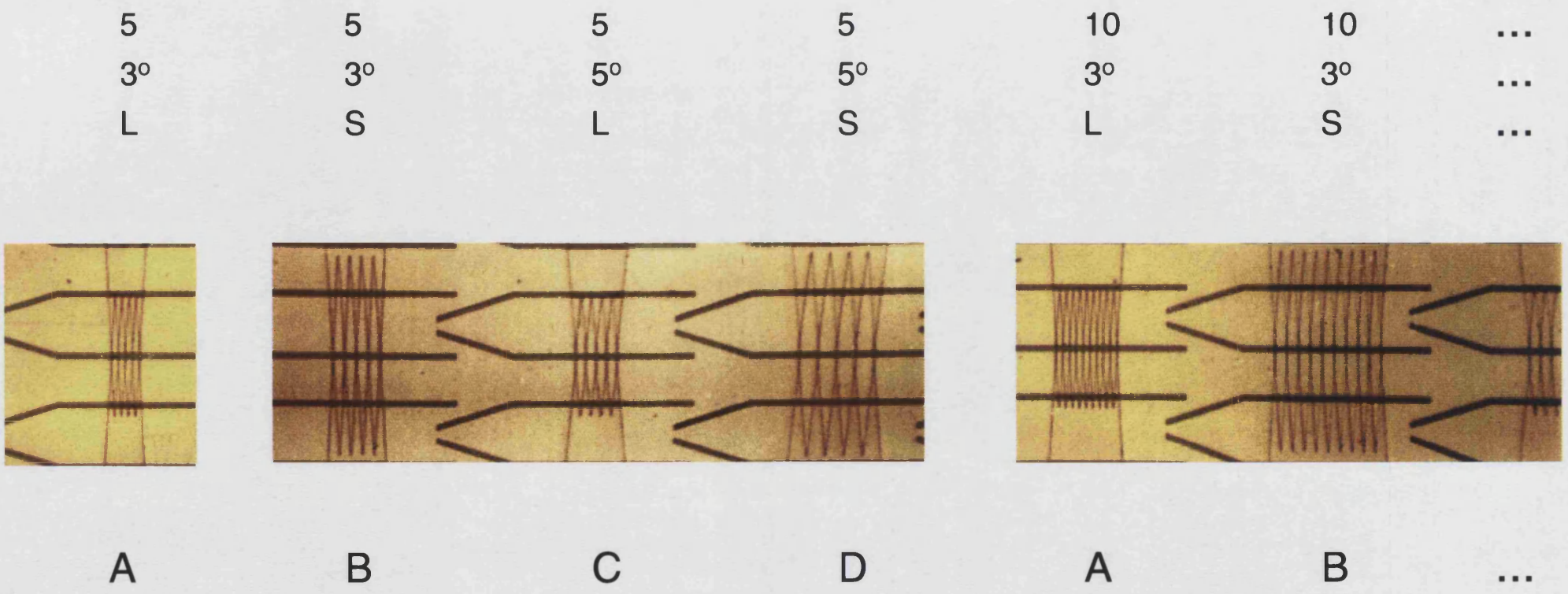

Figure 6.3 *Photographs of Bow Tie Arrays. The five-stripe versions of the four major types A,B,C,D are shown. Brown lines are the etched edges of the patterned current window ridges. Dark horizontal bands are deeper etched trenches which electrically isolated the array into several longitudinal sections. The geometrical parameters indicated above each array are the number of stripes, taper half-angle, and the size of broad area coupling region near to the facets, 'L' long or 'S' short. The pattern repeats for ten stripes, and again with a central stripe width changed from 3 μm to 5 μm.*

The four main types of array structure A, B, C, D are pictured in Figure 6.3. Types B and D are composed of bow ties, parallel to one another, which just overlap at the corners of the tapers. The short overlap region is indicated by the letter 'S'. Tapers with a half-angle of 3° and 5° were tested. Types A and C have a second variation, to increase the region where tapers overlap to just greater than 100μm. The long coupling region, (indicated by 'L' in Figure 6.3) might promote coupling between alternate tapers. The set was replicated with five stripes and ten stripes per array. The set was replicated again with the central stripe widths reduced from 5μm to 3μm. The sixteen variants are grouped into categories A,B,C,D according to Table 6.1. The mask pattern numbers representing each of these are also listed in Table 6.1.[1]

			Mask Pattern Numbers of Variants			
	Description of Class		3 μm centre stripe		5 μm centre stripe	
CLASS	HalfAngle	Overlap	5 stripes	10 stripes	5 stripes	10 stripes
A	3	l	36	40	44	48
B	3	s	37	41	45	49
C	5	l	38	42	46	50
D	5	s	39	43	47	51

Table 6.1 *Mask pattern numbers for each variation of the classes A,B,C,D are shown for reference. The classes refer to the taper half-angle and length of overlap of the taper sections. Eg. type 45 had five 5μm stripes which tapered at 3°to into short overlap regions. The design variations were expected to influence the spatial mode structure and the pulse generation performance.*

6.2 LATERAL MODES OF BOW TIE ARRAY LASERS: EXPERIMENTS

From a set of array lasers fabricated at the University of Bath, the spatial modes were investigated with nanosecond current pulses from below threshold to $10I_{th}$. The lasers reported in this chapter had a single contact, equivalent to the measurements on tapers with all contacts joined. Although multimoded, the arrays showed some unique desirable features in their spatial modes, particularly in the narrow beam waists which were consistently located at the stripe centre and similar for each stripe of an array. The transition from broad area laser behaviour to gain guided array behaviour was demonstrated.

[1] Laser Arrays fabricated in the Dept. of Physics by Dr. F. Laughton

The light-current characteristic was measured, and near-fields of arrays were recorded on a CCD camera, as described in Chapter 3. Measurements were performed under low duty cycle at regulated room temperature. Current pulses of 4-12ns duration in the range of 0.08-8A, (0.1-10I_{th}) were used to drive all of the contacts of the array. Further observations in other arrays were almost independent of the pulse duration from 4ns to 1000ns. The far-field in particular showed some variations in the detail from day to day, as lasers burned in, and for many additional devices, this was the only measurement which was performed. Only results from the stable lasers are presented.

6.3 SPATIAL MODE FEATURES COMMON TO ALL BOW TIE ARRAY TYPES

6.3.1 Near-Field measurements

The series of near-fields of Figure 6.4 display the output of each class of array, A,B,C,D from below threshold current (I_{th}) to at least $8I_{th}$. As the threshold current level was reached, irregular spiked near-fields were observed. In some devices, for instance array 301, one region of the array could function normally at I_{th} whilst the other end was an order of magnitude dimmer. This was due to minor non-uniformity of the laser, small enough that it had insignificant effect on the spontaneous emission at $0.5I_{th}$. These devices had two bond-wires to each contact, symmetrically placed to remove current injection asymmetry, and had no external visible defects. At currents greater than $1.1I_{th}$, laser emission occurred throughout the array, but with several irregular brighter spots. These were not separated by nodes, and tended to widen and coalesce at as current increased through $2I_{th}$. The location and spacing of brightest regions remained approximately constant above $1.1I_{th}$. The number of local maxima in the near-field was approximately 19 per 200μm and 9 per 90μm corresponding to broad area behaviour. The observed filament spacing was 10μm, a little larger than the estimate of 6μm assuming the linear formula of Equation 4.28. The lasing region widened with increasing current, as photon and carrier spreading raised the gain at the fringes of the array to the local threshold level. From twice threshold to at least eight times threshold, the near field distribution was essentially constant.

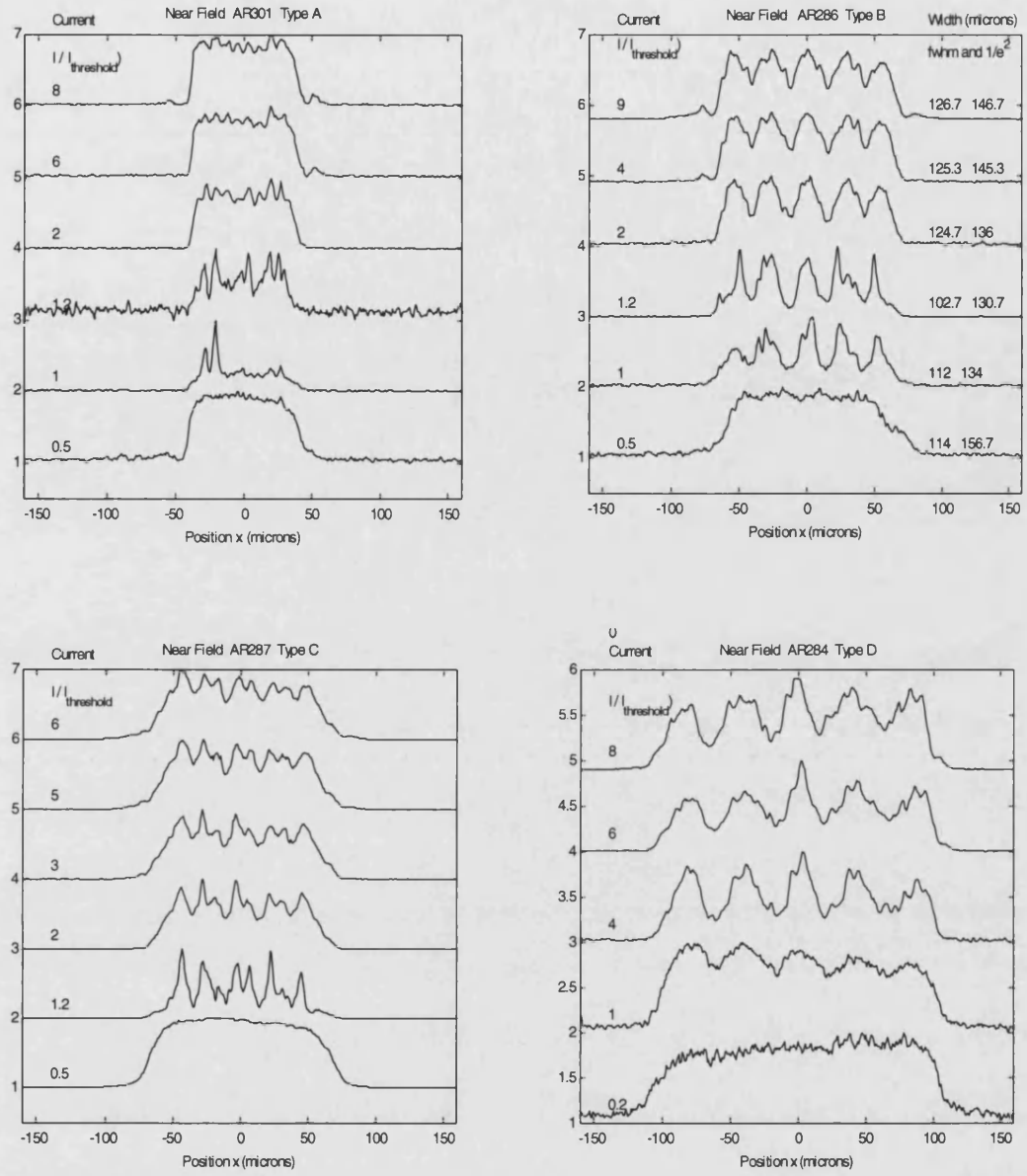

Figure 6.4 *Near-Field Intensity Profiles for each of the types, A,B,C,D of Bow Tie Array. (five-stripe single-contact versions). Current Pulses of 4-12ns (fwhm) were applied at low duty cycle. The highest current traces were obtained at a peak optical power of greater than 1W for each array.*

6.3.2 Observations of Spontaneous Emission in Near-Fields

The spontaneous emission near-field measurements of arrays are included in Figure 6.4 as the lowest trace for each of types A,B,C,D. The spontaneous emission was almost uniform for currents below half threshold (i.e. below transparency). This showed that the devices under study were free of electrical contact nonuniformity and facet optical defects. As the current was increased, some modulation of the near-field into five broad peaks occurred due to amplified spontaneous emission out of the taper centres.

6.3.3 Far-Field measurements

The far-fields for types A,B,C,D are shown in Figure 6.5. At threshold, the far-fields had a local minimum at zero degrees, reminiscent of the gain-guided far-field of the stripe lasers of Chapter 4. There were usually a number of additional pairs of peaks, symmetrically placed about zero degrees. The intensity on axis was never zero, which suggested that the lasers did not operate with adjacent regions in antiphase, as with evanescent coupled arrays[27]. Fine structure was very rarely observed, indicating that if phase-locked supermodes were present then many of them were simultaneously excited.

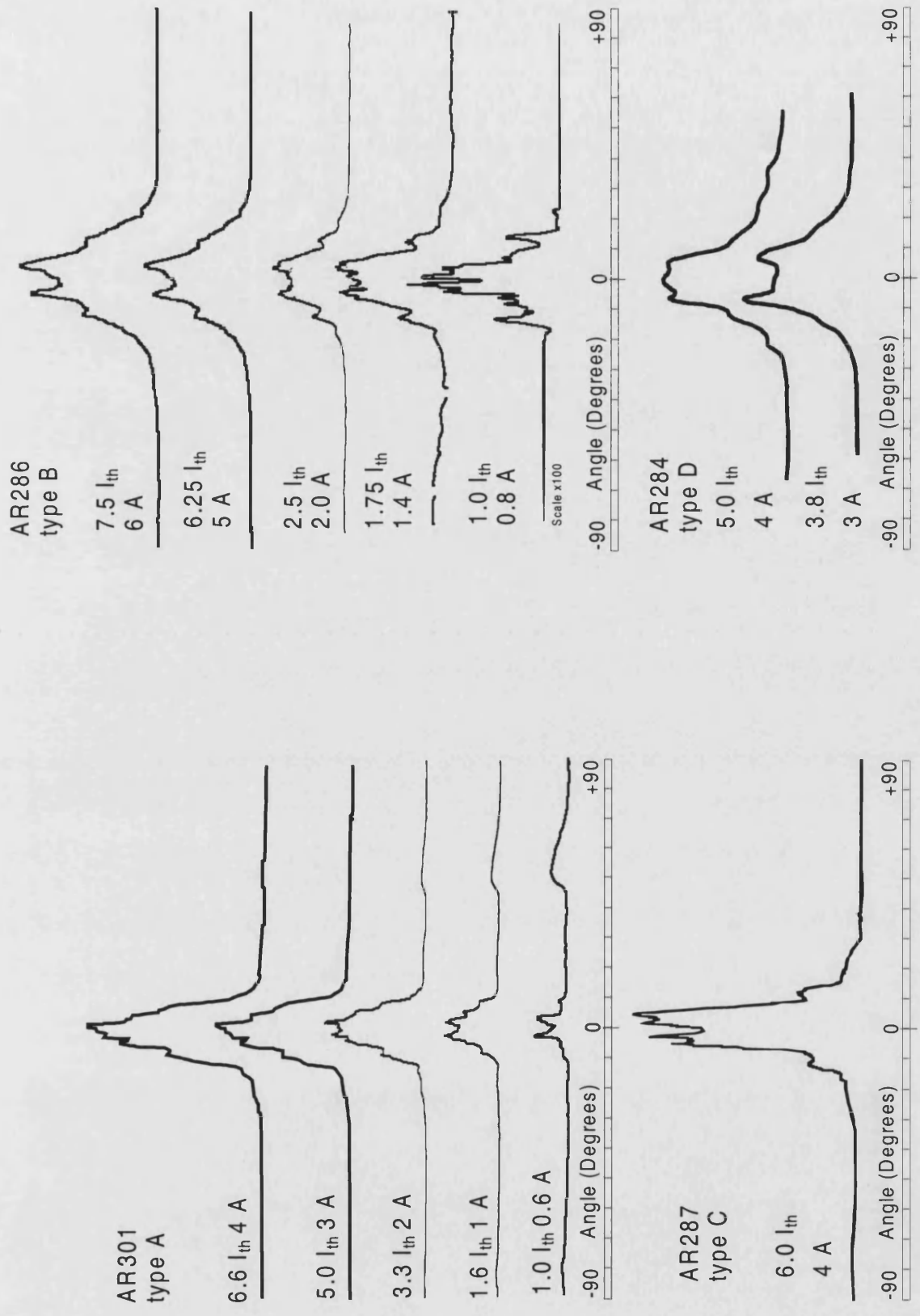

Figure 6.5 Far-field intensity profiles of bow tie array lasers (the same devices as Figure 6.5) during nanosecond pulsed operation. Multimoded operation is indicated by multiple spikes in the far field.

The width of the far-field was ten to thirty times the plane wave diffraction limit for uniform illumination of the whole array aperture. The far-field widths from the arrays above twice threshold were approximately the same as the widths due to a narrow stripe or a single taper, within an envelope function of half-width typically 7-20°, which varied significantly among nominally identical devices[198]. The output of additional duplicate devices is not printed in this thesis. Applying Snell's law at the output facet, the internal maximum angle of propagation was in the range of 2-6°. From twice threshold to at least $8I_{th}$, the far-field distribution was symmetric, on axis, and essentially constant for all of the defect free devices which were studied.

6.3.4 Beam Waist measurements

Above $1.2I_{th}$, arrays showed narrow beam waists, similar to those found in isolated tapers in Chapter 5. Sets of measurements are plotted in Figure 6.6 for the different variants. These were taken immediately after the near-fields of Figure 6.5 by making a small change to the focus of the imaging lens, as described in Chapter 3. As soon as threshold was reached, five beam waists became resolvable, centred on the five stripes, even though most arrays had more than five local maxima in the near-field. The position, width, and astigmatism correction distance δz remained constant up to at least $8I_{th}$.

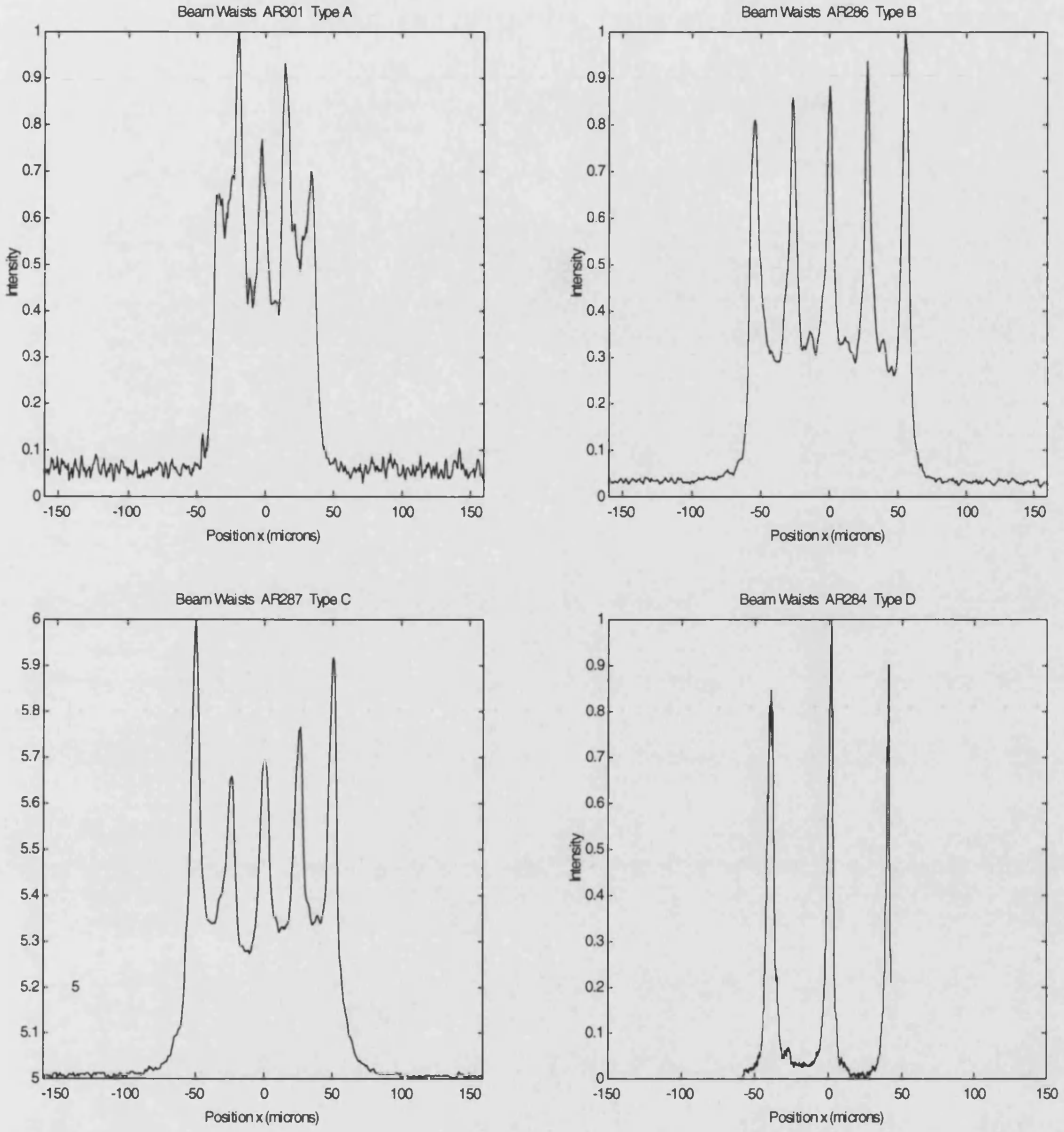

Figure 6.6 *Intensity profiles of beam waists, obtained by near-field imaging onto a CCD with the lens position (z) displaced by a small distance (δz). The waist image plane was located close to the apex of the tapers in the middle of the array chip. The width of the waists was least and the visibility was greatest for type D arrays, indicating the closest match to perfectly cylindrical wavefronts. Type D had the greatest separation of laser stripes*

6.3.5 Spectrum of Bow Tie Arrays

The spectra of array 183 are shown in Figure 6.7. Multi-moded operation was observed under high power conditions. Curiously, well behaved single-moded operation was observed at low power.

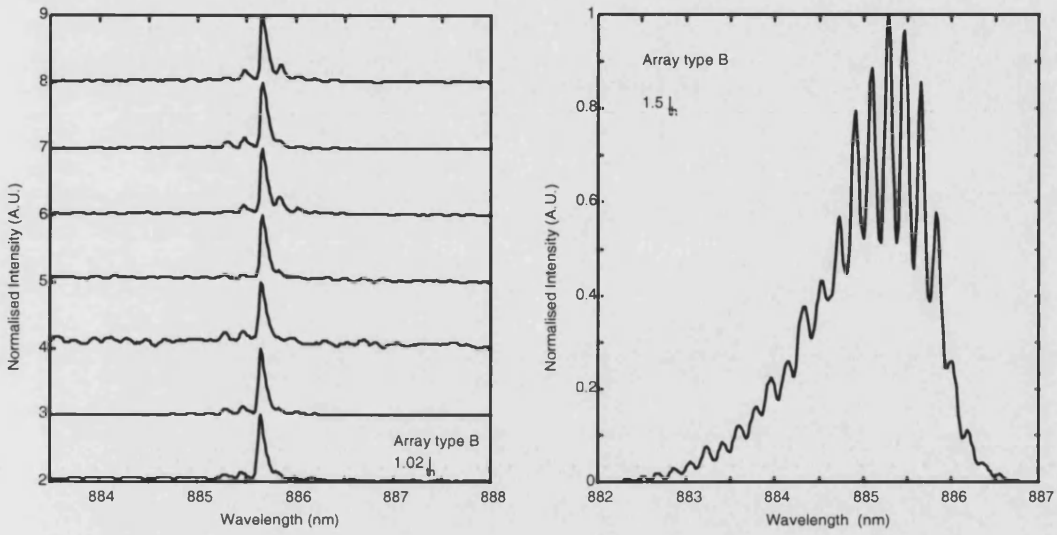

Figure 6.7 *(Left) Spectra from every local maximum of near-field intensity of a type B array at driven at 450mA ($1.02I_{th}$). A single longitudinal mode was dominant through every part of this array in the small range near to threshold.*

(Right)Multi-longitudinal mode operation was always observed at high power, and is shown at 660mA ($1.5I_{th}$). The spectral width increased and coherence length decreased at higher currents.

Within a small range from I_{th} up to $1.02I_{th}$, every maximum of the nearfield intensity was found to emit the same single longitudinal mode at 885.6nm (heat sink at 20°C) with a side mode suppression ratio of 10-15dB. No regions emitted any other dominant longitudinal mode. The measured linewidth of 0.1nm was limited by the instrument resolution of 0.08nm. The maximum optical power in this regime was less than 3mW.

The spectrum above $1.02I_{th}$ was multi-moded. Above $1.5I_{th}$, the spectrum consisted of many longitudinal modes under a smooth envelope function of width 1.7-3.0nm (fwhm). The envelope width increased with current. At a low duty cycle of 0.1%, the envelope peak of the spectrum was fixed at a value close to 885nm. The recorded peak to valley ratio decreased with current, possibly due to thermal chirp during 200ns pulses, or possibly due to multiple lateral modes which the instrument could not fully resolve.

The bandwidth at twice threshold was 2.0nm, corresponding to a coherence length of 0.2mm or a bandwidth of 0.8THz. Spectra recorded in another device at higher currents continued to broaden, and the longitudinal modes ceased to be resolved at approximately twice threshold, presumably due to transient thermal chirp. Under conditions of high power, all bow tie arrays have been found to emit multiple longitudinal modes and to show a short coherence length.

6.4 SPATIAL MODE FEATURES SPECIFIC TO ARRAY TYPES

6.4.1 Near-Field measurements

Well above threshold, the geometric differences between the arrays influenced the near-fields of Figures 6.4 and 6.8. The type A devices had a stripe separation of 16μm between the centres of the stripes, which was only slightly greater than the carrier diffusion length. Therefore the type A was essentially a broad area laser with a 90μm stripe width. Irregular spatial modes were expected.[199-202] The main effect of the tapered structure was to impose longitudinal nonuniformity. The structure directed more current through the end sections than through the middle. The centre stripes only caused a minor perturbation to the almost uniform carrier density. The nearfield of array 301 consisted of bright spots at a broad area preferred filament spacing of 10μm,[169] , in qualitative agreement with linear theory for filamentation.

In the region close to threshold, $<1.05I_{th}$, arrays were strongly influenced by device specific nonuniformity[202]. Very often only a part of the array was above the threshold gain. If one stripe contained a defect which prevented lasing, it modified the field structure of the surrounding stripes.

Types B and C had stripe spacings of 24μm, which were sufficiently far apart that there was significant modulation of the carrier density profile. In type B, four fifths of the length of the array was taper, the remainder being straight, and this led to a modulated near-field envelope with five maxima containing the smaller 10μm periodic features. In type C, the diverging lens power of the shorter tapers was reduced, leading to a more uniform near-field envelope. In type D, the near-field envelope function showed the most modulation, as expected, since the stripe separation was greatest.

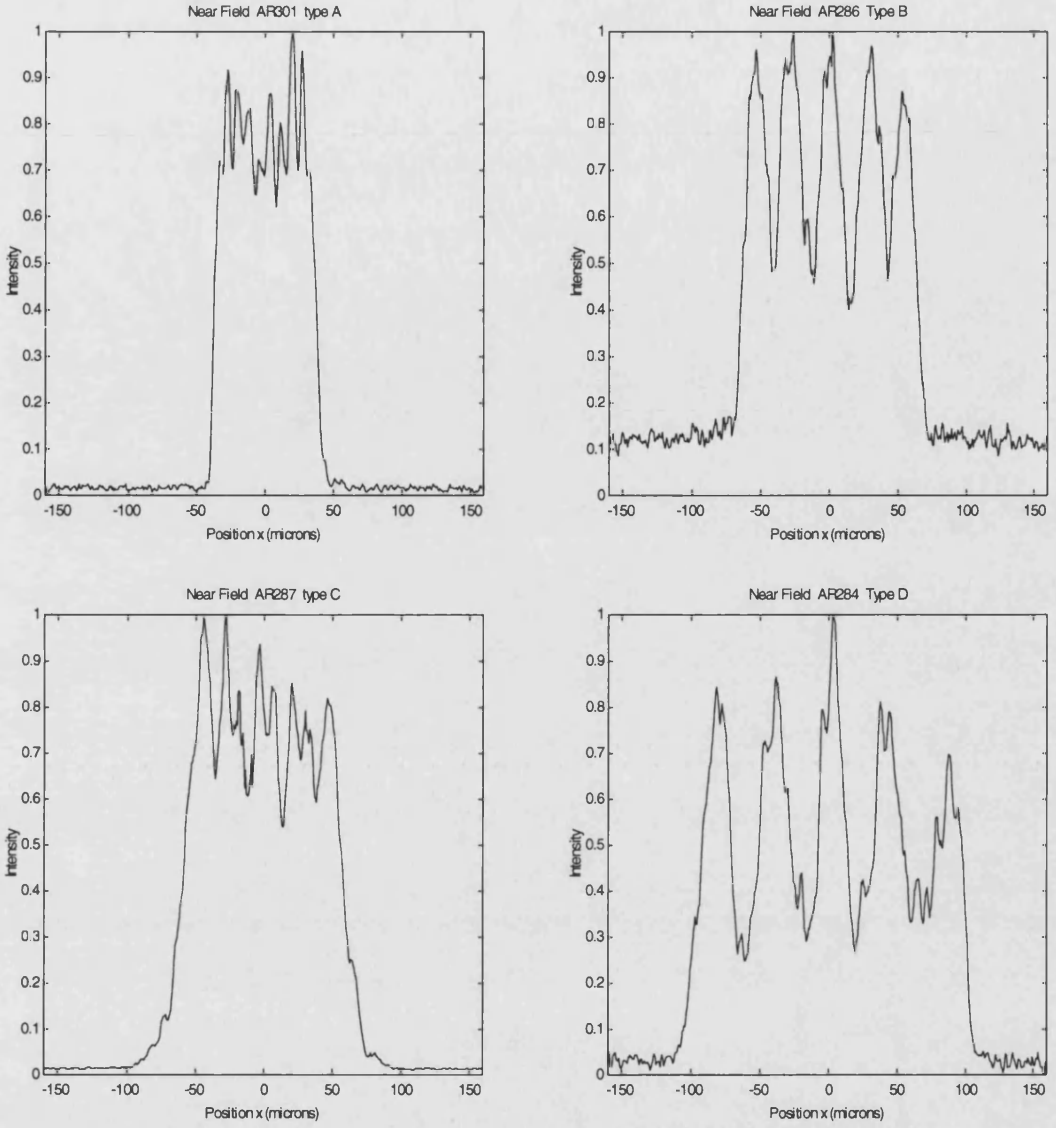

Figure 6.8 Expanded view of near-field intensity profiles, all at $2I_{th}$, showing typical behaviour for each of type A,B,C,D. The five stripes of the array imposed some modulation over a highly multi-lateral moded near field. The modulation was greatest for arrays with short overlap regions, types B and D and was nearly negligible for the arrays of type A.

6.4.2 Far-Field measurements

There was considerable variation of the far-fields[198] between duplicate arrays, suggesting that device non-uniformity was critical. However, all non-damaged arrays showed a far-field that was contained within an almost symmetrical envelope function. This usually showed a local minimum at zero degrees, with peaks to either side, reminiscent of gain guided modes. There was no clear pattern to describe the variation of peak separation with array type or with current.

6.4.3 Beam Waist measurements

The ratio of peak intensity of the waists to minimum power in between waists increased in the order A,C,B,D, which is to be expected as the tapers became more isolated from one another, and the gain distribution consequently became more modulated. The width (fwhm) of the waists also narrowed with increasing separation, down to the diffraction limit of 2μm.

6.5 TOP-WINDOW NEAR-FIELD MEASUREMENTS

Bow tie arrays with etched slots in the top surface emitted some spontaneous emission in the y direction, indicated in Figure 6.9. This was imaged and recorded with a CCD camera, using a similar method to conventional near-field measurements (Chapter 3) but with the laser chip rotated by 90°. Single lines of the image were examined.

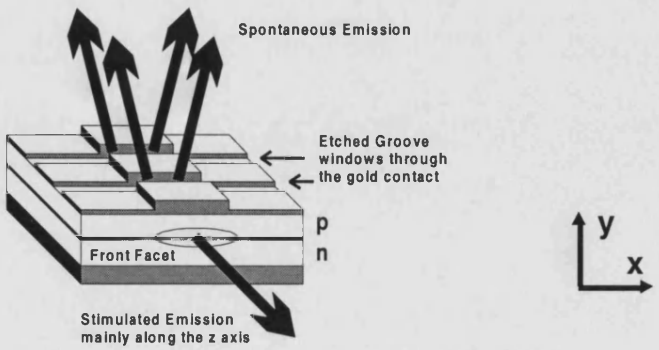

Figure 6.9 *Etched grooves through the gold and p-contact layers allowed observation of a cross-section through the central stripe region. The isotropic spontaneous emission was partly transmitted through the AlGaAs cladding and the top surface grooves.*

As is shown in Figure 6.10, the surface emission from the stripe sections of arrays was a smooth distribution with a small modulation of the near-field intensity peaking over the five current stripes. The observed intensity profile was modulated by 25% in this particular array. Assuming that the spontaneous emission rate was proportional to carrier density squared, the measurement suggests that the carrier density was modulated by only 11%. This was not consistent with the measurements on narrow single stripe lasers reported in Chapter 4, which indicated an effective carrier diffusion length of approximately 5μm. Observations of a duplicate device were substantially different, and found a variation of 60% in the intensity profile over a wide range of current values, corresponding to 26% variation in carrier density in that laser. From carrier diffusion and current spreading, greater than 25% modulation of carrier density was expected in array types B and C, in agreement with the observations.

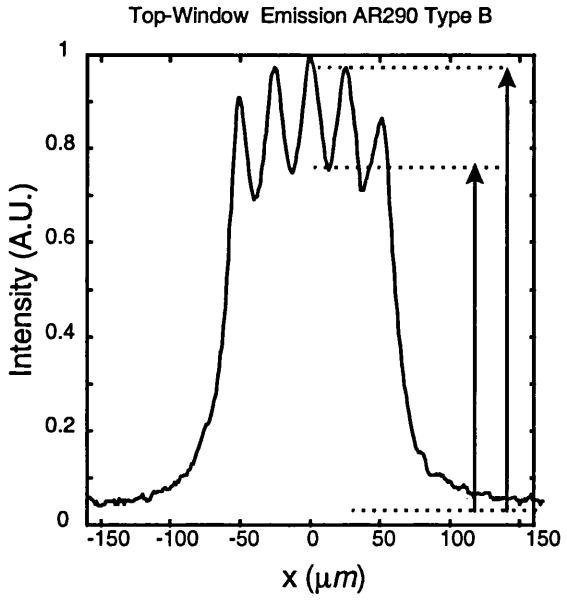

Figure 6.10 *Typical Spontaneous Emission observed through slots in the top surface of array number 290. The emission was not polarised and no speckle or coherence effects were observed. Many similar images were examined and the maximum and local minimum values (examples indicated with arrows) were noted for five maxima and four minima per image. These measurements showed that the degree of modulation of carrier density across the stripes at the array centre was rather low, of the order of 10-30% according to the array type.*

6.6 CONCLUSIONS

The spatial modes of the novel bow tie array were measured. Types B and D are best compared to gain-guided arrays and behaved similarly to them[203-205]. Type A and C behaved similarly broad area lasers with a minor periodic perturbation[206,207]. All types showed a wide far-field divergence filling a similar angular spread to the gain-guided narrow stripe lasers of the same material. They can be described as operating simultaneously in many gain guided array supermodes. Theoretical calculations of the modes of gain guided arrays show symmetric but irregularly spaced near-field maxima.[206-208]. It is believed that the wide far-field and 10μm periodic modulation of the near-field were the consequence of the broad area laser instability reviewed in Chapter 4. [167-171]. Assuming that the near-field remained modulated at higher power, the maximum COD limit should be halved to estimate the COD power from these devices. The revised limit is 4W CW or 25W in picosecond-range pulses. The proximity of neighbouring stripes degraded the width and quality of the beam waists in comparison to those observed in single taper lasers. However, under all operating conditions, one beam waist per stripe could be imaged.

7. Q-Switching of Bow Tie Arrays

7.1 INTRODUCTION

In this chapter, picosecond optical pulse generation at high energy and high peak power from a bow-tie diode laser array with an integrated absorber is reported.[211,212] The pulse energy and power observed was consistent with the expected pulse energy from a broad area device of similar gain volume and inversion ratio showing gain saturation at high optical intensity. The pulse rise-time was reduced to of the order of 1ps, giving single-sided exponential pulses limited by the gain decay time in the laser cavity. The array could be made to operate simultaneously and uniformly, with 50% of the power in well-defined beam-waists. The output is suitable for adaption of photoconductive switching[213-216] to simultaneous picosecond probing of multiple targets with minimal jitter. Pulses of similar duration and energy have been employed in harmonic frequency multiplication,[116,217] and laser range-finding[218].

7.2 MULTI-CONTACT LASER DIODES

Diode laser chips were fabricated with multiple sections separated by etched isolation trenches through the highly doped p-contact, following similar designs to Thredrez, Vasil'ev, and others.[100-105,108]. Narrow-stripe lasers and bow tie lasers with similar multicontact longitudinal structures have been found to be suitable for giant pulse Q-switching, gain-switching, passive Q-switching and mode-locking[176-181].

7.2.1 Waveguide Absorber Sections

The inclusion of material within the laser cavity which is not connected to a current supply implements a simple saturable absorber[93,236]. On receiving incoming spontaneous emission, the carrier density of the unpumped section rises toward transparency. Near to transparency, the absorption decreases. The carrier lifetime in GaAs at $1.8\times10^{18}cm^{-3}$ is approximately 2ns [125]. Much enhanced absorption occurs if negative bias voltage is applied to the p-side of a diode junction. For a semiconductor in a strong electric field, strongly absorbing transition energies are distorted and

redshifted toward the lasing wavelength, which is at the band-edge. The shift of the absorption spectrum by application of reverse bias voltage leads to an increase of up to several hundred cm^{-1} to the optical absorption at the gain-peak wavelength.

7.2.2 Bulk GaAs and Quantum Well Material

Picosecond and subpicosecond mode locking in monolithic multi-contact structures are generally most suited to quantum well material[59,93,219] due to greater gain sublinearity and ultra-fast recovery of absorbing states in the modulator[220-222]. For a reverse biased region in quantum well material, electro-absorbtion shifts a prominent absorption peak over the lasing wavelength, giving an enhanced absorption change[223]. However, the saturation energy is relatively low for quantum wells, due to the limited number of electron and hole states in the quantum well absorption peak, and the relatively slow time for holes to scatter out of those states and transport away the absorbed power[225-226]. Therefore a waveguide containing quantum well material will saturate after less photons have entered than a bulk GaAs waveguide with a similar small-signal extinction ratio. A related process to absorber saturation is gain saturation, by which the external drive current supplying electrons and holes is not able to supply them all at exactly the laser transition energy. There is a delay time while carriers interact with phonons until the electron energy settles a value compatible with the laser emission energy. During this interaction time, high stimulated emission rates deplete the gain at the lasing wavelength. Gain saturation is more severe for quantum well material than for bulk GaAs[227].

The bulk GaAs design was intended to maximise the peak gain and stored energy prior to Q-switching at very high current density of 5-20I_{th},. at the expense of higher transparency and threshold levels than quantum well material. The relatively high number of carriers required to reach transparency was advantageous for creating a compact absorber, to delay giant pulse generation for as long as possible while gain accumulated. The increased capacity of bulk GaAs to store excited carriers in the gain sections and to absorb in the central sections was traded off for having a broader gain spectrum and losing the ultra-low loss α_i of some quantum well structures. The gain

spectrum and related properties are better known for bulk GaAs, and avoid the spectral anomalies that occur when quantum well materials are over-driven.[100,218,225-226]

7.3 TRIPLE CONTACT LASER STRUCTURE

Electrical isolation trenches were designed to avoid perturbing the optical waveguide below. In Chapter 4, this was shown to require that greater than 1.1μm of cladding was left over the active layer for the GaAs/AlGaAs wafer under consideration. The triple contact structure is illustrated in Figure 7.1, for a broad area laser of stripe width *W*. The devices reported in this thesis were bow tie arrays, with additional lateral patterning of the raised contacts which is not shown.

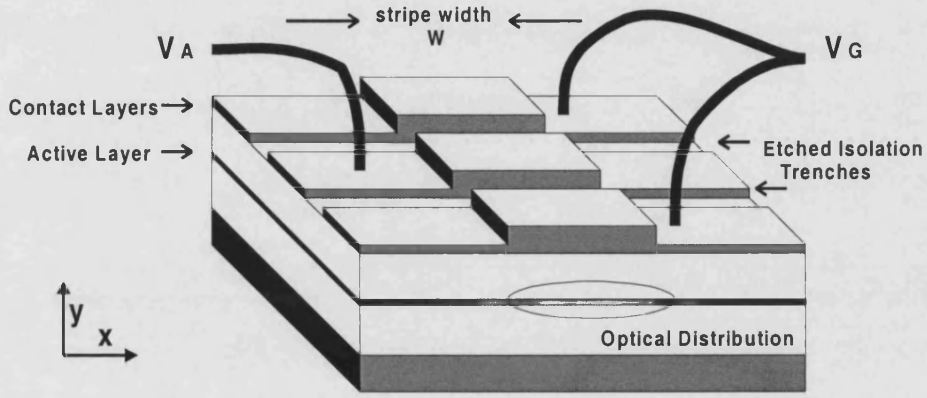

Figure 7.1 *Schematic diagram of triple-contact laser structure, showing etched grooves. Detail of the array structure is not shown, see Figure 6.1-6.4. The wafer composition and structure was described in Table 4.1. The etch depth was a compromise to avoid either perturbing the optical distribution, or allowing a leakage current path through the highly conductive p-doped layers that give electrical contact from GaAs to gold.*

7.3.1 Electrical Connections for Q-Switching of a Multi-Contact Laser

A nanosecond current pulse generator and a kΩ DC voltage supply were connected to the twin gain-sections and absorber section according to Figure 7.2. An avalanche pulse generator (APG) was used to drive the gain sections (both ends of the laser) with nanosecond electrical pulses of amplitude up to 8A at 1-50kHz repetition rate[181].

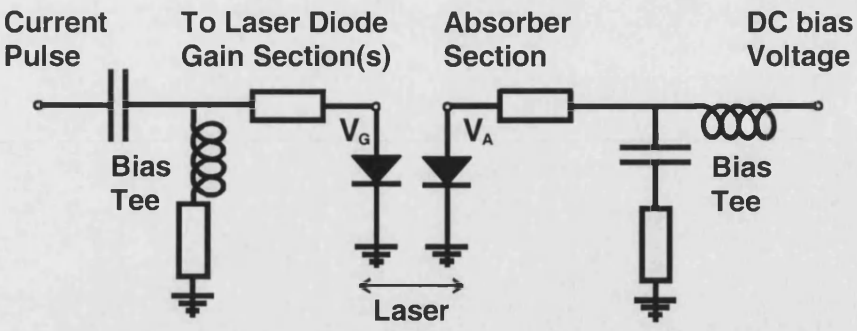

Figure 7.2 External connections using bias tees and resistors for operation of multi-contact diode laser with pulsed gain sections and a DC biased absorber section.

The scheme was similar to gain-switching, using a giant current pulse, preferably shorter than the carrier lifetime of 1ns, and of large amplitude in the range 3-12I_{th}. The optical pulse turn-on time was held back by saturable absorption in the centre contact. The sudden bleaching of the absorber increased the laser cavity Q-factor, releasing stored energy, as described in Chapter 2. The absorption was enhanced by the application of reverse electric field to shift the band edge according to the Franz-Keldysh effect. This allowed a greater inversion ratio to accumulate than for gain switching, giving picosecond pulses of high energy and high peak power. The picosecond pulses were usually accompanied by a tail, shown in Figure 7.3 on the following page.

The tail resulted from the use of current pulses of excessively long duration, and could not be eliminated entirely with the available equipment. Use of a current pulse with a sub-nanosecond duration and 200ps rise-time substantially reduced the energy in the tail, as can be seen in Figure 7.3b. The tail could also be reduced by decreasing the current pulse amplitude to a small fraction above threshold, so that the picosecond pulse occurred near to the maximum of the current pulse. This gave unsatisfactory picosecond pulses of diminished energy and longer duration than for high current operation. The pulse parameters reported in this chapter were taken at an intermediate current, for which the tail was not excessive, and the picosecond pulse had reached 70-90% of the maximised peak intensity.

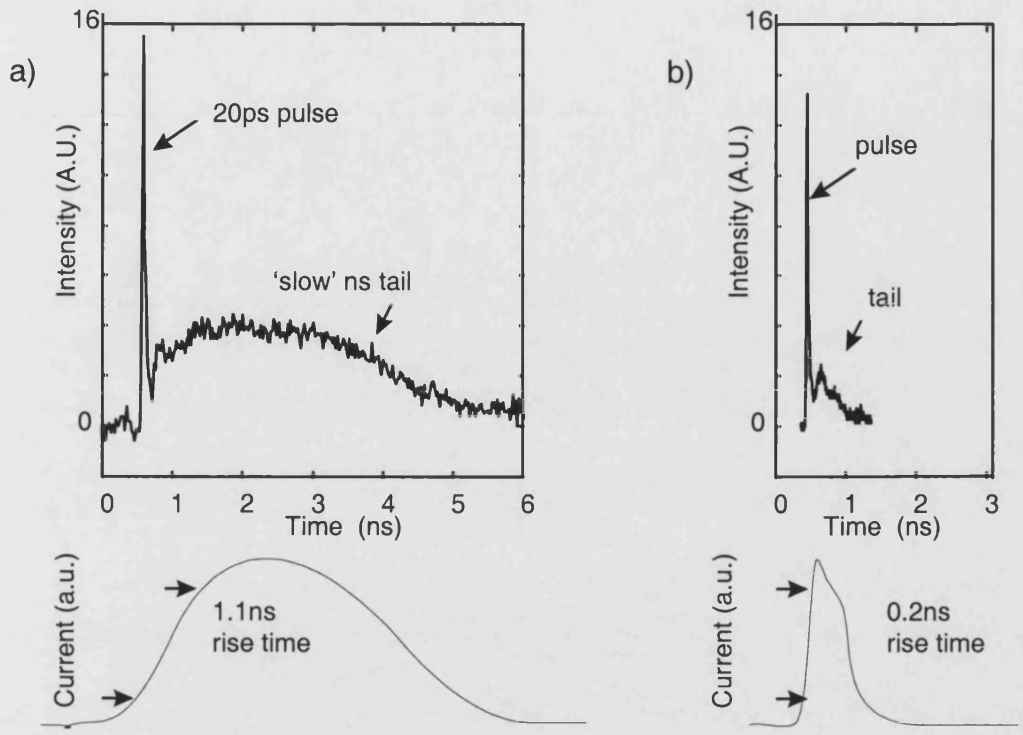

Figure 7.3 *Oscilloscope traces of photodiode signal due to current pulses of $4I_{th}$, with much of the energy in a nanosecond tail following after the main Q-switched pulse. The tail power was consistent with the quasi-CW LI of the laser, at approximately 0.7W. Optical trace A was generated using a 5Ω variable pulse generator from Avtech Instruments, Optical trace B was taken using a 50Ω avalanche pulse generator. The current waveforms are sketched below the measured optical waveforms, and the 20%-80% current rise-times are indicated.*

7.3.2 Average Power measurements

A 1cm^2 silicon photodiode or calibrated optical power meter was placed in the collimated optical beam path. The average power measurement was accurate to 5%, limited by changes to the spatial mode (and hence the collection efficiency of the lenses). The average power was noted at the time of the most critical pulse characterisation experiments, and was later measured systematically over a wider range of current pulse and reverse bias conditions. Dividing by the pulse repetition rate, and correcting for the lens collection efficiency gave the optical energy per pulse per facet. From a set of average power measurements, Figure 7.4 was obtained. The repetition rate was set at 10.5kHz. The average thermal power limit for both the diode laser and the pulse generator were reached at approximately 50kHz. The energy quoted is the total optical energy collected from the front facet during one electrical pulse, and

corresponds to integrating the power under one of the traces of Figure 7.3. The average power measurements were used to calibrate the peak power of scope traces. The peak power estimates were then corrected for deconvolution of the 15ps system response time.

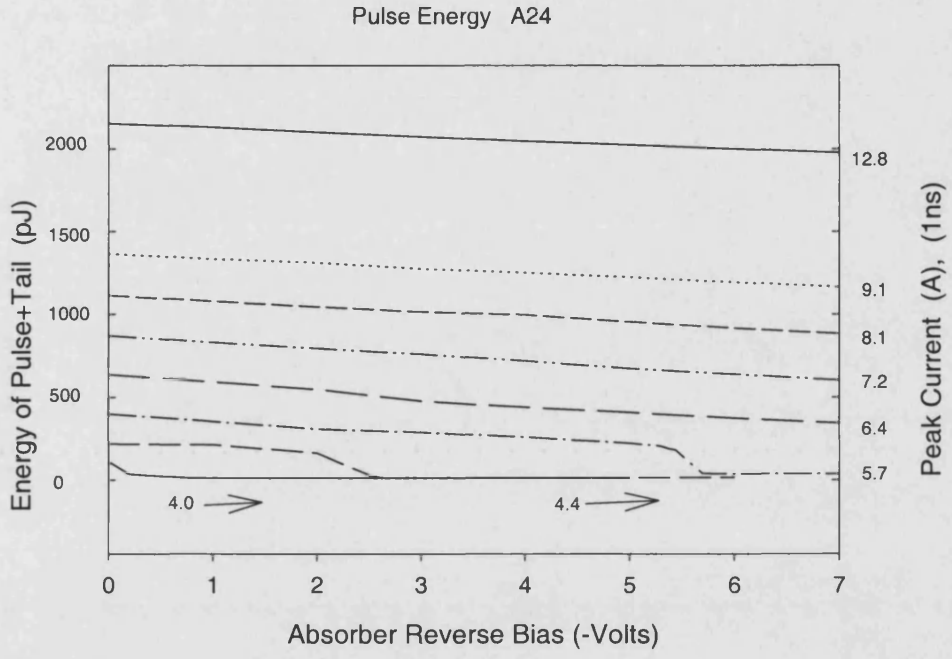

Figure 7.4 *The total pulse energy vs.reverse bias voltage for various current pulse settings. Values were obtained by dividing average power by the repetition rate of 10.5kHz. Each line represents data at a particular peak current.. The pulse duration was fixed at 1ns, with a 200ps rising edge. Threshold was 1.1A when all three contacts of this laser were joined together and driven quasi-CW. For nanosecond pulsed currents of less than 5.7A (peak), laser emission could be suppressed by application of reverse bias. For currents of less than 4.0A peak., the laser did not reach threshold within 1ns.*

7.4 SPATIALLY RESOLVED SCOPE TRACE MEASUREMENTS

7.4.1 Fiber-Coupled Sampling Scope

Using the apparatus of Figure 7.5., the optical output from a small localised region of the arrays was examined by a fiber coupled high speed oscilloscope, with a rise time of 15ps.

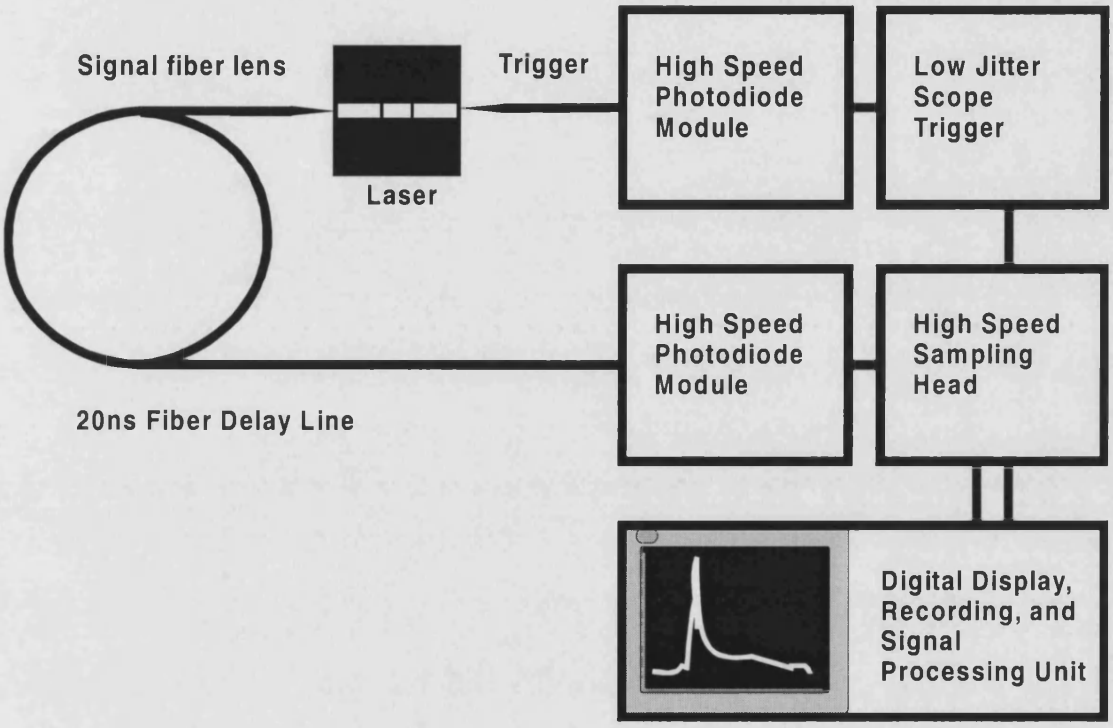

Figure 7.5 *Measurement of the intensity vs. time from a point on a laser facet using a fiber lens into a fast oscilloscope. Best results were obtained using a second fiber lens or equivalent to obtain a trigger signal from a region of the rear facet of the laser. The measurement optical pulse was transmitted through five meters of optical fiber so that it arrived for recording after a delay of several nanoseconds for its trigger to operate. The fiber lenses captured light from a region of approximately 5μm diameter.*

7.4.2 Some Observations from Spatially Resolved Measurements

When the trigger was taken from one fixed region of the reverse facet of the laser, and the position on the front facet of the signal fiber lens was shifted, it was found that the duration, intensity, and the delay time from the electrical pulse to the first optical pulse could vary with position on the array. The peak intensity variation was consistent with

the non-uniform near-fields that were observed under nanosecond pulsed operation and reported in Chapter 6. There were usually several intensity maxima for each taper of an array. Several observations were made:

1. If one taper within an array contained several local maxima, they could pulse at significantly different times. Up to 24ps delay was observed between spots which were located within 10μm in non-uniform or degraded devices.
2. The optical pulse from a local maximum midway between taper centres was always later and weaker than from a local maximum at the taper centre.
3. The optical pulse at a weak maximum of a degraded region was always later and weaker than from non-degraded regions.
4. In devices whose only near-field maxima were near to the taper centres, the start time delay of optical pulses was most uniform.

7.5 PULSE GENERATION FROM BOW TIE ARRAYS

Where each taper produced a spot of similar intensity and spatial profile, the delay and peak power were also as uniform as possible. This was best observed in five-stripe arrays, since there was a drift in the recording instrument trigger time of at least 4ps during extended sets of measurements, so a uniform device could record non-uniform results. A representative set of measurements from a ten stripe array are shown above in Figure 7.6. Additional measurements (not recorded) found that the variation in turn-on times varied by less than 6ps throughout that array.

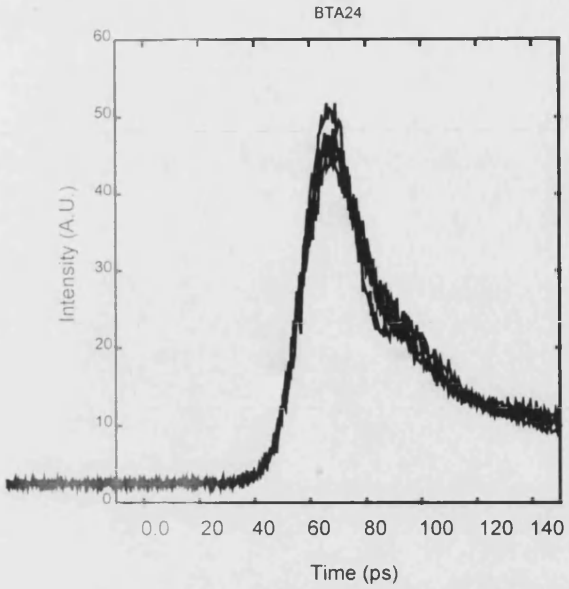

Figure 7.6 Simultaneous and uniform Q-Switched emission from four stripes of Bow Tie Array 24. The device was driven with subnanosecond pulses with an amplitude of $10I_{th}$. V_A = -1.5V. The superimposed scope traces are almost indistinguishable, indicating uniformity.

A duplicate device was tested, and a typical set of scope traces is plotted in Figure 7.7. In this device, spatial and temporal nonuniformity were observed, with delays of up to 7.2ps and peak intensity variations over a factor of two from the brightest region within each stripe.

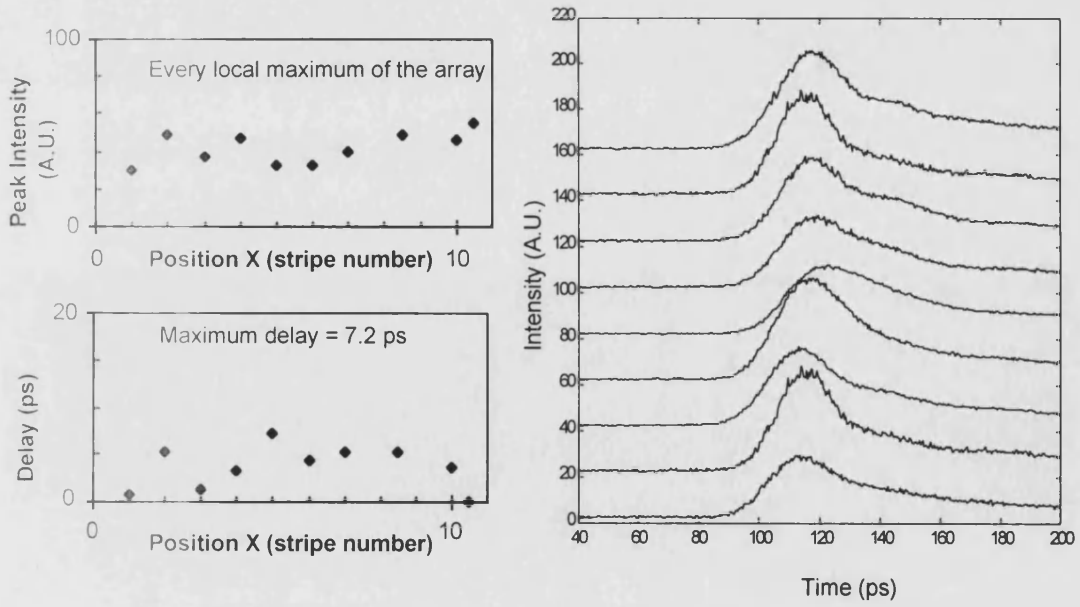

Figure 7.7 Q-switching of bow tie array 23. I_B=1ns, 7.6 A=$10I_{th}$, V_A=-0.6V, I_A=-2mA The ten stripes produced the oscilloscope traces above. The peak intensity and the relative delay

7.5.1 Ten Stripe Arrays

As was stated above, where each taper produced a spot of similar intensity and spatial mode, the delay and peak power were also as uniform as possible. In a ten-stripe array (of type C), relatively uniform peak intensity was observed among all of the stripes, and the maximum delay recorded was 7.2ps, shown in Figure 7.7. This was a repeatable delay, not an artefact of the measurement. This delay was small in comparison to the local pulse duration of 30ps, and the overall output of the array was 35ps (fwhm) The whole scope trace showed an unavoidable tail which contained at least half of the energy that had been measured. Nevertheless, the energy in the front pulse of several duplicate devices was consistently estimated to lie in the range 400-500pJ, almost independent of further increases to current and/or reverse bias and the consequent changes to the energy in the tail. By normalising the area under the 33ps pulse to 500pJ, a peak power of up to14.6W was estimated in this device.

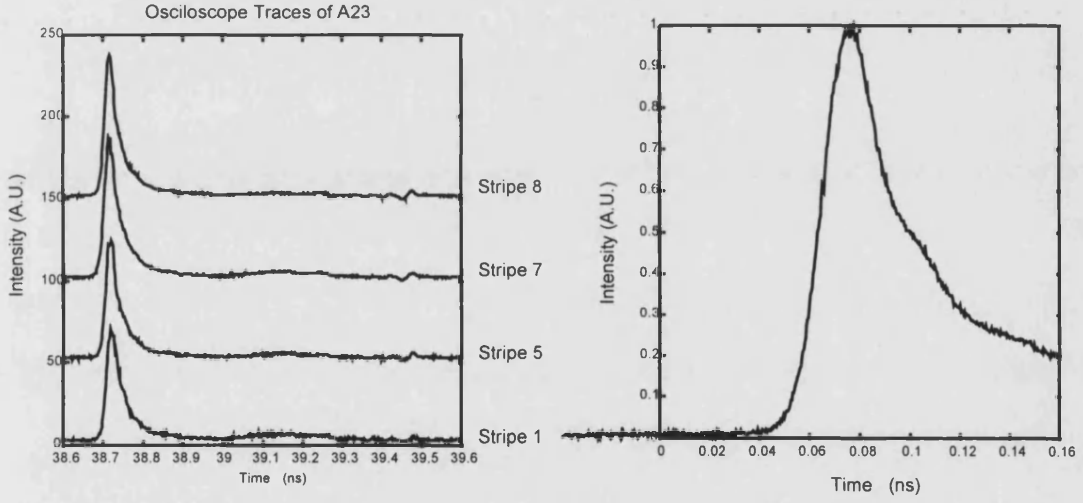

Figure 7.8 *Output of bow tie array 23. Oscilloscope traces were examined at every stripe, and seen to have a low nanosecond tail at least 13dB lower than the peak. The traces recorded from stripes 1,5,7 and 8 were representative of the output of the whole array. The scale was expanded to maximise recording bandwidth, and q full set of ten traces was taken. Their sum (above right) indicated a trace fwhm of 33ps, which deconvolved to 29ps fwhm pulse duration. The total energy, determined from average power measurements, was 495pJ, and the peak power was 10.8W.*

7.5.2 Five Stripe Arrays

In a five-stripe array (of type B), the best uniformity was observed. All of the brightest positions were observed to generate pulses simultaneously to within 3ps, which was limited by the drift in the instrument trigger time. The gain sections received 3ns 1.8A current pulses. Simultaneous pulse generation is illustrated in Figure 7.9. An autocorrelation trace from a similar array had a 1/e full-width of 28.6ps. This gave a pulse 1/e decay time of 14.3ps, (11ps fwhm) for light from one taper section. This was consistent width the duration of the narrowest scope traces, which were less than 24ps fwhm. Opening the aperture of the autocorrelator, the whole device showed a slightly wider autocorrelation function which suggested a pulse duration (fwhm) of 17.5ps. [206] The pulse energy of 300pJ corresponded to a peak power in excess of 17W.

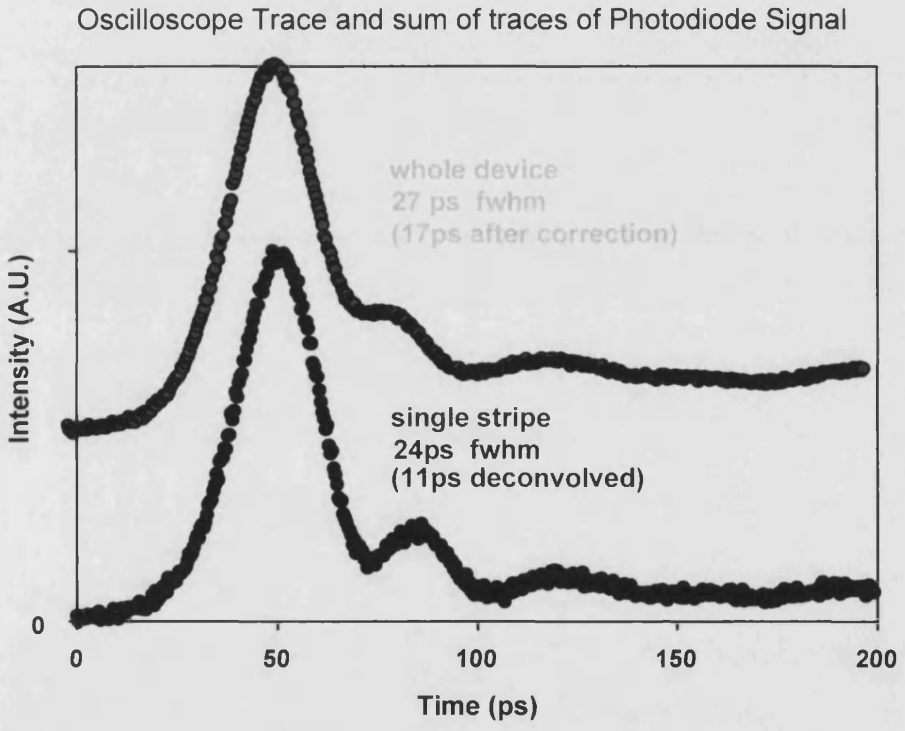

Figure 7.9 *Pulse width during near-simultaneous operation of five-stripe array A275 The oscilloscope trace from a photodiode receiving light from a 3μm area of the array via a fibre lens indicated a single stripe pulse duration of approximately 11*ps. *The sum of many traces (upper) indicated that the pulse width from the whole array was 17*ps.

Table 7.1 summarises the performance of a number of arrays which were tested under gain-switching and Q-switching conditions.

LASER NUMBER	ARRAY TYPE	STRIPES	BEST CONDITIONS V-bias (-V)	I-peak (A)	I-duration (ns)	ENERGY best tail-free pulse (pJ)	excl. tail (pJ)	DURATION whole device, deconvolved (ps)	POWER ><20% (W)
262	B	5	7.5	6	5		130	13	10
349	B	5	3.5	3	5	150		40	3.8
375	B	5	1.5	1.8	3	300	400	17.5	17.1
383	B	5	1.5	1.8	3		400	34	11.8
386	B	5	3.1	1.8	3	162		30	5.4
20	C	5	0	6	1.5		320	not measured	6.4
21	C	10	4	5	1		300	not measured	10
23	C	10	1.5	5	1	495		32	15.4
24	C	10	2	5	1	500	500	33	15.2

Table 7.1 *Best Q-Switched performance of Bow Tie Arrays. The energy within the pulse and excluding the tail, estimated from integrating under scope traces, is listed in the 7^{th} and 8^{th} columns. For the data in the 7^{th} column, the tail was minimised. In the 8^{th} column, the pulse energy was slightly increased by using higher current, which also increased the tail energy.*

The peak power of 10-17W from Q-Switching or gain-switching was a substantial improvement over the single bow-tie laser, and reached power and pulse energy levels which have previously been obtained only from broad area laser diodes or tapered MOPA and post-amplified configurations[97-100, 177,211],. The performance of methods other than Q-Switching were reviewed in Chapter 1. The literature contains few reports of picosecond-range laser arrays.

7.6 PULSE STATISTICS AND JITTER MEASUREMENTS

7.6.1 Definition and measurement of statistical terms

Jitter is defined as the root mean square (rms) variation in the time of a set of events relative to reference events. Values were obtained using a software function on a Hewlett-Packard digital oscilloscope HP54120B. After 1000 traces had been recorded, the standard deviation from a histogram of the points at a reference level was used as a direct measure of jitter. The horizontal window at a reference level is illustrated in Figure 7.10.

Most measurements of jitter were performed with reference to other regions of the array, for which they are termed optical jitter. Further jitter measurements were obtained relative to the current pulse at the APG, which are termed electronic jitter. Jitter in the firing time of the APG relative to a HP214B (used as a 5V trigger) was greater, and was not measured. Using a similar software function, pulse height statistics were calculated by the scope, also illustrated in Figure 7.10. The pulse height variation was described by the standard deviation from a histogram of signal levels at a reference time.

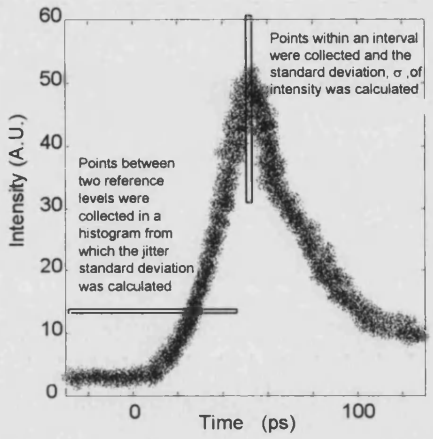

Figure 7.10 Collection of 1000 pulse statistics within user defined intervals, (indicated with rectangular bands) allowed measurement of the rms jitter standard deviation. The rms variation in peak intensity was obtained from a histogram of intensity points within the vertical slot marked above.

It should be noted that the measurements were not strictly independent, since late pulses might not be at their peak in the window in which the pulse height statistics were collected. However, the pulses were always round-topped due to the recording bandwidth limitation of 32GHz, so a few picoseconds of jitter did not significantly modify the peak.

7.6.2 Jitter Values

It was found that the optical jitter could be less than 1.7ps, which should be deconvolved by the instrument sampling time jitter to less than 1ps. This was independent of the distance on the array surface between the trigger collection point and the intensity measurement, as is shown in Figure 7.11.

It was found that the electronic jitter was at least 4ps, usually 8ps, and that this did not vary systematically with position across the array. Since the optical jitter was less than the electronic jitter, it is possible that that an emerging optical pulse in one region of the array initiated optical pulses throughout the whole array. It is also possible that the measured electrical jitter was dictated mainly by current pulse amplitude fluctuations, which effect all stripes of the array.

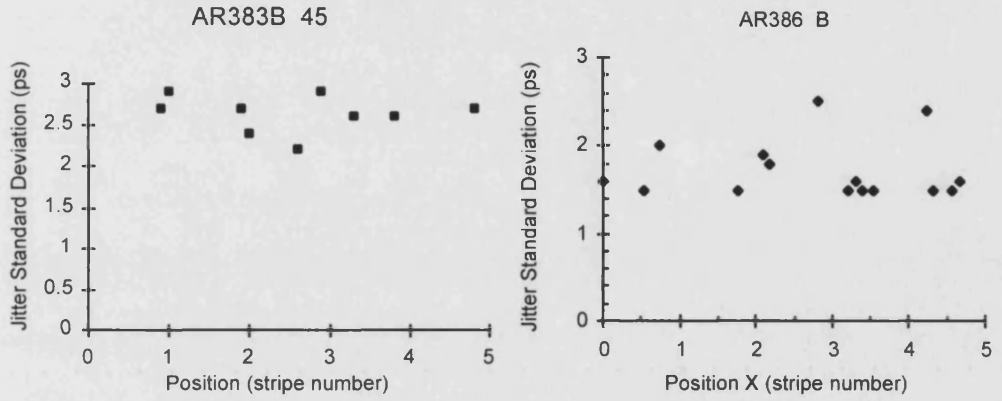

Figure 7.11 The variation of optical jitter across array numbers 383 and 386 (both type B) was random, and did not depend on the distance between the regions of the array used for trigger and signal. In these plots, the trigger came from a fiber lens on stripe 5. Jitter in array 386 was lower than the instrument limit of 1.6ps.

Observing the pulse height using light collected from a localised region of the array by fiber lens, the standard deviation was less than 10% of the peak intensity. At the brighter points the variation was much lower, showing that successive pulses could be similar to one another.

7.7 CONCLUSIONS

Bow tie arrays have been Q-switched using large amplitude single current pulses at 10kHz repetition rate. Energy of up to 0.5nJ per pulse in a duration of 30ps was obtained from ten-stripe arrays. Up to 0.3nJ in 17ps (fwhm) was obtained from five-stripe arrays. Non-uniform output was often observed, but for appropriate reverse bias conditions, the non uniformity could be minimised, and simultaneous operation of the whole array occurred.

8. Performance of Integrated Franz-Keldysh Effect Saturable Absorber for Pulse Generation in Bulk GaAs/AlGaAs Triple-Contact Bow Tie Arrays

8.1.1 History of multi-contact laser structures

The monolithic semiconductor laser with gain and loss sections within one optical cavity was proposed as early as 1964 by Lasher[229]. Experiments with GaAs lasers using multiple contacts isolated by etched trenches (similar to Figure 7.1) were reported within four years by Basov and coworkers, who realised the potential of picosecond switching and bistable components for optical computing[17]. The fabrication technology of two-contact diodes took many years to mature, and such devices can intrinsically show temporal instabilities[230]. The numerous operating regimes which are possible with a loss region and a gain region include CW output, Q-switching (latching) to enhance single Q-switched pulse energy, repetitive self Q-switching (governed by absorber recovery), and mode-locking (due to an absorber with ultra-fast recovery) at repetition rates up to THz.[113-114] The use of a multi-contact structure as an integrated laser-modulator has received much attention in recent years, for optical communication applications. The inclusion of sections with different materials and structures such as DBR gratings has produced very well-developed and high quality devices at communications wavelengths.[231-235] The major functions and configurations of multi-contact laser diodes are reported by Kawaguchi and also by Jones.[236,219]

8.2 EXPERIMENTAL PERFORMANCE OF TRIPLE CONTACT DEVICES

Continuing the Q-Switched single pulse generation experiments reported in Chapter 7, the function of a reverse voltage absorber section within a diode laser array was investigated for the first time. The results presented below indicated that nonuniformity, gain saturation and absorber saturation were significant effects which limited device performance, leaving considerable opportunity for improvements.

8.2.1 Oscilloscope Traces

The pulses reported in the previous chapter were the result of optimisation of gain section current amplitude and absorber DC reverse bias. Additional measurements of the photodiode signal were taken. A selection are plotted in Figure 8.1. The measurement system response time was 15ps.

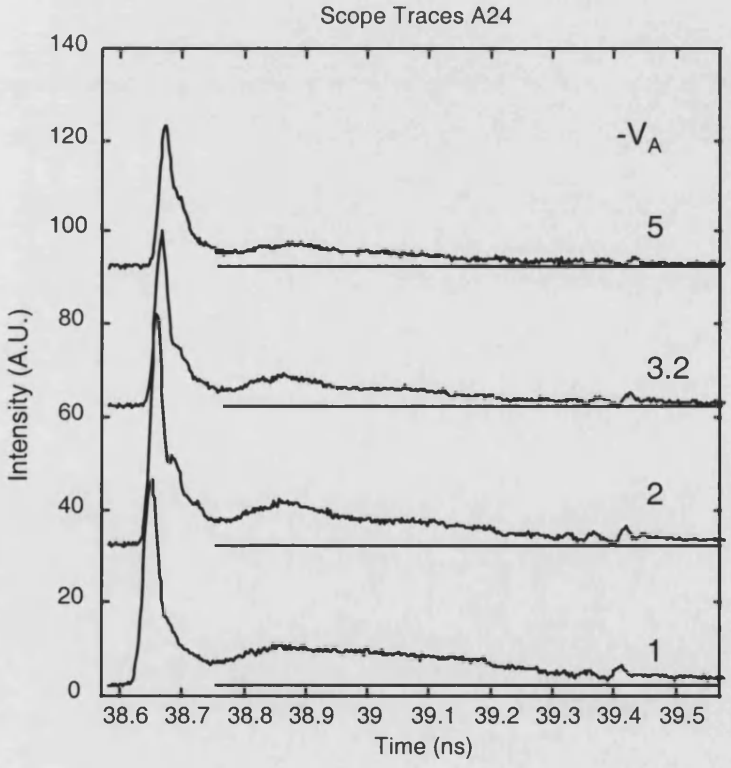

Figure 8.1 *Oscilloscope traces from one near-field local maximum on stripe 2 of a ten-stripe bow tie array 24, type C. The fiber lens position was fine-tuned to follow the centre of the maximum for the signal trace. The trigger was taken from a fixed position. The zero level (offset for display) is marked by horizontal lines. The reverse bias voltage (-V) is indicated above each trace.*

On increasing the magnitude of the absorber reverse voltage from 1.0 to 2.0V, the amplitude of the signal remained constant at 44mV (uncalibrated photodiode signal into 50Ω scope). The pulse duration decreased from 30ps to 23ps, as measured. Deconvolved from the instrument response, this indicated a reduction from 24ps to less than 15ps (fwhm). The traces appear to show delay of approximately 12ps/V but since an optical trigger was used, this should be disregarded. The delay was due mainly to lateral displacement of the near-field maxima within the laser chip. The trigger filament was displaced from its initial position when the absorber was biased. A weaker signal reached trigger threshold levels later, which offset the scope zero time. This might have masked any real delays which might have occurred. For reverse bias of greater than 3V, the pulse did not improve further.

8.2.2 Tail Reduction

It was found that application of reverse bias on the centre contact of arrays allowed tail-free pulse generation at a higher current level than gain-switching. However, the permitted current increase was less than 10%, suggesting that the absorber action was not strong. It was observed that if the Q-switched peak power was improved, then it was mainly due to a reduction of duration at approximately constant pulse energy. The pulse energy never increased by more than 20% on increasing reverse bias.

8.2.3 Autocorrelation Traces

Examples of the second harmonic autocorrelation function (Figure 8.2) from a single stripe within a laser array show how dramatically the local pulse duration could be reduced by activation of the absorber section. As the reverse bias voltage was increased, autocorrelations shortened in duration. There was an optimum bias value, in this case near to 3V, for which the peak intensity was maximised. Further increases to the bias voltage caused non-synchronous output and decreased the energy in the Q-switched pulse, mainly by causing non-uniformity. The number of stripes fully operating and the total pulse energy decreased at bias greater than 3V.

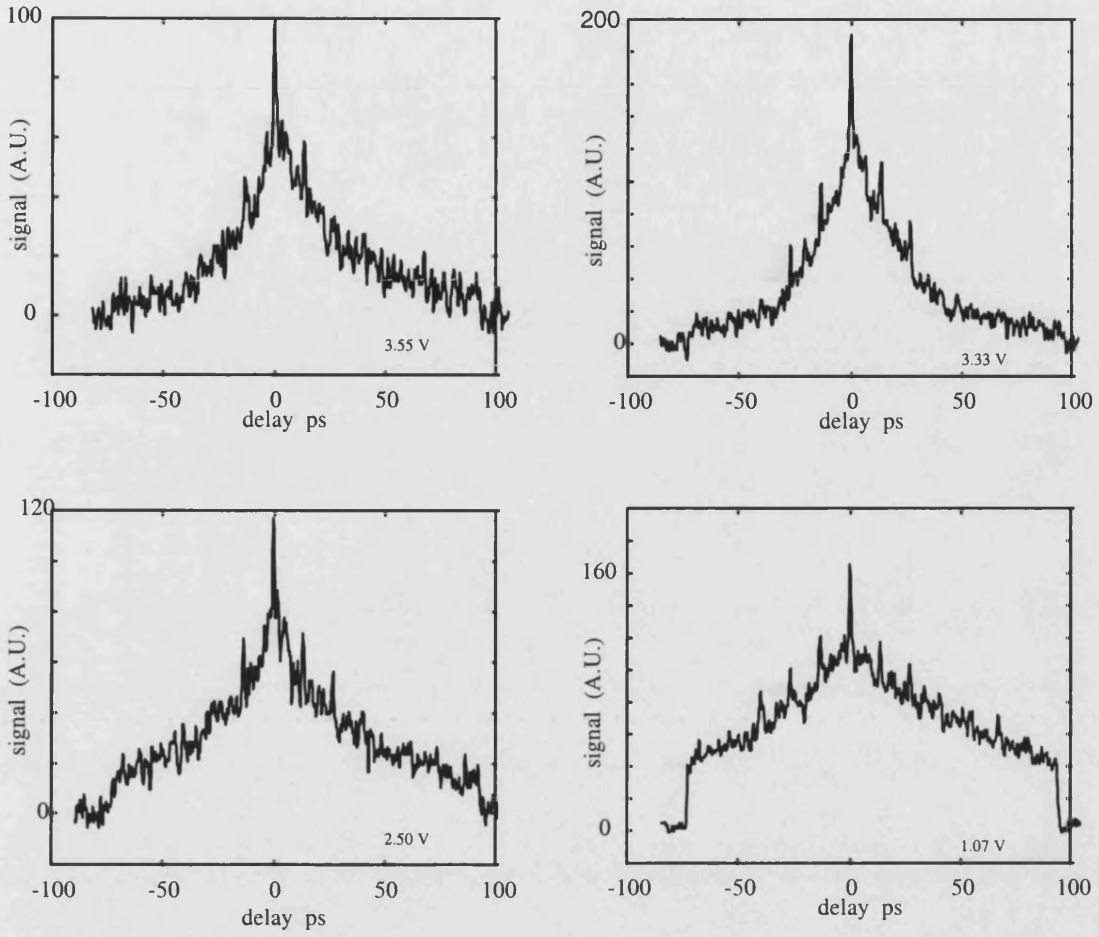

Figure 8.2 *Autocorrelation traces from a near-field maximum on a five-stripe Bow Tie Array 386 with DC bias values of 3.55, 3.33, 2.50, 1.07 Volts. The zero level is indicated by extra data points recorded with a shutter closed at either end of the 170ps scan range of the instrument.*

A full set of autocorrelation traces from one stripe on A386 was used to obtain the following plot of pulsewidth vs. reverse bias in Figure 8.3.

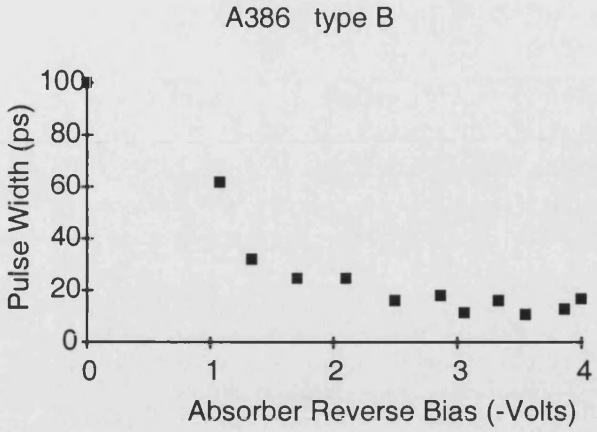

Figure 8.3 *Deconvolved pulse widths from a set of autocorrelation traces obtained from one near-field maximum on Bow Tie Array 386. The pulse width from a localised region was decreased to 11ps (fwhm) by application of 3V or greater to the central contact*

This indicates the transition from mainly gain-switching, at zero bias, to Q-switching. From rate equations simulations without gain saturation, to shorten then simulated pulse duration from 45ps to 11ps required an inversion ratio of 2.3.

This inversion ratio was expected to increase the pulse energy by a factor of 1.9 in comparison to gain switching. The observed picosecond pulsed energy increased by not more than 20% on application of bias.

The triangular log-autocorrelation function in Figure 8.4 shows that the autocorrelation signal was a double-sided exponential function, indicating that the pulse was a single-sided exponential. This is a special case for which there is no ambiguity about the actual pulse shape, except for the direction of the slow exponential decay or rise. The deconvolution factor to convert from autocorrelation width to pulse width was therefore 0.50 for the shorter pulses.

Figure 8.4

The measured autocorrelation function was found to have a bi-exponential shape with a peak as sharp as the coherence spike. This fitted a perfect triangular shape when plotted on a log scale. From a fit to this data (ignoring coherence spikes), the gradient gave the 1/e time of 20ps. The equivalent fwhm is 20 ln(2) = 14ps

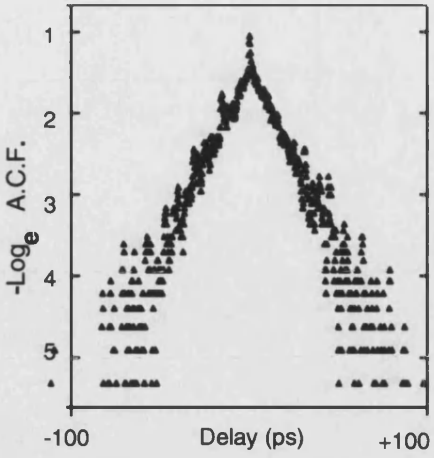

8.2.4 Multiple Pulsations

Autocorrelation traces showed the expected coherence spike at multiples of the laser round-trip time. Some scope traces had substructure after the main pulse peak at non-roundtrip times. Repetitive pulsations did not fully develop in any of the arrays tested, but second pulses were often observed. The amplitude of a second pulse was typically less than 1/3 of the peak. Some double and triple pulses were present in the output of A386 in Figure 8.5

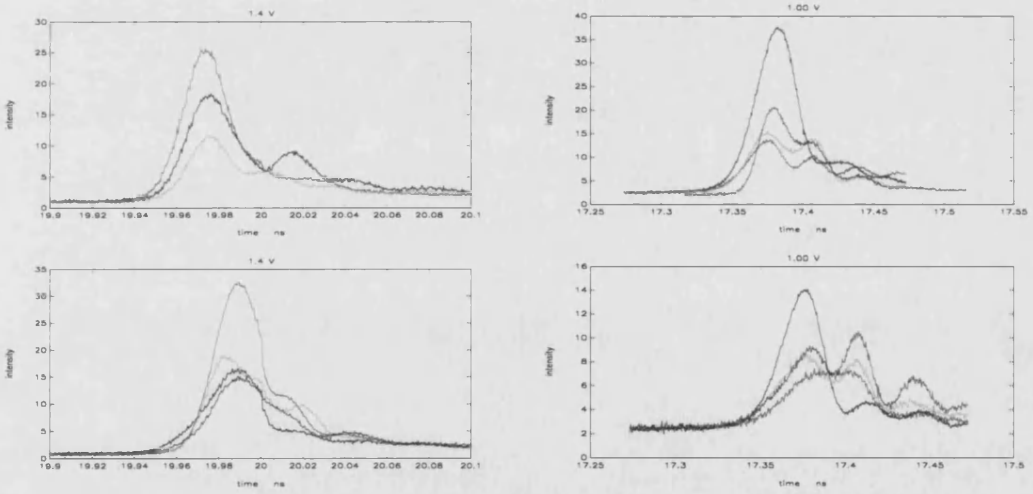

*Figure 8.5 Double-pulse generation from bow tie array 386, type B, five stripes. The magnitude of the absorber reverse bias was 1.4 and 1.0V. Traces were recorded from every near-field maximum. Although the duration of individual pulses could be as low as 11*ps *(deconvolved), there was severe spatial and temporal non-uniformity in this device.*

8.2.5 Nonuniformity and Filamentation

The array was shown to have a near-field modulation spacing of 9-10μm in the quasi-CW measurements of Chapter 6. It had also been observed that at $I < 1.1I_{th}$, a small number of regions of less than 10μm width were up to an order of magnitude more intense than the average across the array aperture. The same was observed under Q-switching conditions. A small number of filaments could reach threshold first, and generate high intensity optical pulses. Typical output from bow tie array 383 is shown in Figure 8.6. Increasing bias values from 0 to 3V caused most regions to produce high peak intensity, which increased with bias. For further bias increases, most filaments went below threshold. A set of rogue filaments at a delayed time benefited from the excess gain that was now stored instead of being taken by the main filament group.

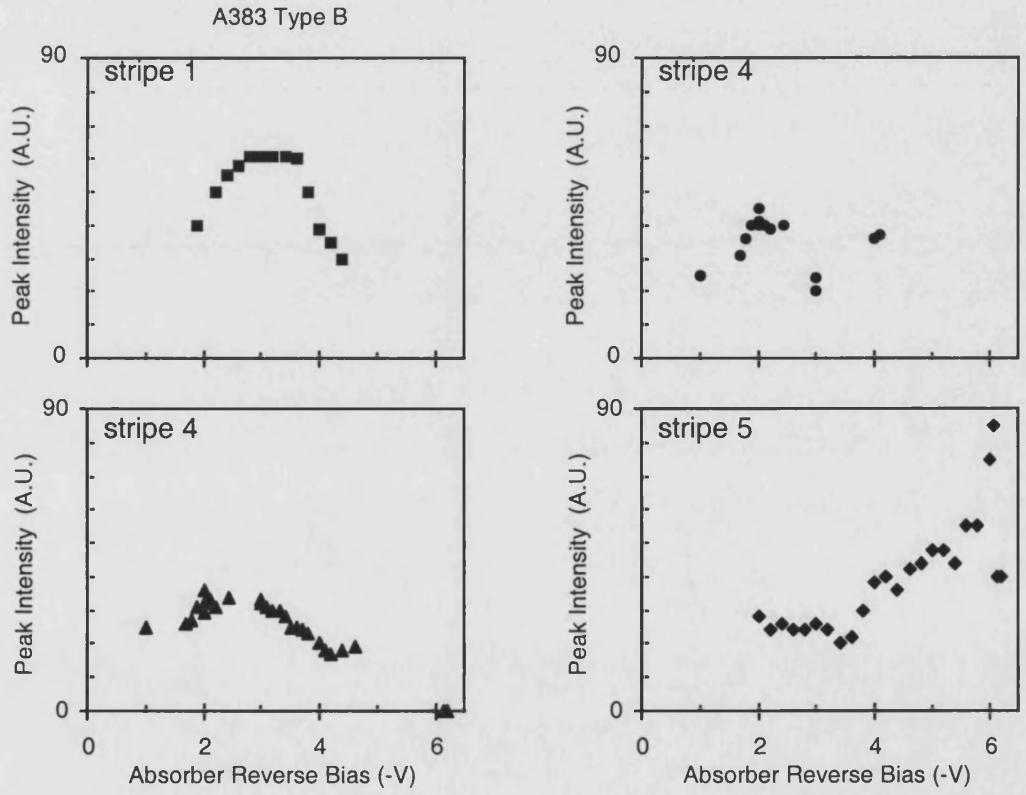

Figure 8.6 *Peak intensity obtained from scope traces at several near-field local maxima. The fiber position was fine-adjusted to maximise the signal for each measurement point, to follow minor displacements of the centre of the near-field maximum. DC bias of -3 to -4 Volts was found to maximise the peak intensity of optical pulses from 'normal' parts of the five-stripe type B arrays. A (reversible) spatial mode transition occurred in this laser, with much of the power being diverted into a particular group of bright spots at high reverse bias. The maximum in stripe 5 increased dramatically at a reverse bias of -6V*

It was found that adjacent filaments within one taper could emit pulses with maxima at substantially different times, with delay of up to 40ps. The spatial and temporal nonuniformity was observed to be most severe at high reverse bias, under exactly the conditions which generated pulses of the shortest local duration.

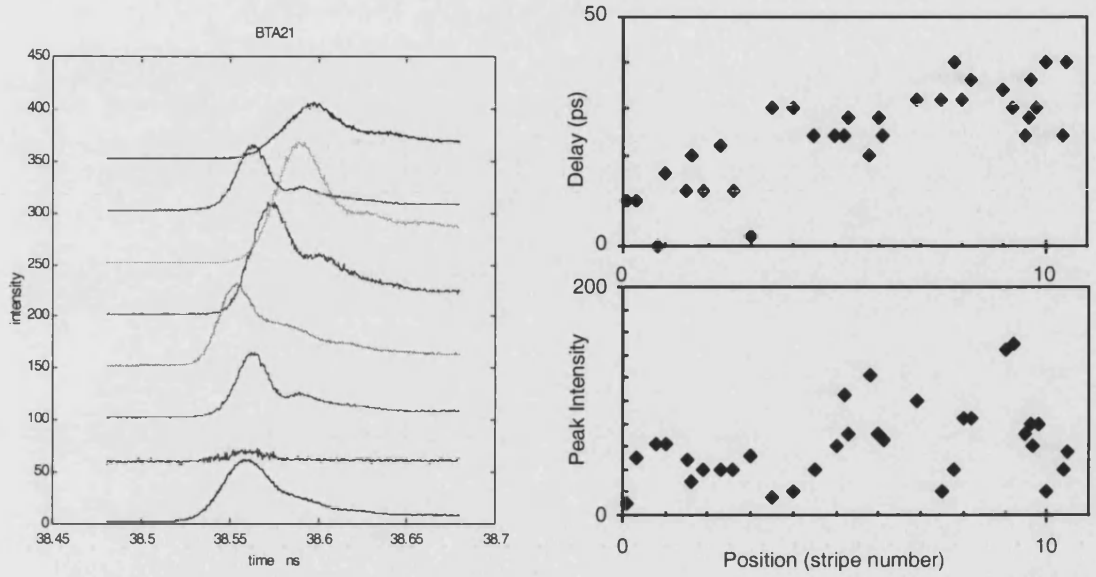

Figure 8.7 *Typical output of Bow Tie Array 21. A set of scope traces for the maximum in each stripe showed up to 30*ps *relative delay between the rising edge of pulses from adjacent stripes. Further traces were observed but not stored, giving the additional data points for peak intensity and delay as a function of position.*

The performance of degraded bow tie arrays was useful for evaluation of the effect of non-uniformity on the pulse generation process. Some areas of the array were found to emit high intensity pulses as long as 40ps after the first Q-switched pulse had begun. In some cases, these delayed pulses appeared from almost the same position on the output facet as earlier pulses. If the initial Q-switched pulse was highly non-uniform, then it caused severe lateral spatial hole burning, leaving a network of excited laser material. The regions of the array which were missed by the first set of pulses could produce their own pulses shortly afterwards.

8.3 SPECTRUM

8.3.1 Q-Switched Spectrum

Using a single fiber-lens to collect light from a small region of the array facet, other fiber coupled instruments could be interchanged with the sampling scope. An optical spectrum analyser was used to record time-averaged spectra from each maximum in the near-field of an array, shown in Figure 8.8.

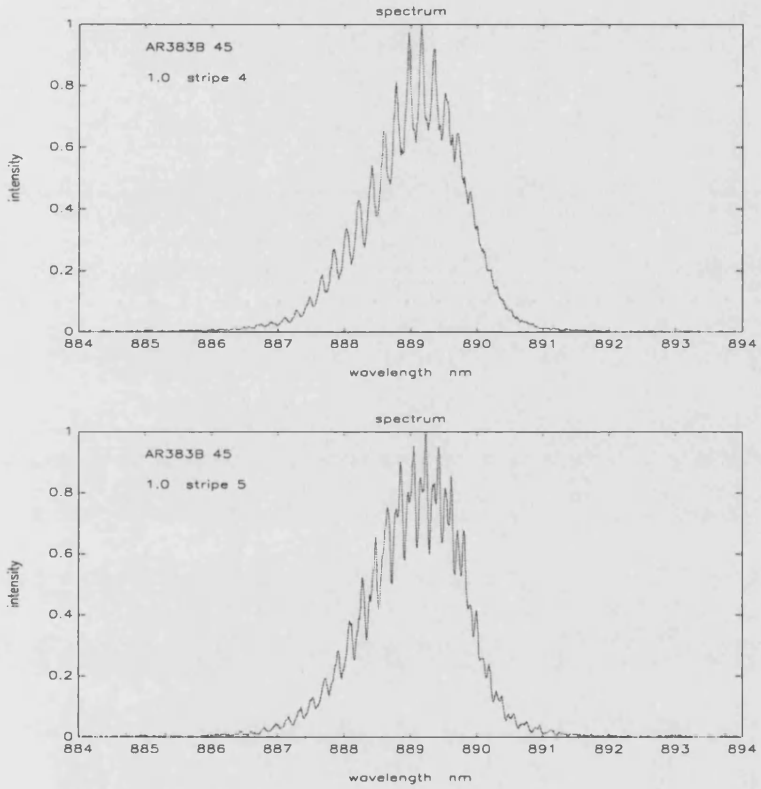

Figure 8.8 Measured spectra from two regions of a typical multi-contact bow tie array. In some regions, the each longitudinal mode was split into multiple sub-peaks

The spectra showed poorly defined longitudinal modes, often interspersed with additional peaks. This was consistent with several lateral modes for each of the longitudinal modes. The average longitudinal mode spacing was not exactly equal to the value expected from the effective index of the wafer structure. The exact pattern of sub-peaks between the longitudinal modes was not stable, and was found to change with reverse bias. This was possibly due to spatial mode hops when bias, feedback, or degradation conditions changed.

9. Final Summary

9.1 REVIEW

In Chapter 1, an introduction to laser diodes and their uses was presented. The available wavelength ranges from the mid infra-red (4μm) to near-UV were stated.

The continuous power delivered within a diffraction-limited spot was used as a measure for comparison of the various laser diode structures which have been developed to date (until April 1998) and reported in the literature. From this comparison, it emerged that tapered laser oscillators, resonant optical waveguide (ROW) arrays, and unstable resonators all performed better than common single-stripe lasers by one order of magnitude. Master oscillator power amplifier structures showed a further increase, to multi-Watt power levels. In all cases, the width of the output facet of a laser structure was increased in order to raise the power without exceeding the practical limitations of catastrophic optical damage (COD) or catastrophic contact failure which are inherent to all known semiconductor laser material systems. It was noted that a substantial futher increase to the CW power was obtained in structures which used facet coating technologies. Facet coatings have removed the weak link in the power delivery chain due to COD, but the higher power density limit due to contact failure still required wide area laser structures for high average power.

A further substantial increase to peak power is possible in pulsed lasers, since the thermal components of COD are relaxed in comparison to CW. A review of the peak power obtained by use of various optical pulse generation schemes was presented. It was noted that peak power may be improved beyond the performance of simple modulation of the laser by increasing the complexity of the laser diode structure, the electrical drive circuitry, and/or external optical structures. Due to the use of high current density electrical drive, the scaling of power with the size of the active area of semiconductor that was systematically examined for CW lasers still applied to pulsed lasers.

Enlarged laser diode structures for pulse generation included arrays, tapers and MOPA diffraction-limited sources. The highest peak power and energy per pulse, approaching kW and μJ levels were from non-diffraction limited broad area lasers.

A second figure of merit, the pulse duration was also examined. This was generally poor for multimoded high power lasers. Mode locked MOPA structures and re-compressed chirped pulse systems of high complexity were required to produce >Watt power levels in picosecond to sub-picosecond timescales.

In Chapter 2, the fundamental requirements for production of optical gain by electrical injection into laser diode structures were briefly introduced. The gain function for GaAs and a sublinear approximation suitable for laser simulations was presented. The rate equations were stated for a monochromatic homogenous laser, and were used to state the CW threshold conditions. The rate equations were used to illustrate dynamic laser behaviour with output of numerical simulation. Gain switching, using pulsed current much greater than CW threshold to obtain peak optical power much greater than the CW was explained, and the importance of a high inversion ratio was stated. This described a high stored carrier population much greater than the CW value to give maximum gain prior to pulse generation. Using the output of rate equation simulations, the use of a saturable semiconductor absorber within the laser cavity was investigated. It was shown that Q-switching can give a large enhancement of the peak power in a pulse.

In Chapter 3 experimental methods were described. Electrical drive, optical power measurement, and spatial intensity profile measurement systems were presented.

Chapter 4 introduced the theoretical basis required to understand practical limitations to the maximum size of single moded lasers. The width may be increased slightly by avoiding the conventional approach of using a strong effective index step to create index guided narrow stripe lasers. The choice of etch depth in the lasers under study was analysed, and shown to be unable to give significant lateral index guiding.

Experimental measurements on narrow stripe lasers were well explained by an analytic model of gain-guiding, which was used to estimate the parameters which determined the spatial mode structure. These are the peak gain at the stripe centre, the maximum loss at the stripe edge, and the real refractive index profile due to the gain or loss profile in the laser.

The self-induced filamentation that is often observed in GaAs broad area lasers was reviewed. It was stated that the lasers under test were expected to spontaneously develop self-organised filaments with a period of the order of 6μm in devices with sufficient width to contain more than one filament.

Chapter 5 presented systematic measurements of spatial intensity profiles of single tapered laser structures with multiple contacts along the length of the device. It was found that the tapered gain guided lasers were multimoded under high power quasi-CW conditions. Single moded operation could only be obtained by avoiding the injection of gain into the narrow segment including the apex of the taper. The difference in loss between the stripe centre (saturated to transparency) and the stripe edges (unsaturated; high loss) gave a self-organised structure similar to a gain guide. The ratio of refractive index perturbations at the stripe centre to stripe edge was decreased by a factor of three in comparison to a tapered laser with uniform contact voltage. This was observed to decrease the multimodedness of the lateral optical distribution, and to restore symmetry to the far-field intensity profile.

In all of the single tapered gain guided devices studied, the optical distribution could be approximated by circular wavefronts originating from a point source at the apex of the taper.

In Chapter 6, a novel bow tie array structure was described. The first measurements of spatial intensity profiles were presented. The arrays of overlapping tapers showed behaviour similar to a broad area laser of the same facet width. Arrays of just-overlapping tapers showed one high quality beam waist per stripe, similar to isolated single tapers, which could be well imaged to five high intensity spots. The near-field

profile at the laser facet was more complex. The far-field of the devices had a similar width to the far-field of single moded narrow stripe lasers in the same material.

In Chapter 7, the achievements of multi-contact Q-switched bow tie arrays were presented. Photodiode signals with spatial resolution by use of a fibre-lens showed that an array could be Q-switched to give near-simultaneous output from all of the tapers in the array. Thus the output of a scaleable large area device (width $W > 120\mu m$) was useful for high peak power high energy picosecond pulse generation. The relative delays of less than 3ps among the tapers were compatible with gain switched or Q-switched pulse generation. Pulses with low short term jitter (<1.6ps) up to power supply limited repetition rates >50kHz with single shot energy 500nJ in <33ps and 300nJ in <17ps were obtained.

In Chapter 8, the function of the intra-cavity saturable absorber in the bow tie array was examined in more detail. The properties of multi-contact laser diodes in the literature were reviewed. Experimental measurements found an increase to the complexity and a decrease to the quality of the optical pulses under non-optimum conditions of gain current pulse amplitude and absorber DC reverse bias. The use of a relatively high DC bias to give maximum saturable absorption in the laser cavity was attempted. Second harmonic autocorrelation measurements showed the expected decrease to the local pulse duration as the absorption increased. The autocorrelation also showed that one taper could produce optical pulses with a sub-picosecond rise time. However, to make use of the extra power from replication of many tapers in the array, simultaneous pulse generation is required. High speed photodiode measurements showed that in the present devices, high reverse bias for optimisation of a single taper within the array led to severe spatial nonuniformity and a consequent large variation in the delay times before pulses emerged from all regions.

Non-uniform and non-simultaneous output of the array occurred under conditions which minimised the pulse duration within one stripe of the array. This is believed to be related to the spontaneous self-organised filamentation that is well-known in broad area lasers. An increase to the carrier density occurs prior to Q-switching, and this should be

maximised for high energy and short pulse generation, as was shown in Chapter 2. Filamentation is known to become more severe as the linewidth enhancement factor increases, and this is especially severe in the regime of gain saturation prior to Q-switching.

9.2 SUGGESTIONS FOR FURTHER WORK

The arrays tested for this thesis were composed of taper sections which were slightly too large to achieve single-moded operation in each taper under the conditions of high current injection. If material systems with a high gain at low carrier density are used, then the filamentation spatial frequency decreases with the square root of the linewidth enhancement factor. This might be used to increase the size of single moded taper structures before multiple near-field peaks develop. The performance of multimoded broad area lasers with low loss quantum well material show that quantum well material narrowed the far-field divergence and improved near-field uniformity.

Current spreading into the regions between the stripes led to a reduction in the absorption, which is required to define effective gain guides. Ion implantation or strong lateral confinement of the carrier population by stripes of wide band-gap material should help to confine gain to the stripe centres.

Possible improved structures might use a deeper etch to totally remove the highly conductive p material in the AlGaAs cladding. The desired etch forms a ridge waveguide by a weak effective index change. Variation of the dopants (eg. avoiding the use of zinc doping in the contact) might give a sharper boundary between the conductive contact layers and the thin layer of optical cladding on the p side of the active layer. This must be achieved without increasing the series resistance, and is a major development project in itself. Deep etch also imposes index guiding. This reduces the width permitted for a single moded stripe from 6μm to 2μm or less. The narrow sections of the tapers would be made more similar to conventional strongly index guided single mode stripe lasers. The deep etch also makes the tapers multimoded. This is not a problem for outward travelling waves, since they diverge from a virtual

waist at the apex. However, waves reflected at the facet continue to diverge, and interfere as they return down the taper. Therefore the higher modes of the taper can be easily excited. To avoid multimoded laser emission in the taper, a MOPA architecture, using an anti-reflection coated travelling wave amplifier is recommended. Using a coherent array for the master oscillator would permit several single moded taper amplifiers to be used simultaneously. However, the potential for kilowatt Q-Switched diode laser systems will not be realised without much process development to achieve large (mm^2) areas of defect-free material.

1 Hall, R.N., Fenner, G.E., Kingsley, J.D., Soltys, T.J. and Carlson, R.O., "Coherent light emission from GaAs p-n junctions," Phys.Rev.Lett. 9 (Nov.), 366 (1962).

2 Nathan, M.I., Dumke, W.P., Burns, G., Dill, F.H. and Lasher, G.J., "Stimulated emission of radiation from GaAs p-n junctions," Appl.Phys.Lett. 1 (Nov.), 62 (1962).

3 Holonyak, N.Jr. and Bevacqua, S.F., "Coherent (visible) light emission from Ga(AsP) junctions," Appl.Phys.Lett. 1 (Dec.), 82 (1962).

4 Quist, T.M., Rediker, R.H., Keyes, R.J., Krag, W.E., Lax, B., McWhorter, A.L. and Zeiger, H.J., "Semiconductor maser of GaAs," Appl. Phys. Lett. 1 (Dec.), 91 (1962).

5 Booth, I.J., Mackechnie, C.J. and Ventrudo, B.F., "Operation of Diode Laser Pumped Tm^{3+} ZBLAN Upconversion Fiber Laser at 482nm," IEEE Journal of Quantum Electronics 32 (1), 118-123 (1996).

6 Waarts, R., Nam, D., Sanders, S., Harrison, J. and Dinerman, B.J., "Two-dimensional Er:YSGG microlaser array pumped with a monolithic two-dimensional laser diode array," Optics Letters 19 (21), 1738-1740 (1994).

7 Sumida, D.S. and Fan, T.Y., "Room-temperature 50mJ/pulse side-diode-pumped Yb:YAG laser," Optics Letters 20 (23), 2384-2386 (1995).

8 Yamaguichi, S., Kobayashi, T., Saito, Y. and Chiba, K., "Efficient Nd:YAG laser end pumped by a high-power multistripe laser-diode bar with multiprism array coupling," Applied Optics 35 (9), 1430-1435 (1996).

9 Tsunekane, M., Taguchi, N. and Inaba, H., "High Power operation of diode-end pumped Nd:YVO_4 laser using composite rod with undoped end," Electronics Letters 32 (1), 40 (1996).

10 Le Garrec, B.J., Raze, G.J., Thro, P.Y. and Gilbert, M., "High average power diode array pumped frequency doubled YAG laser," Optics Letters 21 (24), 1990-1992 (1996).

11 Zawischa, I. and Ferguson, A.I., "Diode-pumped CW single mode, tunable Cr^{3+}:$LiSrAlF_6$ ring laser," Optics Letters 21 (1), 45 (1996).

12 Choi, H. K., Turner, G. W. and Manfra, M. J., "High CW Power (Greater-Than-200mW/facet) At 3.4μm From InAsSb/InAlAsSb Strained-Quantum-Well Diode-Lasers," Electronics Letters 32 (14), 1296-1297 (1996).

13 Yakovlev, Y. P., Baranov, A. N., Imendov, A. N., Popov, A. A. and Sherstnev, V. V., "Tunable Diode-Lasers Based On Quaternary III-V Alloys in the Spectral Range of 2-4μm For Laser Spectroscopy Applications," Journal De Physique IV 4 (C4), 671-676 (1994).

14 Desjardins, P., Izquierdo, R. and Meunier, M., "Diode laser induced chemical vapour deposition of WSi_x on TiN from WF_6 and SiH_4," J.Appl.Phys. 73 (10), 5216 (1883).

15 Arjavalingam, G., Opprysko, M.M. and Hirst, J.E.Jr., Mater.Res.Soc.Symp.Proc. 101 (81) (1988).

16 Karlsons, D., Reno, C.W. and Hannan, W.J., "Room Temperature GaAs Laser Voice-Communication System," Proc. IEEE 52 (Nov.), 1354-1355 (1964).

17 Basov, N.G., "0-1 Dynamics of Injection Lasers," IEEE Journal of Quantum Electronics 4 (11), 855-864 (1968).

18 Karbowiak, A.E., "The Birth of Optical Communications," IEE Proceedings 133 (3), 202 (1986).

19 Kao, K.C., "Dielectric-fibre surface waveguides for optical freqencies," IEE Proceedings 113 (7), 1151 (1966).

20 Oe, K., Ando, S. and Sugiyama, K., Jap.J.Appl.Phys. 16, 1273 (1977).

21 Kobayashi, N. and Horikoshi, Y., Jap.J.Appl.Phys. 18, 1005 (1979).

22 Borella, M.S., Jue, J.P., Banerjee, D., Ramamurthy, B. and Mukherjee, B., "Optical Components for WDM Lightwave Networks," Proceedings of the IEEE 85 (8), 1272-1307 (1997).

23 Favre, F., Le Guen, D., Moulinard, M.L., Henry, M. and Georges, T., "320 Gbit/s soliton WDM transmission over 1300km with 100km dispersion-compensated spans of standard fibre," Electronics Letters 33 (25), 2135-2136 (1997).

24 Nakazawa, M., Suzuki, K., Kubota, H., Sahara, A. and Yamada, E., "100Gbit/s WDM (20Gbit/s x 5 channels) soliton transmission over 10000km using in-line synchronous modulation and optical filtering," Electronics Letters 33 (14), 1233-1234 (1995).

25 Favre, E., Le Guen, D. and Devaux, F., "4x20Gbit/s soliton WDM transmission over 2000km with 100km dispersion-compensated spans of standard fibre," Electronics Letters 33 (14), 1234-1235 (1997).

26 SDL, Product Catalog , 1997.

27 Botez, D. and Scrifres, D., *Diode Laser Arrays* (1995).

28 Report No. ISO/TC 172/SC9/WG1 N 56, 1993.

29 Choi, H.K., Walpole, J.N., Turner, G.W., Eglash, S.J., Missaggia, L.J. and Conners, M.K, "GaInAsSb-AlGaAsSb Tapered Lasers Emitting at 2μm," IEEE Photonics Technology Letters 5 (10), 1117-1119 (1993).

30 Mehuys, D. G., Major, J. S., Plano, W. E. and Welch, D. F., "620 mW Near-Diffraction-Limited, 1.8μm Tapered Laser," Electronics Letters 30 (14), 1131-1133 (1994).

31 Groves, S.H. , Donnelly, J.P. , Walpole, J.N. , Woodhouse, J.D. , Missaggia, L.J. , Bailey, R.J. and Napoleone, A., "Strained-Layer InGaAsP Diode Lasers with Tapered Gain Region for Operation at 1300nm," IEEE Photonics Technology Letters 6 (11), 1286-1288 (1994).

32 Walpole, J. N., Donnelly, J. P., Groves, S. H., Missaggia, L. J., Woodhouse, J. D., Bailey, R. J. and Napoleone, A., "Diffraction-Limited 1.3μm Wavelength Tapered-Gain-Region Lasers With Greater-Than-1-W CW Output Power," IEEE Photonics Technology Letters 8 (11), 1429-1431 (1996).

33 Welch, D.F., "New dawn beckons for semiconductor lasers," Physics World (Feb.), 35-37 (1994).

34 Mehuys, D., Goldberg, L., Waarts, R. and Welch, D.F., "4.5W CW Near-Diffraction-Limited Tapered-Stripe Semiconductor Optical Amplifier," Electronics Letters 29 (2), 219-221 (1993).

35 Mehuys, D. , Goldberg, L. and Welch, D.F., "5.25W CW Near-Diffraction-Limited Tapered-Stripe Semiconductor Optical Amplifier," IEEE Photonics Technology Letters 5 (10), 1179-1182 (1993).

36 O'Brien, S., Schoenfelder, A. and Lang, R. J., "5W CW diffraction-limited InGaAs broad-area flared amplifier at 970 nm," IEEE Photonics Technology Letters 9 (9), 1217-1219 (1997).

37 O'Brien, S., Mehuys, D., Major, J., Lang, R., Parke, R., Welch, D. F. and Scifres, D., "1.3W CW, Diffraction-Limited Monolithically Integrated Master Oscillator Flared Amplifier At 863nm," Electronics Letters 29 (24), 2109-2110 (1993).

38 Welch, D. F., Parke, R., Mehuys, D., Hardy, A., Lang, R., O'Brien, S. and Scifres, S., "1.1W CW, Diffraction-Limited Operation of a Monolithically Integrated Flared-Amplifier Master Oscillator Power-Amplifier," Electronics Letters 28 (21), 2011-2013 (1992).

39 Bhattacharya, A., Mawst, L. J., Nesnidal, M. P., Lopez, J. and Botez, D., "0.4W CW Diffraction-Limited Beam Al Free 0.98μm Wavelength 3 Core Arrow-Type Diode-Lasers," Electronics Letters 32 (7), 657-658 (1996).

40 Ou, S. S., Yang, J. J., Jansen, M., Hess, C., Sergant, M., Tu, C., Alvarez, F. and

Lembo, L. J., "High-Power Ingaas/Gaas Singlemode Laser-Diodes With Reactive-Ion-Etched Ridges," Electronics Letters 28 (25), 2345-2346 (1992).

41 Biellak, S.A., Fanning, G.C., Sun, Yan, Wong, S.S. and Siegman, E., "Reactive-Ion-Etched Diffraction-Limited Unstable Resonator Semiconductor Lasers," IEEE Journal of Quantum Electronics 33 (2), 219-229 (1997).

42 Srinvasan, S.T., Schaus, C.F., Sun, S-Z., Armour, E.A., Hersee, S.D. and McInerney, J.G., "High Power Spatially Coherent Operation of unstable resonator semiconductor lasers with regrown lens-trains," Appl.Phys.Lett. 61 (11), 1272-1274 (1992).

43 Chang-Hasnain, C.J., "Characteristics of the off-centred apertured mirror external cavity laser array," Appl.Phys.Lett. 54 (6), 484-485 (1989).

44 Pillai, R. and Garmire, E., "External-cavity semiconductor-laser array insensitive to paraxial misalignment," Optics Letters 20 (20), 2108-2110 (1995).

45 Pillai, R. and Garmire, E., "Paraxial misalignment Insensitive External Cavity Semiconductor Laser Array Emitting Near Diffraction Limited Single Lobed Beam," IEEE Journal of Quantum Electronics 32 (6), 996-1008 (1995).

46 Maccormack, S. and Eason, R. W., "Near-Diffraction-Limited Single-Lobe Emission From a High-Power Diode-Laser Array Coupled to a Photorefractive Self-Pumped Phase- Conjugate Mirror," Optics Letters 16 (10), 705-707 (1991).

47 Waarts, R., Mehuys, D., Nam, D., Welch, D., Streifer, W. and Scifres, D., "High-power, CW, diffraction-limited, GaAlAs laser diode array in an external Talbot cavity," Appl.Phy.Lett. 58 (23), 2586-2588 (1991).

48 Zmudzinski, C., Mawst, L. J., Botez, D., Tu, C. and Wang, C. A., "1W Diffraction-Limited-Beam Operation of Resonant-Optical-Wave-Guide Diode-Laser Arrays At 0.98μm," Electronics Letters 28 (16), 1543-1544 (1992).

49 Mawst, L. J., Botez, D., Jansen, M., Roth, T. J. and Rozenbergs, J., "1.5W Diffraction-Limited-Beam Operation From Resonant-Optical-Wave- Guide (ROW) Array," Electronics Letters 27 (4), 369-371 (1991).

50 Kaneko, Y., Kikuchi, A., Nomura, A. and Kishino, K., Electronics Letters 26, 657 (1990).

51 Valster, A.M.N., Finke, M.J.B., Boermans, J.M.M., van der Heijden, C.J., Spreuwenberg, G.R. and Liedenbaum, C.T.H.F., presented at the PD-12 Semiconductor Laser Conf. , 1990

52 Nurmikko, A. V. and Gunshor, R. L., "Blue-Green Emitters in Wide-Gap II-VI Quantum-Confined Structures," IEEE Journal of Quantum Electronics 30 (2), 619-630 (1994).

53 Ohki, A., Ohno, T., Matsuoka, T. and Ichimura, Y., "Continuous-wave operation of ZnSe-based laser diodes homoepitaxially grown on semi-insulating ZnSe substrates," Electronics Letters 33 (11), 990-991 (1997).

54 Nakayama, N., Itoh, S., Okuyama, H., Ozawa, M., Ohata, T., Nakano, K., Ikeda, M., Ishibashi, A. and Mori, Y., "Continuous-Wave Operation of 489.9nm Blue Laser-Diode At Room-Temperature," Electronics Letters 29 (25), 2194-2195 (1993).

55 Linden, K. J. and Reeder, R. E., "Diode-Laser Arrays With High-Power in the 4 - 5μm Infrared Region," Optical Engineering 23 (5), 685-686 (1984).

56 Choi, H. K., Turner, G. W. and Liau, Z. L., "3.9μm InAsSb/AlAsSb Double-Heterostructure Diode-Lasers With High- Output Power and Improved Temperature Characteristics," Applied Physics Letters 65 (18), 2251-2253 (1994).

57 Xu, J., Lambrecht, A. and Tacke, M., "Lead Chalcogenide Implanted Diode-Lasers in CW Operation Above 77-K," Electronics Letters 30 (7), 571-573 (1994).

58 Ishida, A., Sakurai, N., Aikawa, K. and Fujiyasu, H., "PbSrS-MQW Lasers and the Effect of Quantum-Well On Operation Temperature," Solid-State Electronics 37 (4-6), 1141-1144 (1994).

59 Agrawal, G.P and Dutta, N.K., *Semiconductor Lasers*, 2 ed. (Van Nostrand Reinhold, New York, 1993).

60 Chen, T. R., Ungar, J., Iannelli, J., Oh, S., Luong, H. and Barchaim, N., "High-Power Operation of InGaAsP/InP Multiquantum-Well DFB Lasers At 1.55μm Wavelength," Electronics Letters 32 (10), 898-898 (1996).

61 Botez, D., Mawst, L. J., Bhattacharya, A., Lopez, J., Li, J., Kuech, T. F., Iakovlev, V. P., Suruceanu, G. I., Caliman, A. and Syrbu, A. V., "66-Percent CW Wallplug Efficiency From Al-Free 0.98μm -Emitting Diode-Lasers," Electronics Letters 32 (21), 2012-2013 (1996).

62 Sarzala, R.P. and Nakwaski, W., "Thermal properties of buried-heterostructure diode lasers," International Journal of Optoelectronics 8 (5), 705-725 (1993).

63 Casey, H.C.Jr. Panish, M.B., *Heterostructure Lasers* (Academic Press, Orlando, New York, London, 1978).

64 DeLoach, B.C., Hakki, B.W.Jr., Hartman, R.L. and D'Asaro, L.A., Proc.IEEE 61, 1042 (1973).

65 Peek, J.A.F., "Water Vapor, Facet Erosion, and the Degradation of (AlGa)As DH Lasers Operated at CW output powers of Up to 3mW /μm Stripewidth," IEEE Journal of Quantum Electronics 17 (5), 781-786 (1981).

66 Yoo, J. S., Lee, H. H. and Zory, P., "Temperature Rise At Mirror Facet of CW Semiconductor-Lasers," IEEE Journal of Quantum Electronics 28 (3), 635-639 (1992).

67 Lee, H. H., "Effects of Lateral Heat and Carrier Diffusion On Thermal Runaway of CW DH Semiconductor-Lasers," IEEE Journal of Quantum Electronics 29 (10), 2619-2624 (1993).

68 Yoo, J. S., Fang, S. and Lee, H. H., "Condition For No Thermal Runaway in CW Semiconductor-Lasers," Journal of Applied Physics 74 (11), 6503-6510 (1993).

69 Nakwaski, W., "Thermal-Model of the Catastrophic Degradation of High-Power Stripe- Geometry GaAs/(AlGa)As Double-Heterostructure Diode-Lasers," Journal of Applied Physics 67 (4), 1659-1668 (1990).

70 Shaw, D.A. and Thornton, P.R., Solid-State Electronics 13, 919 (1970).

71 Lammert, R.M. Smith, G.M. Forbes,D.V. Osowski,M.L. Coleman,J.J., "Strained Layer InGaAs-GaAs-AlGaAs buried heterostrucure lasers with nonabsorbing mirrors fabricated by selective-area MOCVD," Electronics Letters 31 (13), 1070-1072 (1995).

72 Hendrix, J., Morthier, G. and Baets, R., "Influence of laser parameters and unpumped regions near the facets on the power level for catastrophic optical damage in short wavelength lasers," IEE Proc.Optoelectronics 144 (2), 109-114 (1997).

73 Matsumoto, M., Sasaki, K., Kondo, M., Takeoka, T., Nakatsu, H., Watanabe, M., Ishizumi, T., Yamamoto, O., Yamamoto, S. and Hijikata, T., "High-Power Laser Diode With Window Grown On Facets," Sharp Technical Journal (50), 33-36 (1991).

74 Matsumoto, M., Sasaki, K., Kondo, M., Takeoka, T., Yamamoto, S. and Ishizumi, T., "High-Power Algaas Single-Stripe Laser-Diode With Window-Grown-On- Facets," Electronics and Communications in Japan Part II-Electronics 78 (11), 45-54 (1995).

75 Morimoto, T., Ogawa, M. and Kaneiwa, S., "High-Power Laser Diode For Magnetooptical Disk Systems," Sharp Technical Journal (50), 53-58 (1991).

76 Sasaki, K., Matsumoto, M., Kondo, M., Ishizumi, T., Takeoka, T., Yamamoto, S. and Hijikata, T., "Highly Reliable 150 mW CW Operation of Single-Stripe Algaas Lasers With Window Grown On Facets," Japanese Journal of Applied Physics Part 2-Letters 30 (5B), L 904-L 906 (1991).

77 Shima, A., Tada, H., Motoda, T., Tsugami, M., Utakouji, T. and Higuchi, H., "Reliability study on 50-100-mW CW operation of 680-nm visible laser diodes with a window-mirror structure," IEEE Journal of Selected Topics in Quantum Electronics 3

(2), 443-449 (1997).

78 Shima, A., Tada, H., Ono, K., Fujiwara, M., Utakouji, T., Kimura, T., Takemi, M. and Higuchi, H., "Highly reliable 60 degrees C 50-mW operation of 650-nm band window- mirror laser diodes," IEEE Photonics Technology Letters 9 (4), 413-415 (1997).

79 Syrbu, A. V., Yakovlev, V. P., Suruceanu, G. I., Mereutza, A. Z., Mawst, L. J., Bhattacharya, A., Nesnidal, M., Lopez, J. and Botez, D., "ZnSe-Facet-Passivated InGaAs/InGaaSP/InGaP Diode-Lasers of High CW Power and Wallplug Efficiency," Electronics Letters 32 (4), 352-354 (1996).

80 Tsunekawa, Y., Watanabe, K., Seki, T., Asaka, T., Yamasaki, Y., Takamura, T. and Iwano, H., "High-Power Operation of AlGaAs/GaAs Large-Optical-Cavity Laser Diode With ZnS_xSe_{1-x}(X=0.06) Layer Grown By Adduct-Source Metalorganic Chemical Vapor-Deposition Method," Japanese Journal of Applied Physics Part 2-Letters 28 (11), L2085-L2088 (1989).

81 Watanabe, M., Tani, K., Takahashi, K., Sasaki, K., Nakatsu, H., Hosoda, M., Matsui, S., Yamamoto, O. and Yamamoto, S., "Fundamental-Transverse-Mode High-Power Algainp Laser-Diode With Windows Grown On Facets," IEEE Journal of Selected Topics in Quantum Electronics 1 (2), 728-733 (1995).

82 Hakki, B.W. and Nash, F.R.Jr., J.Appl.Phys. 45, 3907 (1974).

83 Moser, A., "Thermodynamics of facet damage in cleaved AlGaAs lasers," Appl.Phys.Lett. 59 (5), 522-524 (1991).

84 Temkin, H.A., Mahajan, A., Di Giuseppe, M.A. and Dentai, G., Appl.Phys.Lett. 40, 562 (1982).

85 Plano, W. E., Major, J. S. and Welch, D. F., "High-Power 875-nm Al-Free Laser-Diodes," IEEE Photonics Technology Letters 6 (4), 465-467 (1994).

86 Botez, D., Mawst, L.J., Bhattacharya, A., Lopez, J., Li, J., Kuech, T.F., Iakovlev, V.P., Suruceanu, G.I., Caliman, A., Syrbu, A.V. and Morris, J., "6W CW front-facet power from short-cavity (0.5mm), 100μm stripe Al-free 0.98mu-m emitting diode lasers," Electronics Letters 33 (24), 2037 (1997).

87 Ohkubo, M., Ijichi, T., Iketani, A. and Kikuta, T., "Aluminum Free InGaAs/GaAs/InGaAsP/InGaP Grinsch Sl-sqw Lasers At 0.98μm," Electronics Letters 28 (12), 1149-1150 (1992).

88 Zhang, G., Nappi, J., Ovtchinnikov, A. and Asonen, H., "Aluminium-Free GaAs/GaInAsP Quantum Well Lasers," Electronics Letters 29 (5), 429-431 (1993).

89 Ueda, O., Imai, H., Yamaguchi, A., Komiya, S., Umebu, I. and Kotani, T., J.Appl.Phys. 40, 562 (1984).

90 Garbuzov, D.Z. , Gokhale, M.R. , Dries, J.C. , Studenkov, P. , Martinelli, R.U. , Connolly, J.C. and Forrest, S.R., "13.3W quasi-continuous operation of 0.99μm wavelength SCH-QW InGaAS/GaAs/InGaP broadened waveguide lasers," Electronics Letters 33 (17), 1462-1463 (1997).

91 Wade, J.K. , Mawst, L.J. , Botez, D. , Jansen, M. , Fang, F. and Nabiev, R.F., "High continuous wave power, 0.8μm -band Al-free active-region diode lasers," Appl.Phys.Lett. 70 (2), 149-151 (1997).

92 O'Brien, S , Zhao, H. and Lang, R.J., "High Power wide aperture AlGaAs based lasers at 870nm," Electronics Letters 34 (2), 184-185 (1998).

93 Lau, K.Y., "Short-Pulse and High-Frequency Signal Generation in Semiconductor Lasers," IEEE Journal of Lightwave Technology 7 (2), 400-419 (1989).

94 Hahn, D. and Schlachetzki, A., "Monolithic Integration of InGaAsP Laser with Transferred-Electron Device as Fast Laser Driver," IEEE Journal of Quantum Electronics 32 (1), 14-19 (1996).

95 Lui, Pao-Lo , Kaminow, I.P. and Hsieh, J.J., "Picosecond Pulse Generation from

InGaAsP Lasers at 1.25 and 1.3μm by Electrical Pulse Pumping," IEEE Journal of Quantum Mechanics 17 (5), 671-674 (1981).

96 Chang, C. T., Sun, C. K., Albares, D. J. and Jacobs, E. W., "High-Energy (59 pJ) and Low-Jitter (250 fs) Picosecond Pulses From Gain-Switching of a Tapered-Stripe Laser-Diode Via Resonant Driving," IEEE Photonics Technology Letters 8 (9), 1157-1159 (1996).

97 Stelmakh, N., Lourtioz, J. M., Marquebielle, G., Volluet, G. and Hirtz, J. P., "Generation of high-energy (0.3μJ) short pulses (<400 ps) from a gain-switched laser diode stack with subnanosecond electrical pump pulses," IEEE Journal of Selected Topics in Quantum Electronics 3 (2), 245-249 (1997).

98 Kume, M., Naito, H., Ohya, J., Ohta, I., Shimizu, H., Kazumura, M. and Teramoto, I., "A High-Power Short-Pulse Laser Diode For Wave-Guide 2nd Harmonic-Generation," Solid-State Electronics 34 (12), 1329-1333 (1991).

99 Williams, K. A., Sarma, J., White, I. H., Penty, R. V., Middlemast, I., Ryan, T., Laughton, F. R., Roberts, J. S., "Q-Switched Bow-Tie Lasers For High-Energy Picosecond Pulse Generation," Electronics Letters 30 (4), 320-321 (1994).

100 Thedrez, B.J. Saddow, S.E. Liu,YuanQun Wood,C. Wilson,R. and Lee, Chi H., "Experimental and Theoretical Investigation of Large Output Power Q-Switched AlGaAs Semiconductor Lasers," IEEE Photonics Technology Letters 5 (1), 19-22 (1993).

101 Weisser, S. , Larkins, E.C. , Czotscher, K. , Benz, W. , Daleiden, J. , Esquivias, I. , Fleissner, J. , Ralston, J.D. , Romero, B. , Sah, R.E. , Schonfelder, A. and Rosenweig, J., "Damping-Limited Modulation Bandwidths up to 40GHz in Undoped Short-Cavity InGaAs-GaAs Multiple-Quantum-Well Lasers," IEEE Photonics Technology Letters 8 (5), 608-610 (1996).

102 Zhang, X., Gutierrezaitken, A. L., Klotzkin, D., Bhattacharya, P., Caneau, C. and Bhat, R., "0.98μm Multiquantum-Well Tunneling Injection-Lasers With Ultra-High Modulation Bandwidths," Electronics Letters 32 (18), 1715-1717 (1996).

103 Tsang, D.Z. , Walpole, J.N. , Liau, L. , Groves, S.H. and Diaduik, W., "Q-Switching of low-threshold buried-heterostructure diode lasers at 10GHz," Appl.Phys.Lett. 45 (3), 204-206 (1984).

104 Dykaar, D.R. , Berthold, K. , Levi, A.F.J. , Tanbun-Ek, T. and Logan, R.A., "Large-signal picosecond response of InGaAs/InP quantum well lasers," Appl.Phys.Lett. 56 (17), 1629-1631 (1990).

105 Vasil'ev, P. P., White, I. H., Burns, D. and Sibbett, W., "High-Power, Low-Jitter Encoded Picosecond Pulse Generation Using an Rf-Locked Self-Q-Switched Multicontact GaAs/GaAlAs Diode-Laser," Electronics Letters 29 (18), 1593-1594 (1993).

106 Kidoguchi, I., Adachi, H., Kamiyama, S., Fukuhisa, T., Mannoh, M. and Takamori, A., "Low-noise 650-nm-Band AlGaInP visible laser diodes with a highly doped saturable absorbing layer," IEEE Journal of Quantum Electronics 33 (5), 831-837 (1997).

107 Bessho, Y., Uetani, T., Hiroyama, R., Komeda, K., Shono, M., Ibaraki, A., Yodoshi, K. and Niina, T., "Self-Pulsating 630nm Band Strain-Compensated MQW AlGaInP Laser-Diodes," Electronics Letters 32 (7), 667-668 (1996).

108 Gavrilovic, P., Stelmakh, N., Zarrabi, J. H. and Beyea, D. M., "High-Energy CW Q-Switched Operation of Multicontact Semiconductor- Laser," Electronics Letters 31 (14), 1154-1155 (1995).

109 Vainshtein, S., Rossin, V. V., Kilpela, A., Kostamovaara, J., Myllyla, R. and Maatta, K., "Internal Q-Switching in Semiconductor-Lasers - High-Intensity Pulses of the Picosecond Range and the Spectral Peculiarities," IEEE Journal of Quantum Electronics 31 (6), 1015-1021 (1995).

110 Technoexan, "Picosecond Injection Lasers," *Product Catalog* (Uni-Export Instruments Ltd., International House, The Common, Stokenchurch, High Wycombe,

Bucks. HP14 3UH, 1997).

111 Portnoi, E. L., Venus, G. B., Khazan, A. A., Gadjiev, I. M., Shmarcev, A. Y., Frahm, J. and Kuhl, D., "Superhigh-po ner picosecond optical pulses from Q-switched diode laser," IEEE Journal of Selected Topics in Quantum Electronics 3 (2), 256-260 (1997).

112 Sanders, S. , Eng, L. , Paslaski, J. and Yariv, A., "108GHz passive mode locking of a multiple quantum well semiconductor laser with an intracavity absorber," Appl.Phys.Lett. 56 (4), 310-311 (1990).

113 Arahira, S., Oshiba, S., Matsui, Y., Kunii, T. and Ogawa, Y., "Terahertz-Rate Optical Pulse Generation From a Passively Mode-Locked Semiconductor-Laser Diode," Optics Letters 19 (11), 834-836 (1994).

114 Wu, M.C. , Chen, K. , Tanbun-Ek, T. , Logan, R.A. , Chin, M.A. and Raybon, G., "Transform-limited 1.4ps optical pulses from a monolithic colliding-pulse mode-locked quantum well laser," Appl.Phys.Lett. 57 (8), 759-761 (90).

115 Poelker, M., "High-Power Gain-Switched Diode-Laser Master Oscillator and Amplifier," Applied Physics Letters 67 (19), 2762-2764 (1995).

116 Goldberg, L. and Mehuys, D., "Blue-Light Generation Using a High-Power Tapered Amplifier Mode- Locked Laser," Applied Physics Letters 65 (5), 522-524 (1994).

117 Mar, A., Helkey, R., Bowers, J., Mehuys, D. and Welch, D., "Mode-Locked Operation of a Master Oscillator Power-Amplifier," IEEE Photonics Technology Letters 6 (9), 1067-1069 (1994).

118 Zhu, B., White, I. H., Williams, K. A., Laughton, F. R. and Penty, R. V., "High-Peak-Power Picosecond Optical Pulse Generation From Q-Switched Bow-Tie Laser With a Tapered Traveling-Wave Amplifier," IEEE Photonics Technology Letters 8 (4), 503-505 (1996).

119 Stelmakh, N. and Lourtiez, J-M., "230fs 25W Pulses from Conventional Mode-Locked Laser Diodes with Saturable Absorber Created by Ion Implantation," Electronics Letters 29 (2), 160-161 (1993).

120 Schrans, T., Salvatore, R. A., Sanders, S. and Yariv, A., "Subpicosecond (320fs) Pulses From CW Passively Mode-Locked External Cavity 2-Section Multiquantum Well Lasers," Electronics Letters 28 (16), 1480-1482 (1992).

121 Chusseau, L. and Delevaque, E., "Nonlinear optical compression of Er^{3+}-fiber amplified 1.5μm laser diode pulses," IEEE Journal of Selected Topics in Quantum Electronics 2 (3), 500-507 (1996).

122 Gunning, P., Kashyap, R., Siddiqui, A. S. and Smith, K., "Picosecond Pulse Generation of Less-Than-5ps From Gain-Switched dfb Semiconductor-Laser Diode Using Linearly Step-Chirped Fiber Grating," Electronics Letters 31 (13), 1066-1067 (1995).

123 Miyamoto, M., Tsuchiya, M., Liu, H. F. and Kamiya, T., "Generation of Ultrashort (Similar-to-65fs) Pulses From 1.55μm Gain-Switched Distributed-Feedback (DFB) Laser With Soliton Compression By Dispersion Arrangements," Japanese Journal of Applied Physics Part 2-Letters 35 (10B), L1330-L1332 (1996).

124 Ohta, H. and Oki, T., "310-Femtosecond Optical Pulse Generation From a Gain-Switched Laser- Diode Using Soliton Compression," Japanese Journal of Applied Physics Part 2-Letters 33 (11B), L1604-L1606 (1994).

125 Casey, H.C. and Panish, M.B., *Heterostructure Lasers* (Academic Press, Orlando, New York, London, 1978).

126 Sze, S.M, *Semiconductor Devices, Physics and Technology* (John Wiley and Sons, New York, 1985).

127 Kressel, H. and Butler, J.K., *Semiconductor Lasers and Heterojunction LEDs* (Academic Press, Orlando, New York, London, 1977).

128 Thompson, G.H.B., *Physics of Semiconductor Laser Devices* (Wiley, Chichester, New York, Brisbane, Toronto, 1980).

129 Agrawal, G.P and Dutta, N.K., *Semiconductor Lasers*, 2 ed. (Van Nostrand Reinhold, New York, 1993).

130 Hess,O. Kuhn,T."Spatio-Temporal Dynamics of Semiconductor Lasers: Theory, Modelling and Analysis," Progress in Quantum Electronics 20 (2), 85-179 (1996).

131 Basov, N.G., Krokhin, O.N. and Popov, Y.M., "Production of Negative Temperature States in p-n Junctions of Degenerate Semiconductors," JETP 13, 1320-1321 (1961).

132 Halperin, B.I. and Lax, M., Phys.Rev. 148, A553 (1966).

133 Summers, Huw, "Gain Spectra of bulk GaAs," Private Communication and QBasic program (1994).

134 Lowery, A.J., Olesen, H., Morthier, G., Verhoeve, P., Baets, R., Buss, J., Mc.Donald, D. and Marcenac, D.D., "A proposal for standardized parameters for semiconductor lasers," International Journal of Optoelectronics 10 (5), 347-355 (1995).

135 Claisse, P.R. and Taylor, G.W., "Internal Quantum Efficiency of Laser Diodes," Electronics Letters 28 (21), 1991-2 (1992).

136 Marcuse, D., "Classical Derivation of the Laser Rate-Equation," IEEE Journal of Quantum Electronics 19 (8), 1228-1231 (1983).

137 Carrol, J.E., *Rate equations in semiconductor electronics* (Cambridge University Press, Cambridge, 1985).

138 Wilson,J and Hawkes,J.F.B. *Optoelectronics, an introduction* (Prentice-Hall international series in Optoelectronics, Cambridge University Press, 1989)

139 Lau,K.M. "Short Pulse and High-Frequency Signal Generation in Semiconductor lasers" IEEE Journal of Lightwave Technology, 7 (2) 400-419 (1989)

140 Mηller, J., Laughton, F. R., White, I. H., Penty, R. V., Sarma, J., Middlemast, I., Ryan, T. and Button, C., "Q-Switched Bow-Tie Lasers At 1.5μm Driven By an Overshoot- Compensated Avalanche Pulse-Generator," International Journal of Optoelectronics 10 (1), 35-38 (1995).

141 Rahman, Kamil Abd, "Computer Controlled Measurement of The Electrical and Optical Characteristics of Tapered Semiconductor Lasers," M.Phil, Optoelectronics Group, Dept.of Physics, University of Bath, 1995.

142 Burrato, S.K. , Hsu, J.W. , Trautman, J.K. , Betzig, E. , Bylsma, R.B. Bahr and C.C. Cardillo, M.J., "Imaging InGaAsP quantum-well lasers using near-field scanning optical microscopy," Journal of Applied Physics 76 (12), 7720-7725 (1994).

143 Reng, N. Eppich, B., "Definition and measurement of high-power laser beam parameters," Optical and Quantum Electronics 24 ('S'), 973-992 (1992).

144 Goldberg, B. Unlu, M.S. Herzog,W.D. Ghaemi,H.F. Towe,E., "Near-Field Optical Studies of Semiconductor Heterostructures and Laser Diodes," IEEE Selected Topics in Quantum Electronics 1 (4), 1073-1080 (1995).

145 Courjon, D. and Bainier, C., "Near-Field microscopy and Near Field Optics," Rep.Prog.Phys. 57, 989-1028 (1994).

146 Cook, D.D. Nash, F.R., "Gain-induced guiding and astigmatic output beam of GaAs lasers," Journal of Applied Physics 46 (4), 1660-1671 (1975).

147 Born, M. and Wolf, E., *Principles of Optics*, VI ed. (Pergamon Press, Oxford, New York, Toronto, Sydney, Frankfurt, 1980).

148 Anderson, W.W., "Mode Confinement and Gain in Junction Lasers," IEEE Journal of Quantum Electronics 1 (6), 228-236 (1965).

149 Byer, N.E. Butler, J.K., "Optical Field Distribution in Close-Confined Laser Structures," IEEE Journal of Quantum Electronics 6 (6), 291-296 (1970).

150 Marcuse, Dietrich, *Theory of Dielectric Optical Waveguides* (Academic Press, New York, San Francisco, London, 1974).

151 Tamir, Theodor, *Guided Wave Optoelectronics* (Springer-Verlag, Berlin, New York, London, 1988).

152 Yariv, Amnon, *Optical Electronics*, 3rd ed. (Holt-Saunders, London, 1985).

153 Landau, L.D. and Lifshitz, E.M., "Electrodynamics of Continuous Media," (Pergamon Press, 1960), pp. p.256.

154 Selway, P.R. Thompson, G.H.B. Henshall,G.D. Whiteaway,J.E.A., "Measurement of the effect of injected carriers on the p-n refractive index step in single heterostructure diode lasers," Electronics Letters 10, 453 (1974).

155 Thompson, G.H.B., "A theory for filamentation in semiconductor lasers including the dependence of dielectric constant on injected carrier density," Opto-electronics 4 (1972), 257 (1972).

156 Osinski, M. Buus, J., "Linewidth broadening factor in semiconductor lasers -an overview," IEEE Journal of Quantum Electronics 23, 9-29 (1987).

157 Lee, S.S., Figueroa, L. and Ramaswamy, R., "Variations of Linewidth Enhancement Factor and Linewidth as a Function of Laser Geometry in AlGaAs LAsers," IEEE Journal of Quantum Electronics 25 (5), 862-870 (1989).

158 Hochholzer, M. and Jordan, V., "Discussion of the linewidth enhancement factor alpha of GaAs/GaAlAs quantum well lasers," IEE Proc.Optoelectronics 141 (5), 311-315 (1994).

159 Bossert, D.J. and Gallant, D., "Gain, Refractive Index, and alpha Parameter in InGaAs-GaAs SQW Broad-Area lasers," IEEE Photonics Technology Letters 8 (3), 322-327 (1996).

160 Henry, C.H., "Theory of the Linewidth of Semiconductor Lasers," IEEE Journal of Quantum Electronics 18 (2), 259-264 (1982).

161 Hakki, B.W., "Striped GaAs lasers: mode size and efficiency," Journal of Applied Physics 46, 2723 (1975).

162 Epstein, P.S., Proc.Nat.Acad.Sci. 16, 627 (1930).

163 Adams, M.J., Opt.Quant.Elec. 10, 17 (1978).

164 Osinski, M., Opt.Quant.Elect. 9, 361 (1977).

165 Dickson, L.D., "Characteristics of a Propagating Gaussian Beam," Applied Optics 9 (8), 1854-1861 (1970).

166 Tatum, J. A., Staszewski, R., Macfarlane, D. L. and Serreze, H. B., "Beam Quality of High-Power Broad-Area Visible Diode-Lasers," Optical and Quantum Electronics 26 (9), 911-928 (1994).

167 Sun, Y. and Siegman, A. E., "Optical-Mode Properties of Laterally Offset Gain and Index Guiding Structures," IEEE Journal of Quantum Electronics 32 (5), 790-795 (1996).

168 Constance, J., Chang-Hasnain, Kapon, E. and Colas, E., "Spatial Mode Structure of Index-Guided Broad Area Quantum-Well Lasers," IEEE Journal of Quantum Electronics 26 (10), 1713-1715 (1990).

169 Marciante, J. R. and Agrawal, G. P., "Lateral Spatial Effects of Feedback in Gain-Guided and Broad-Area Semiconductor-Lasers," IEEE Journal of Quantum Electronics 32 (9), 1630-1635 (1996).

170 Mehuys, D., Lang, R.J., Mittlestein, M., Salzman, J. and Yariv, A., "Self-Stabilized Nonlinear Lateral Modes of Broad Area Lasers," IEEE Journal of Quantum Electronics 23 (11), 1909-1919 (1987).

171 La Comb, R., Wagner, D.K., DiMarco, L. and Conolly, J., "Stable Operation of multiple lateral mode ridge waveguide lasers for high speed printing," Elec.Lett. 33 (3), 214 (1997).

172 Fischer, I., Hess, O., Elsaber, W. and Gobel, E., "Compex spatio-temporal dynamics in the near-field of a broad-area semiconductor laser," Europhysics Letters 35 (8), 579-594 (1996).

173 Marciante, J.R. and Agrawal, G.P., "Spatio-Temporal Characteristics of Filamentation in Broad-Area Semiconducot Lasers," IEEE Journal of Quantum Electronics 33 (7), 1174-1179 (1997).

174 Casares, S. F., Balle, S. and Menendezvaldes, P., "Mode Beating and Spontaneous Emission Noise Effects in a Variable- Wave-Guide Model For the Dynamics of Gain-Guided Semiconductor-Laser Arrays," IEEE Journal of Quantum Electronics 30 (11), 2449-2457 (1994).

175 Martinregaldo, J., Balle, S. and Abraham, N. B., "Spatiotemporal Dynamics of Gain-Guided Semiconductor-Laser Arrays," IEEE Journal of Quantum Electronics 32 (2), 257-276 (1996).

176 Williams, K.A., Sarma, J., White, I.H., Penty, R.V., Middlemast, I., Ryan, T. and Laughton, F.R., "High Energy Q-Switched pulse generation using bow-tie laser diodes," presented at LEOS, San Jose, 1994.

177 Zhu, B., White, I.H., Williams, K.A., Laughton, F.R. and Penty, R.V., "High peak power picosecond pulse generation from Q-switched bow-tie laser with a tapered travelling wave amplifier," IEEE Photonics Technology Letters 8 (4), 503-505 (1996).

178 Williams, K., Sarma, J., White, I.H., Penty, R.V., Middlemast, I., Ryan, T., Laughton, F.R. and Roberts, J.S., "Tapered bow-tie lasers for high energy Q-switched pulse generation," presented at CLEO, Anaheim, 1994.

179 Summers, H.D., White, I.H., Laughton, F.R., Ralston, J.D., Penty, R.V., Williams, K.A., Sarma, J., Middlemast, I. and Ryan, T., "Passively mode-locked p-doped MQW bow-tie lasers," presented at CLEO, Baltimore, 1995.

180 Williams, K.A., White, I.H., Laughton, F.R., Sarma, J., Penty, R.V., Middlemast, I., Ryan, T. and Roberts, J.S., "Passive mode-locking of bow-tie lasers," presented at CLEO, Amsterdam, 1994.

181 Muller, J., Laughton, F.R., White, I.H., Penty, R.V., Sarma, J., Middlemast, I., Ryan, T. and Button, C., "Q-Switched Bow-Tie Lasers at 1.5 μm driven by an overshoot-compensated avalanche pulse generatior," Int.Opt.J.Optoelectronics 10, 35-38 (1996).

182 Sun, Y., Fanning, C. G., Biellak, S. A. and Siegman, A. E., "Thermally Controlled Lateral Beam Shift and Beam-Steering in Semiconductor-Lasers," IEEE Photonics Technology Letters 7 (1), 26-28 (1995).

183 Sun, Y. and Siegman, A. E., "Optical-Mode Properties of Laterally Offset Gain and Index Guiding Structures," IEEE Journal of Quantum Electronics 32 (5), 790-795 (1996).

184 Petrescu-Prahova, I.B. Buda, M.B. Van de Roer,T.G., "Design of a 1W Single Filament Laser Diode," IEICE Trans.Electronics E77-C (9), 1472-1478 (1994).

185 Wessel, J.G., Battle, P.R. and Carlsten, J.L., "Mode Structure and the noise performance of a gain-guided amplifier," Phys.Rev.A 50 (3), 2587-2593 (1994).

186 Petermann, K., IEEE Journal of Quantum Electronics 15, 566 (1979).

187 Asbeck, P.M., Cammack, A., Daniele, J.J. and Klebanoff, V., "Lateral Mode Behaviour in Narrow Stripe Lasers," IEEE Journal of Quantum Electronics 15 (8), 727-733 (1979).

188 Lang, R., "Lateral Transverse Mode Instability and its Stabilization in Stripe Geometry Injection Lasers," IEEE Journal of Quantum Electronics 15 (8), 719-726 (1979).

189 Jiang, Z., White, I.H., Laughton, F.R., Penty, R.V., McCall, M.W. and Tsang, H.K., "High Power diffraction-limmited ultrashort pulse generation from double tapered semiconductor laser diodes," presented at the OSA Topical meeting on semiconductor lasers, Keystone, Colorada, 1995.

190 Brooks, N., Sarma, J. and Middlemast, I., "A New Design for Tapered-Geometry High-Power Semiconductor Optical Sources," presented at LEOS, Boston, 1996.

191 Elyumin, S., Komori, K., Arai, S. and Bendelli, G., "Taper-Shape Dependence of Tapered-Wave-Guide Traveling-Wave Semiconductor-Laser Amplifier (TTW-SLA)," IEICE Transactions On Electronics E77C (4), 624-632 (1994).

192 GhafouriShiraz, H., Tan, P. W. and Aruga, T., "Picosecond pulse amplification in tapered-waveguide laser-diode amplifiers," IEEE Journal of Selected Topics in Quantum Electronics 3 (2), 210-217 (1997).

193 Bendelli, G., Komori, K. and Arai, S., "Gain Saturation and Propagation Characteristics of Index-Guided Tapered-Wave-Guide Traveling-Wave Semiconductor-Laser Amplifiers (TTW-SLAS)," IEEE Journal of Quantum Electronics 28 (2), 447-458 (1992).

194 Nakatsuka, S. and Uchida, K., "High-Power Single-Mode Flared Laser-Diode With an Intermediate-Width Stripe At the Flare Base," Japanese Journal of Applied Physics Part 1-Regular Papers Short Notes & Review Papers 35 (2A), 619-623 (1996).

195 Williams, K.A., White, I.H., Laughton, F.R., Jiang, Z. and Penty, R.V., "Gain-switched dynamics of tapered waveguide bow-tie lasers," presented at CLEO, Anaheim, 1996.

196 Sánchez, M. Camps, I. Gonzaléz,J.C. Diaz,P. Prutski,T.A., "Cavity Length dependence of the peak conversion efficiency in AlGaAs lasers," Journal of Applied Physics 79 (7), 3796-3797 (1996).

197 Claisse, P.R. Taylor, G.W., "Internal Quantum Efficiency of Laser Diodes," Electronics Letters 28 (21), 1991-1992 (1992).

198 Kitcher, D.J., Transfer Report, Dept.of Physics, University of Bath, 1995.

199 Tchelnokov, A. V., Lourtioz, J. M. and Gavrilovic, P., "Spatial and Spectral Dynamics of the Optical-Emission of Broad-Area Semiconductor Laser/Amplifiers," Annales De Physique 20 (5-6), 637-638 (1995).

200 Marciante, J. R. and Agrawal, G. P., "Nonlinear Mechanisms of Filamentation in Broad-Area Semiconductor Lasers," IEEE Journal of Quantum Electronics 32 (4), 590-596 (1996).

201 Marciante, J. R. and Agrawal, G. P., "Lateral Spatial Effects of Feedback in Gain-Guided and Broad-Area Semiconductor-Lasers," IEEE Journal of Quantum Electronics 32 (9), 1630-1635 (1996).

202 Landry, M. J., Rupert, J. W. and Mittas, A., "Multiple-Stripe and Broad-Area Diode-Lasers Operating At High-Power - Aging and Thermal-Degradation Influences On Performance," Optical Engineering 32 (1), 157-165 (1993).

203 Fischer, I., Hess, O., Elsaber, W. and Gobel, E., "Compex spatio-temporal dynamics in the near-field of a broad-area semiconductor laser," Europhysics Letters 35 (8), 579-594 (1996).

204 Tang, X. F., Vanderziel, J. P. and Chin, A. K., "Characterization of the Array Modes of High-Power Gain-Guided GaAs Single-Quantum-Well Laser Arrays," IEEE Journal of Quantum Electronics 32 (8), 1417-1426 (1996).

205 Tihanyi, P. L., Jain, F. C., Robinson, M. J., Dixon, J. E., Williams, J. E., Meehan, K., Oneill, M. S., Heath, L. S. and Beyea, D. M., "High-Power Algaas-Gaas Visible Diode-Lasers," IEEE Photonics Technology Letters 6 (7), 775-777 (1994).

206 Bryan, R.P., Miller, L.M., Cokerill, T.M., Langsjoen, S.M. and Coleman, J.J., "High-Power Pulsed Operation of a Optimized Nonplanar Corrugated Substrate Laser

Diode Array," IEEE Journal of Quantum Electronics 26 (2), 222 (1990).

207 Mroziewicz,B. "Broad area semiconductor laser with spatially modulated reflectivity of the mirrors," Electronics Letters 32 (4), 329 (1996).

208 Verdiell, J. M., Frey, R. and Huignard, J. P., "Analysis of Injection-Locked Gain-Guided Diode-Laser Arrays," IEEE Journal of Quantum Electronics 27 (3), 396-401 (1991).

209 Marshall, W.K. and Katz, J., "Direct Analysis of Gain-Guided Phase-Locked Semiconductor Laser Arrays," IEEE Journal of Quantum Electronics 22 (6), 827-832 (1986).

210 Alishev, Y. V., Hatzkevich, O. A. and Yamaykin, V. E., "Performance Studies of Semiconductor-Laser Arrays in the Fresnel Region," Doklady Akademii Nauk Belarusi 36 (9-10), 806-809 (1992).

211 Williams, K.A., Kitcher, D.J., Laughton, F.R., White, I.H. and Penty, R.V., "Picosecond Q-switched bow-tie laser array," presented at IQEC, Sydney, 1996.

212 Khrushchev, I. Y., Kitcher, D. J., Williams, K. A., White, I. H., Laughton, F. R. and Penty, R. V., "Picosecond Q-switched bow-tie laser diode array," Electronics Letters 33 (5), 426-428 (1997).

213 Wu, H. H., Lin, G. R. and Pan, C. L., "Optoelectronic Phase Tracking and Electrooptic Sampling of Free-Running Microwave Signals Up to 20 GHz in a Laser-Diode-Based System," IEEE Photonics Technology Letters 7 (6), 670-672 (1995).

214 Wu, H. H., Wang, C. L., Lin, G. R., Chang, C. S. and Pan, C. L., "Optoelectronic Phase-Tracking and Wave-Form Display of Microwave Signals Up to 8 GHz Using Gain-Switched Laser-Diodes," Japanese Journal of Applied Physics Part 2-Letters 33 (5B), L 760-L 762 (1994).

215 Breglio, G. and Cutolo, A., "Optoelectronic Measurement of Voltage Pulse Repetition Frequency By Picosecond Laser-Diodes," IEEE Transactions On Instrumentation and Measurement 43 (1), 7-12 (1994).

216 Breglio, G., Casavola, R., Cutolo, A. and Spirito, P., "The Bipolar Mode Field-Effect Transistor (BMFET) As an Optically Controlled Switch - Numerical and Experimental Results," IEEE Transactions On Power Electronics 11 (6), 755-767 (1996).

217 Kume, M., Naito, H., Ohya, J., Ohta, I., Shimizu, H., Kazumura, M. and Teramoto, I., "A High-Power Short-Pulse Laser Diode For Wave-Guide 2nd Harmonic-Generation," Solid-State Electronics 34 (12), 1329-1333 (1991).

218 Kompa, G., "Recent Advances in Laser Radar Technology with New Facilities for Quality Control," presented at the Modern Design, Manufacturing and Measurement, Tsinghua University, Bejing, China, 1993.

219 Jones, D.J., Zhang, L.M., Carroll, J.E. and Marcenac, D.D., "Dynamics of Monolithically Passively Mode-Locked Semiconductor Lasers," IEEE Journal of Quantum Electronics 31 (6), 1051-1058 (1995).

220 Hess, K., *Advanced Theory of Semiconductor Devices* (Prentice-Hall, EngleWod Cliffs, New Jersey, 1988).

221 Moseley, A.J., Robbins, D.J., Marshall, A.C., Kearley, M.Q. and Davies, J.I., "Quantum Confined Stark Effect in GaInAs/InP Single Quantum Wells Grown by LP MOVPE," Electronics Letters 24 (21), 1301 (1988).

222 Collings, D. and Schumacher, K.L., "Ultrafast transient absorption measurement of the electron-LO phonon scattering time in GaAs-Al(0.33)Ga(0.67)As multiple quantum wells," Appl.Phys.Lett. 7 (14), 889-891 (1994).

223 Schmitt-Rink,S. Chemla, D.S. and Miller, D.A.B., Adv.Phys. 38 (89) (1989).

224 Suzuki,M., Tanaka, H. and Akiba, S., "Effect of Hole Pile-up at heterointerface on modulation voltage in GaInAsP Electroabsorption Modulators," Electronics Letters 25 (2), 88-89 (1989).

225 Devaux,F., Bordes, P., Ougazzaden, A., Carre, M. and Heut, "Experimental optimisation of MQW electroabsorption modulators with up to 40 GHz bandwidths," Electronics Letters 30 (16), 1347 (1994).

226 Grupen, M. and Hess, K., "Severe gain suppression due to dynamic carrier heating in quantum well lasers," Appl.Phys.Lett. 70 (7), 808-810 (1997).

227 Collings, D. and Schumacher, K.L., "Ultrafast transient absorption measurement of the electron-LO phonon scattering time in GaAs-Al(0.33)Ga(0.67)As multiple quantum wells," Appl.Phys.Lett. 7 (14), 889-891 (1994).

229 Lasher, G.J., "Analysis of a proposed bistable injection laser," Solid State Electronics 7, 707-716 (1964).

230 Erneux, T. and Mandel, P., "Bifurcation Phenomena in a Laser with a Saturable Absorber I," Z.Phys.B.-Condensed Matter 44, 353-363 (1981).

231 Ferreira, M., "Frequency Noise and Modulation of a Four-Section DBR Laser," IEEE Journal of Quantum Electronics 32 (4), 851-858 (1996).

232 Zeilinski, E., Lach, E., Bouayas-Amine, J., Haisch, H., Kuhn, E., Schilling, M. and Weber, J., "Monolithic Multisegment Mode-Locked DBR Laser for Wavelength Tunable Picosecond Pulse Generation," IEEE Selected Topics in Quantum Electronics 3 (2), 230-232 (1997).

233 Phelan, P., Mc.Donald, D., Egan, A., Hegarty, J., O'Dowd, R., Farrel, G. and Lindgren, S., "Comparison of self-pulsation in multisection lasers with distributed feedback and intracavity saturable absorbers," IEE Proc.Optoelectronics 141 (2), 114-118 (1994).

234 Nirmalathas, A., Liu, H.F., Ahmed, Z., Novak, D. and Ogawa, Y., "Subharmonic Synchronous and Hybrid Mode-Locking of a Monolithic DBR Laser Operating a Millimeter-Wave Frequencies," IEEE Photonics Technology Letters 9 (4), 434 (1997).

235 Correc, Pascal, "Tunability of Multisection DFB Lasers," IEEE Journal of Quantum Electronics 32 (6), 972-980 (1996).

236 Kawaguchi, H., "Progress in optical functional devices using two-section laser diodes/amplifiers," IEE Proceedings 140 (1), 3-15 (1993).